

RESEARCH REPORT

Research project TACR TRANSPORT 2020+
No. CK02000321

Authors:

Vladimír Socha
Petr Došel
Lenka Hanáková
Boris Oniščenko
Stanislav Kušmírek
Jan Petříček



CTU

**CZECH TECHNICAL
UNIVERSITY
IN PRAGUE**



Institute of Aviation Medicine, Prague

T A
C R

Technology
Agency of the
Czech Republic

Programme **Transport 2020+**

Authors

Vladimír Socha, Petr Došel, Lenka Hanáková, Boris Oniščenko, Stanislav Kušmírek, Jan Petříček

© 2024 Czech Technical University in Prague, Faculty of Transportation Sciences, Department of Air Transport

© 2024 Institute of Aviation Medicine, Prague

Users are permitted to apply the methods described in this document for any purpose, provided that it is used as is without any modifications or alterations. Users are not allowed to make any changes to the source document. The content must remain intact and unaltered in any form or manner. Republishing, distributing, or using the content of this document in any form is prohibited without prior written permission from the authors. The data supporting the findings of this study will be made publicly available following the publication of all related results. Until then, the data will be available upon request. In recognition of the intellectual effort and contributions of the authors, any use of the report must be accompanied by an appropriate citation to the source document. This citation should acknowledge the authors and reference the title and publication year of the source document.

Contents

1	Introduction	1
2	Methods	2
2.1	Participants	2
2.2	Experimental setup	3
2.2.1	Stage 1	4
2.2.2	Stage 2	8
2.3	Physiological measurements	14
2.3.1	Cardiac activity	14
2.3.2	Brain activity	15
2.4	Stabilometry and motion tracking	16
2.4.1	Postural stability	18
2.4.2	Motion tracking	19
2.5	Equipment	20
2.6	Data processing	22
2.6.1	Flight data	22
2.6.2	Cardiac activity	26
2.6.3	Brain activity	34
2.6.4	Stabilometry	35
2.7	Statistical analysis	38
2.7.1	Cardiac activity	38
2.7.2	Brain activity	40
2.7.3	Stabilometry	42
2.7.4	Structured interviews	43
3	Results	44
3.1	Structured interview	44
3.2	Flight data	45
3.2.1	Somatogravic illusion	45
3.2.2	Coriolis Illusion	51
3.2.3	Somatogravic Illusion	54
3.3	Cardiac activity	57
3.3.1	Somatogravic illusion	57
3.3.2	Coriolis illusion	59
3.3.3	Somatogyral illusion	62
3.4	Postulography	64
4	Conclusion	67

Appendices	71
Appendix 1 – Flight profile 1 for Stage 1	72
Appendix 2 – Flight profile 2 for Stage 1	80
Appendix 2 – Flight profile 3 for Stage 1	89
Appendix 4 – Flight profile 1 for Stage 2	97
Appendix 5 – Flight profile 2 for Stage 2	105

1 Introduction

The phenomenon of vestibular illusions presented a significant challenge in aviation, particularly under instrument flight rules (IFR) conditions, where pilots must rely heavily on their instruments due to the lack of visual cues. These illusions could lead to spatial disorientation, a leading factor in many aviation accidents. Recognizing the importance of addressing this challenge, the project aimed to pioneer the development and incorporation of vestibular illusion simulators into initial pilot training programs. This initiative sought not only to enhance pilots' ability to recognize and manage spatial disorientation but also to foster a safer aviation environment by integrating practical, illusion-based training scenarios into standard flight education.

The primary goal of the project was to establish certified methodologies and procedures that enabled the effective use of vestibular illusion simulators in ab-initio pilot training. By simulating various flight conditions that induce spatial disorientation, such as somatogravic, Coriolis, and somatogyral illusions, the training aimed to equip pilots with the skills necessary to navigate these challenges effectively. This approach aligned with the broader objective of increasing safety in air transport by directly addressing one of its most elusive dangers.

To achieve these goals, the project engaged in comprehensive research activities designed to underline the significance of vestibular illusion training within simulator-based pilot training. By systematically identifying flight tasks susceptible to inducing vestibular illusions and evaluating the impact of these illusions on pilots' performance and psycho-physiological condition, the project aimed to build a robust body of evidence supporting the incorporation of this training. The research was conducted across four cohorts of pilots, ranging from beginners to experienced aviators, to ensure the findings were comprehensive and applicable across different stages of pilot training.

The controlled and safe confines of a flight simulator offered an unparalleled platform for this kind of training. Within this environment, pilots were afforded the opportunity to encounter and engage with complex spatial illusions in a manner that was free from the high-risk stakes of actual flight. This exposure was invaluable, equipping pilots with the experience and confidence to recognize, confront, and correct for the disorienting effects of vestibular illusions in real-world scenarios. Such training was anticipated not only to bolster a pilot's psychological and physiological resilience to disorientation triggers but also to enhance their overall situational awareness and decision-making capabilities under stress.

Furthermore, the structured repetition of these simulated illusions facilitated a deeper understanding and memorization of appropriate compensatory strategies, thereby embedding instinctual reactions that could be relied upon during critical moments of actual flight operations. It fostered a mindset that prioritized instrument readings over misleading sensory perceptions, a fundamental skill in navigating the complexities of modern aviation.

This document serves as a research report for project CK02000321, summarizing research activities and presenting the main findings within the context of the project's established goals. In addition, it includes a description of the methodological approaches, ensuring that this research is reproducible. The conducted research represents the largest study in this field worldwide in terms of measurements carried out and data collected. We consider the presented results to be generalizable.

2 Methods

The primary goal of the project No. CK02000321 was to develop evidence-based methodologies and procedures to incorporate vestibular illusion simulators into pilots’ initial training, in a manner that would allow acceptance of flight hours as part of pilots’ training along with the benefit of practical spatial disorientation training. The project objectives were achieved through research activities, thus providing an evidence base for the methodology (other project result), as the incorporating of new procedures in areas characterized by a high degree of safety, particularly in aviation, requires evidence-based approaches and methods of investigation. Project activities and the overall solution approach were therefore designed in a way that reflects this approach. In this context, research activities were divided into two stages:

Stage 1: measurements involving experienced pilots (instructors), based on which final flight profiles were defined among other things, and

Stage 2: measurements involving pilots with varying levels of flight experience using the final flight profiles.

2.1 Participants

A total of 25 subjects participated in Stage 1 of the experimental measurements, while 114 subjects participated in Stage 2.

In Stage 1, 25 instrument rating instructors on volunteering basis were participating. These were active pilots who had no previous experience with the GYRO IPT-II simulator or other desorientation simulator. The pilots ranged in age of 40 ± 13 years. The overall flight hours were 7105 ± 4598 and IFR flight hours were 5401 ± 4157 . Since they all held a Class 1 medical certificate as per Commission Regulation (EU) No 1178/2011, Annex IV (Part-MED), as amended, they had normal visual acuity, and any vestibular or visual impairments were excluded.

In Stage 2, each subject was classified into groups 1 to 4 based on their flying experience, with group 4 including the most experienced pilots. These groups encompass pilots undergoing initial IFR training (Gr. 1), pilots in the post-simulator training phase (Gr. 2), pilots who have recently completed IFR training (Gr. 3), and experienced pilots with approximately 250 hours or more of IFR flight experience (Gr. 4). A detailed overview of the population included in each subject group is provided in Table 1.

Table 1: Population included in Stage 2

Group	Sex		Age	Overall flight hours	IFR flight hours
	F	M			
Gr. 1	4	26	26 ± 6	186 ± 152	2 ± 4
Gr. 2	1	24	25 ± 7	236 ± 267	30 ± 19
Gr. 3	3	26	25 ± 5	306 ± 282	92 ± 54
Gr. 4	1	29	38 ± 11	4215 ± 4158	3172 ± 3507

While the original plan was to equally distribute the subjects into 4 groups, i.e. have 120 subjects, 30 in each group, it was problematic to find a sufficient number of subjects, especially in the case of group 2, where this group of pilots was the most specific regarding the training phase, which has a continuous form. The identification and acquisition of subjects from this cohort thus depended to a large extent on the time when, after a relatively short period, the subject no longer had to meet the project's requirements.

Considerable effort was made to recruit subjects for various groups. The aim was to find suitable pilots to complete the full complement of tested pilots using various platforms and advertisements. Unfortunately, finding ideal candidates proved challenging. An advertisement was published targeting a group of pilots under the patronage of the Czech Civil Aviation Authority, those who were either undergoing or had completed ATPL exams. Awareness of the measurement spread among the national carrier's pilots, where many young pilots joined after a selection process. However, due to the workload of entry requirements, simulators, and ground school, they couldn't participate. Additionally, awareness spread through many aeroclubs via flight operations managers. Unfortunately, the response from aeroclubs was not sufficiently positive. An appropriate alternative was to approach commercial flight schools, which sent pilots for measurement. Unfortunately, there weren't enough pilots to fulfill the targeted number of participants.

The 114 selected pilots were then recruited through the previously mentioned channels (i.e. CTU students, CTU alumni, aeroclubs, flight schools, social networks etc.). All subjects were healthy adults, there were medical requirements pursuant to a class 2 medical certificate as per Commission Regulation (EU) No 1178/2011, Annex IV (Part-MED), as amended.

All subjects received basic information regarding the principles and requirements of the experiment, the non-invasive methods of data collection, and the procedures for anonymizing personal and collected data, in line with the ethical principles for medical research involving human subjects [1]. The experiments were approved by the Committee for Ethics in Research of the Czech technical university in Prague Scientific Council (formerly Committee for Research Ethics at the Czech Technical University in Prague) under the reference number 0000-01/21/51902/EKČVUT, and all subjects signed informed consents.

However, the subjects were not briefed on the specific details of the simulation device to prevent bias resulting from anticipated cabin movements during illusion induction. Nonetheless, all subjects were informed about the potential for motion sickness and were provided with sickness bags. Additionally, subjects were informed about the simulator's stop button in case of motion sickness. Throughout the entire flight, the subjects maintained radio communication with the simulator operator and were instructed to immediately report any health issues. The measurements took place at the Institute of Aviation Medicine, Prague, located in the Military University Hospital Prague, under medical supervision.

2.2 Experimental setup

The experimental measurements, divided into two stages, were both based on predefined simulated flights using desorientation simulator GYRO IPT-II Spatial Disorientation Trainer (ETC Aircrew Training Systems, Southampton, PA, United States). The measurements were supplemented by the monitoring of the psychophysiological state, postural stability measurements, and structured interviews in both stages of the project.

2.2.1 Stage 1

The experimental Stage 1 aimed to obtain feedback from instructors and design final flight profiles. For this purpose, an experimental setup consisting of three simulated flights was designed. Additionally, the subjects were monitored for their psychophysiological state using electrocardiography (ECG) and electroencephalography (EEG), motion using a motion capture system (MoCap), and postural stability using a stabilometry platform. Following each flight, feedback was obtained through structured interviews, as illustrated in Fig.1.

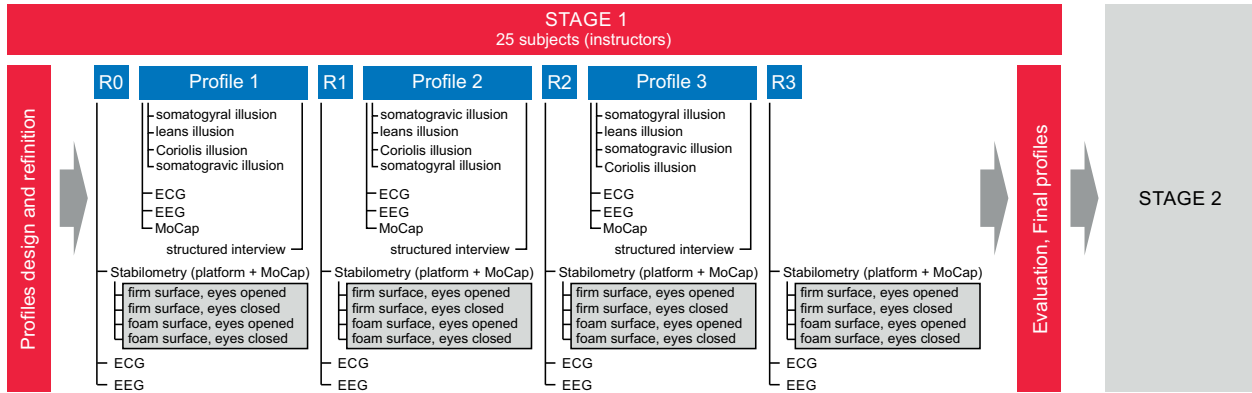


Figure 1: Schematic depiction of experimental setup for Stage 1.

Prior to initiating experimental measurements, potential methods of inducing vestibular illusions and their integration into specific flight phases were identified. In this context, three flight profiles were programmed and progressively refined in the presence of experienced instructors from both participating institutions. These flight profiles, each approximately 30 minutes long, were further used for experimental measurements in Stage 1.

Flight profiles

Apart from the profiles themselves, subjects were allowed an initial 30-minute familiarization period with the simulator's behavior. The profiles were created based on the outline of classical IFR simulator training. All flights took place at PHNL – Daniel K. Inouye International Airport using radio navigation aids and without additional traffic. The inspiration for the profiles came from those commonly used for military pilot training, but they were significantly modified for the purposes of the project. Within these profiles, four illusions were examined: somatogravic, Coriolis, somatogyral, and leans illusions. The programming of profiles took place directly within the simulator's software environment.

The first flight profile contained elements corresponding to the initial phase of IFR simulator training, such as basic instrument flying, straight and level flight, climbs, descents, turns, speed changes, configuration changes, frequency changes, maintaining a given vertical speed, etc. This profile was programmed based on specific times for instructions and then based on specific flight conditions, primarily exceeding the heading, roll, or pitch parameter to trigger the illusion. The first programmed illusion was the somatogyral illusion during a turn with a sudden transition of the aircraft to the horizon. The second illusion was the leans


illusion, which was implemented again during a turn. Another illusion was the Coriolis illusion, where the subject was tasked with turning while simultaneously moving their head. The somatogravic illusion was the last one and was triggered during a go-around. The sequence of profile phases along with conditions and voice instructions is described in Appendix 1.

The second flight profile corresponded to the mid-phase of IFR simulator training. This profile thus included basic IFR procedures such as holding, procedure turn, base turn, and navigation using radio navigation aids. For this profile, the subject was provided with a map showing the individual procedures and was thoroughly briefed beforehand. The map with marked procedures available to the subject is shown in Fig. 2. The profile started on runway 26R, followed by a departure straight along the runway heading. The pilot was then vectored over VOR HNL to perform a base turn, followed by a smooth transition into holding. After the holding, the pilot was instructed to fly R-138 and make a right procedure turn at a distance of 5 NM.

This profile was programmed primarily based on the fulfillment of certain conditions, whether it be exceeding parameters such as pitch, heading, altitude, speed, bank angle, etc. The first illusion, somatogravic illusion, occurred immediately after takeoff. The leans illusion was programmed for the turn during the base turn. In the first turn onto the departure course during the holding pattern, the Coriolis illusion was implemented. The last one, the somatogyral illusion, was located in the final turn during the procedure turn. The sequence of the profile along with programming conditions, individual instructions, and illusions is described in detail in Appendix 2.

The third profile corresponded to the final phase of IFR simulator training. In this profile, the pilot should be capable of executing the previous elements and conducting a continuous flight from takeoff to landing. For this flight profile, the pilot again had maps available (see Figure 3). The beginning of the third profile was once again on the runway, specifically runway 04R in this case. Subsequently, the pilot was tasked with flying to R-125 from VOR HNL. To save time, the entire departure route was not flown, but the pilot was instructed to make a right turn back to VOR HNL. After passing VOR HNL, the pilot could smoothly proceed to the ILS approach RWY 04R and, at DA(H), perform a go-around and continue according to the published missed approach to the ALANA waypoint and hold.

After completing the holding pattern, the pilot was permitted to proceed to NDB EWABE, marking the end of the flight. The first illusion occurred after takeoff during the turn back to VOR HNL, which was the somatogyral illusion. The leans illusion was programmed during the procedure turn on approach. The somatogravic illusion occurred during the go-around. The Coriolis illusion was in the first turn onto the departure course during the holding over the ALANA waypoint. The sequence of the third profile along with programming conditions, instructions, and illusions is illustrated step by step in Appendix 3.

-  In Appendices 3–5, the timeline of the profile events includes times of events, which may give the impression that the profile lasted for an unreasonably short period. These times are defined solely to establish the timeline of events. In this context, the defined conditions to which the simulator reacts upon fulfillment are important. This means that the overall duration of the profile is somewhat variable, depending on the fulfillment of specific conditions at specific (real) time points.

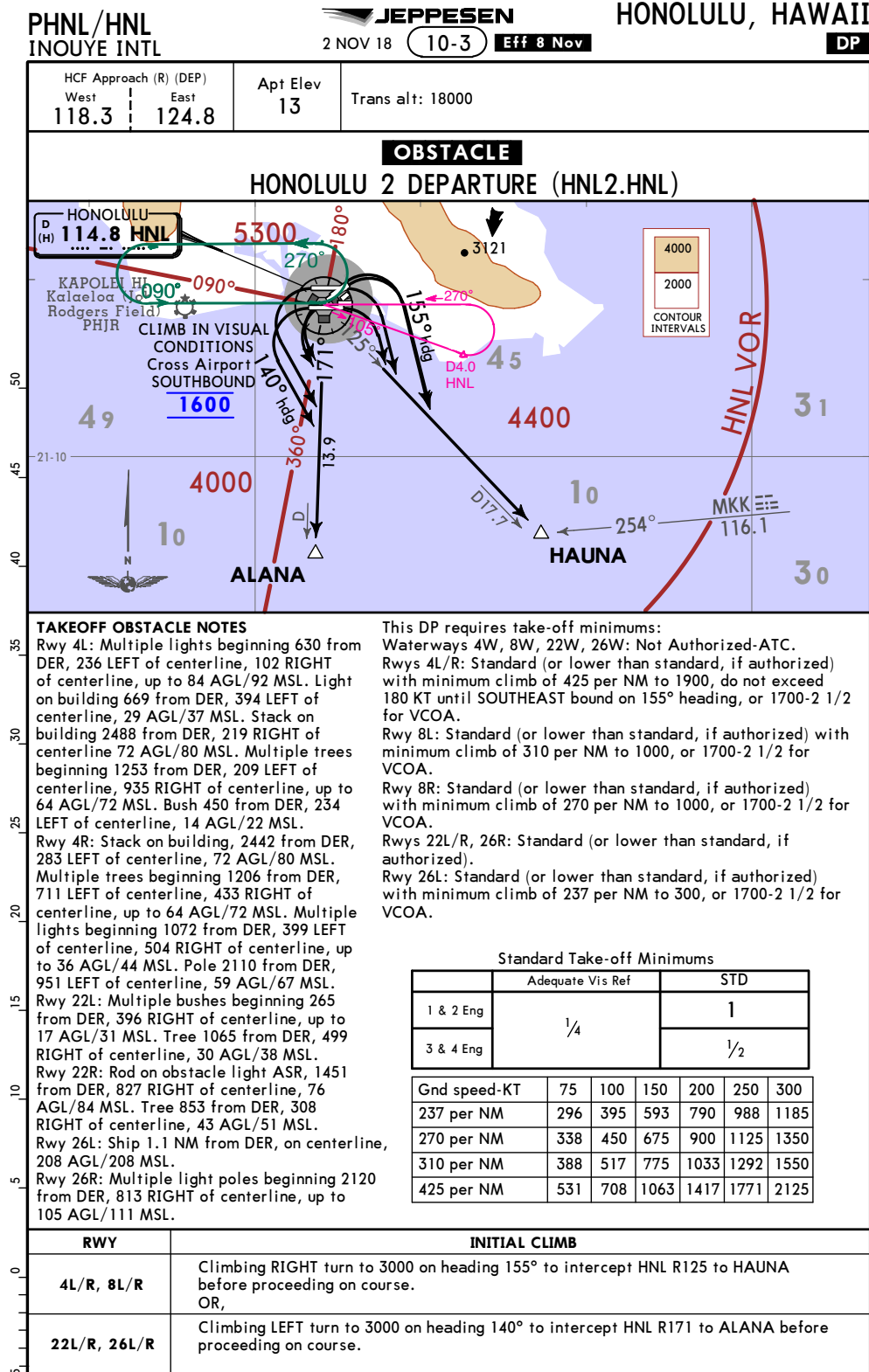


Figure 2: Map with procedures marked for flight profile 2 (Stage 1).

PHNL/HNL
INOUEY INTL

JEPPESEN
2 NOV 18 (11-3)

HONOLULU, HAWAII
ILS Rwy 4R

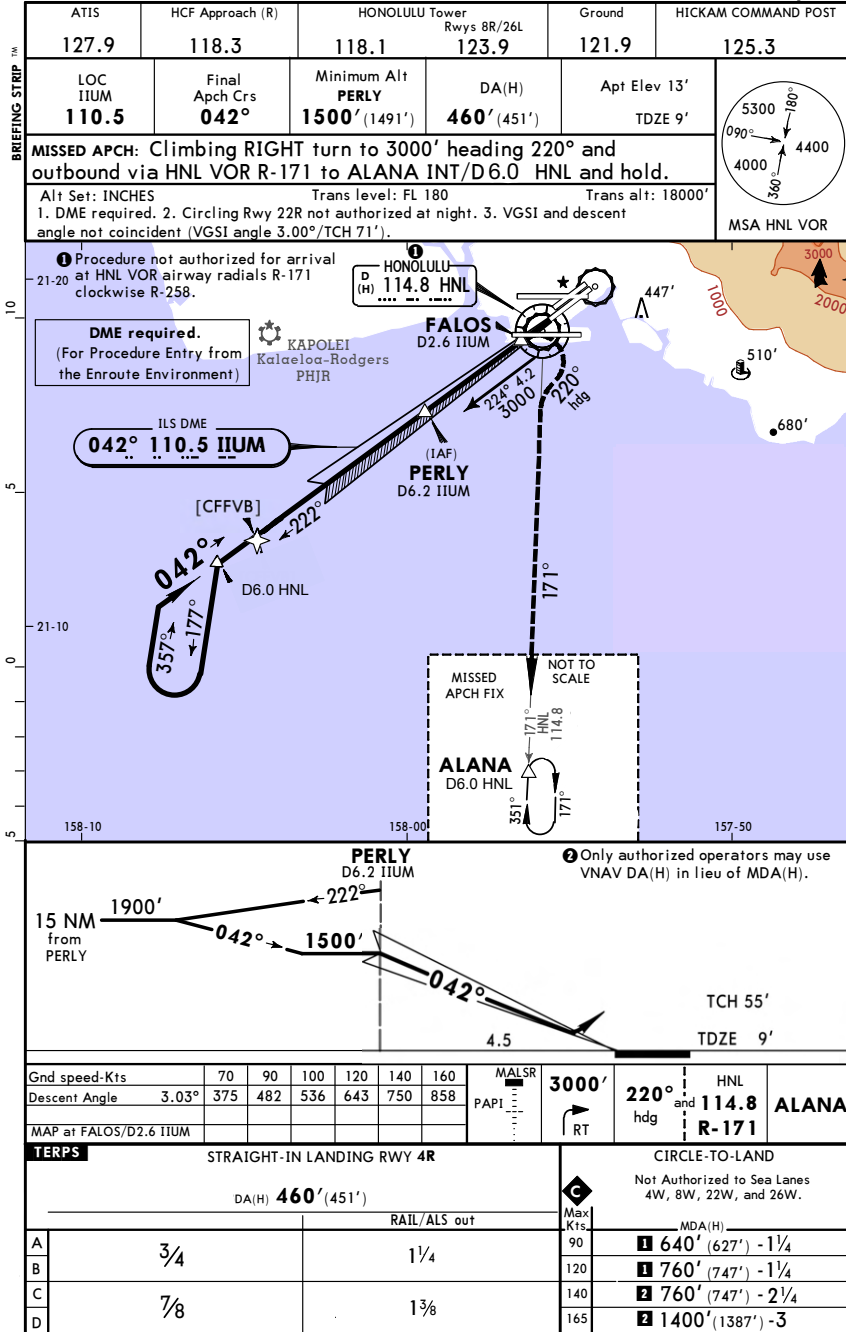



Figure 3: Map with procedures marked for flight profile 3 (Stage 1).

Structured interview

After each flight profile, the subjects provided feedback through structured interviews. Information obtained during these interviews with the instructors was crucial for designing the final two profiles used in Stage 2. The interviews consisted of a total of six questions.

- Q1:** Flight Profile 1 – impressions, illusions (realness, intensity), composition
- Q2:** Flight Profile 2 – impressions, illusions (realness, intensity), composition
- Q3:** Flight Profile 3 – impressions, illusions (realness, intensity), composition
- Q4:** Incorporation of practical simulator-based training for vestibular illusions into IFR training?
Yes/no + justification.
- Q5:** At what stage of IFR training should this vestibular illusion training be incorporated?
- Q6:** Which flight profile to use in case of incorporation?

In the first three questions, the subjects were asked to report impressions from the given profiles. This primarily involved identifying which illusions were experienced, which was the most intense, which was the weakest, etc. Furthermore, there was room for evaluating the composition of the profile. This led, among other things, to the exclusion of the leans illusion from the final profiles, as subjects reported its unrealistic induction during flight. Based on collected information, two profiles were then selected as the basis for the final profiles used in the subsequent stage of the project.

 The results of Stage 1 structured interviews are presented in document CK02000321-V1 Methodology of Vestibular Illusion Training Using a Flight Simulator which is available online at <http://kld.fd.cvut.cz> and/or upon request via email (sochavla@fd.cvut.cz).

2.2.2 Stage 2

Experimental setup for Stage 2 was similar as for Stage 1. The setup of each measurement consisted of 2 simulated flights, accompanied by psychophysiological state monitoring, stabilometry and motion tracking, see Fig. 4. To evaluate the effect of vestibular training, each subject absolved two measurements, separated by approx. one week.

Flight profiles

Since the most preferred profiles were the first and second ones, elements from these mentioned profiles were incorporated into the final ones. Considering that not only experienced pilots but also pilots in the initial phase of IFR training participate in activity A3, the profiles had to be designed in a way that ensured all pilots are able to fly these profiles without significant difficulties.

Both profiles were designed to assess and compare susceptibility to vestibular illusions and the training undergone for vestibular illusions. All flights took place again at PHNL – Daniel K. Inouye International

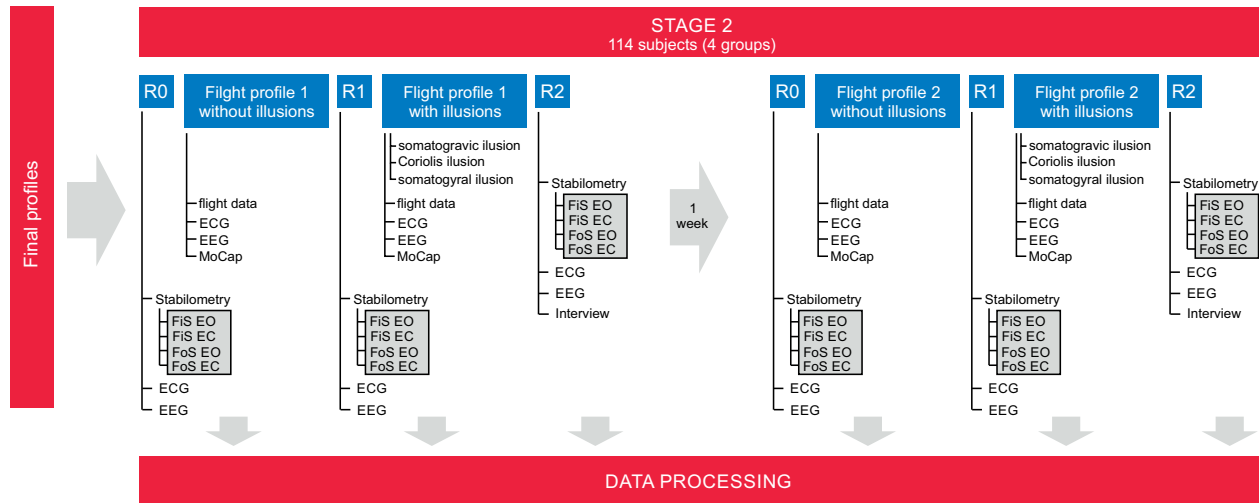


Figure 4: Schematic depiction of experimental setup for Stage 2. Note that, FiS means Firm surface, FoS means Foam surface, EO means Eyes opened, and EC means Eyes closed.

Airport using radio navigation aids and without additional traffic. Within these profiles, three flight illusions were induced: somatogravic, Coriolis, and somatogyral illusions. Both profiles contained the same elements to ensure similarity. Those profiles were flown during 2 sessions with approximately a one week time gap between them.

The first flight profile began with a takeoff from runway 08R. During takeoff, the somatogravic illusion was implemented. Then, the subject was tasked with climbing to an altitude of 1500 ft and then turning to heading 160. After reaching this heading, the subject was instructed to continue climbing to an altitude of 2000 ft and, after a certain time, make a left turn to heading 270. During this turn, the Coriolis illusion was implemented. The next instruction was to fly directly to VOR HNL. Then, the subject was instructed to fly heading 250 and descend to an altitude of 1500 ft. After reaching this altitude, the instruction was to make a left turn to heading 045. During this turn, the somatogyral illusion was implemented. The next instruction was to descend below the cloud cover to 800 ft, and the subject was instructed to land on runway 08R. This profile was flown twice by each subject, immediately one after the other without unnecessary delay. The first time without implemented illusions and the second time with illusions. The sequence of the profile is shown in Appendix 4. Prior to the actual flight profile, each subject completed a 30-minute free flight to familiarize themselves with the simulator’s behavior. Then, two versions of the first flight profile followed. Each version of the profile lasted approximately 20 minutes.

The second flight profile began with a takeoff from runway 04R. During takeoff, the somatogravic illusion was again implemented. The subject received instructions to climb to an altitude of 1500 ft before takeoff. Even before reaching this altitude, the subject was instructed to turn left to heading 300 and continue climbing to an altitude of 2000 ft. After reaching this altitude, the subject was to make a right turn to heading 190. During this turn, the Coriolis illusion was programmed. The next instruction was to fly directly to VOR HNL. After passing VOR HNL, the subject was to descend to an altitude of 1500 ft and then turn left to heading 110, followed by a right turn to heading 315. During this turn, the somatogyral

illusion was implemented. The next instruction was to descend below the cloud cover to 800 ft, with the subject being tasked to land on runway 26R. This profile was flown twice by the subject immediately one after the other without unnecessary delay, with the first flight without implemented illusions and the second flight with illusions, see Appendix 5. The profile lasted approximately 20 minutes. Prior to the actual flight profile, the subject again completed a free flight. Compared to the previous profile, the duration of the free flight was shortened to 10 minutes considering the previous experience.

Illusions induction

After liftoff and while climbing over the runway in the departure direction, if the longitudinal pitch exceeds 5° , the simulator initiates a pitch-up movement of the cabin by $+12$ degrees. This results in an angular acceleration of $1.3 \text{ }^\circ/\text{s}^2$ and a maximum rotational velocity of $4 \text{ }^\circ/\text{s}$. Immediately achieving 12° pitch, the simulator cabin returns to its initial position of 0° , achieving this with an angular deceleration of $0.3 \text{ }^\circ/\text{s}^2$ and a rotational speed of $1 \text{ }^\circ/\text{s}$. A schematic representation of the mechanics of inducing the somatogravic illusion is illustrated in Fig. 5. In the figure, the induction of the somatogravic illusion in the second flight profile is demonstrated. However, this procedure was also applied to the first profile.

The Coriolis illusion was induced in the first major turn of both profiles. During the aircraft's turn in the simulation, the simulator device performs a rotation around its axis. This rotation achieves a total rotational speed of $60^\circ/\text{s}$ with angular acceleration of $2^\circ/\text{s}^2$, lasting a total of 30 seconds. After this period and once the condition that the aircraft is in the midst of a turn is met, the pilots received an audio command to read and announce a sequence of numbers located behind their shoulder. The label with the sequence of numbers is placed below the natural field of vision, forcing a head movement also downward. This command compels the pilot to make a significant head movement, both towards and back along a trajectory that stimulates the vestibular apparatus, leading to sensations associated with the Coriolis illusion. The initial head movement is forced in the direction of the simulator's rotation.

The rotation of the simulator continues until a condition of completing a turn to a specific course is met. From this point, the simulator device begins to decelerate from a rotational speed of $60^\circ/\text{s}$ at a rate of $1^\circ/\text{s}^2$ for 60 seconds until a rotation of $0^\circ/\text{s}$ is achieved. A schematic representation of the mechanics of inducing the somatogravic illusion is illustrated in Fig. 6. This figure demonstrates the induction of the illusion for the second flight profile. The approach was identical for the first flight profile, with the only difference being that the simulator's rotation and the instruction for the pilot to turn their head were in the opposite direction, as the turn was made to the left.

In the experiment, the somatogyral illusion was triggered during the second major turn in both flight profiles. A critical factor in inducing this illusion involves the simulator's gradual acceleration into rotational motion to reach high rotation speeds. For the purposes of this study, the acceleration rate was experimentally determined to be $1.5^\circ/\text{s}$, allowing the simulator to attain a rotational speed of $60^\circ/\text{s}$ after 40 seconds. The initiation of the simulator's rotation coincided with the aircraft entering a steady turn, maintaining a rotation speed of $60^\circ/\text{s}$ until the maneuver's completion, that is, until the aircraft began to align with the intended course. The gentle initial acceleration and the consistent rotation speed play a vital role in the swift stabilization of the fluid within the vestibular apparatus's semicircular canals.

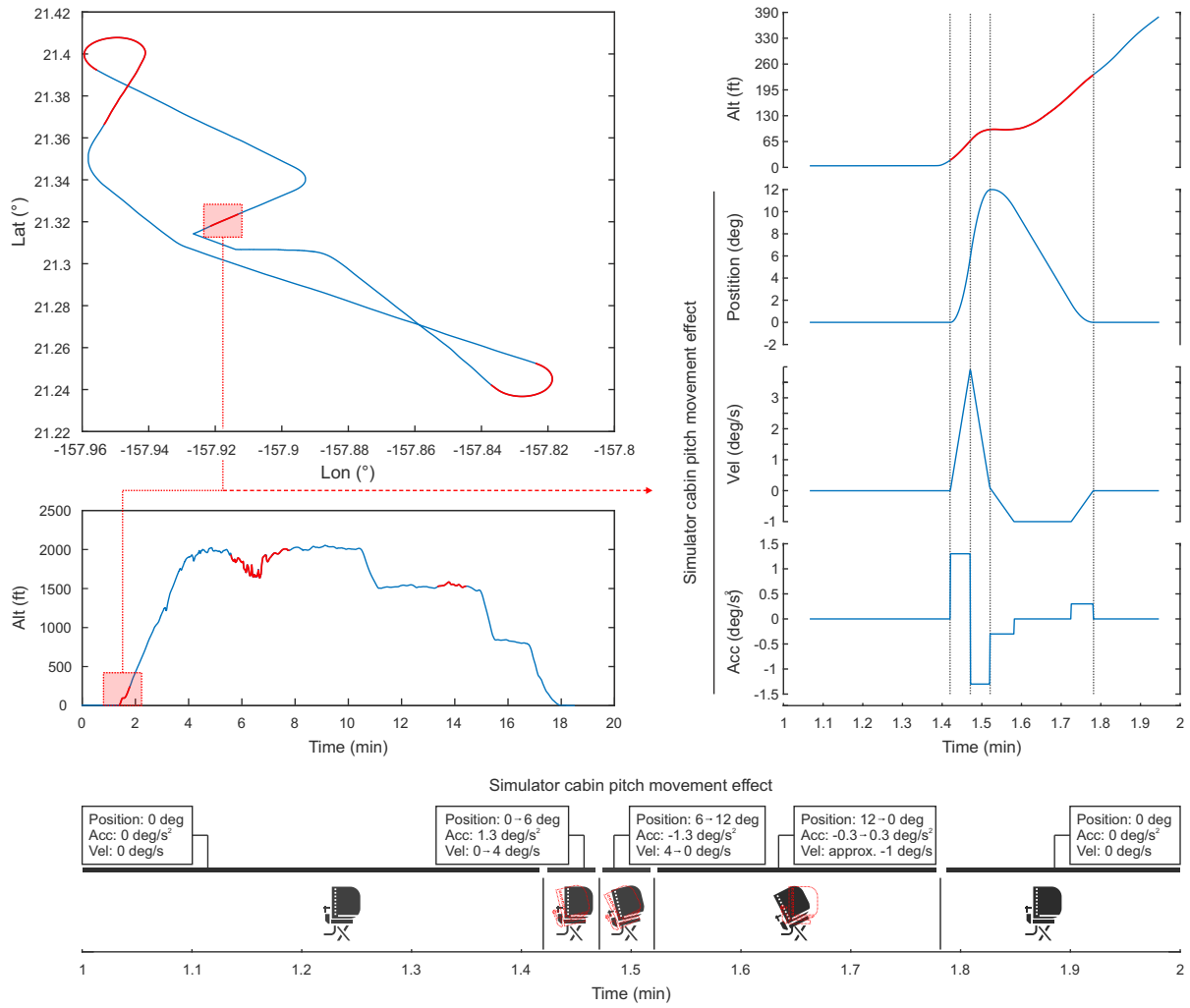


Figure 5: Principle of inducing the somatogravic illusion

A pivotal moment in the induction of the somatogravic illusion occurs as the aircraft exits the turn, transitioning into level flight. At this point, the simulator undergoes rapid deceleration and ceases its rotation within 5 seconds, equivalent to a deceleration rate of $12^\circ/\text{s}$. This sudden deceleration introduces a dramatic and disorienting shift in vestibular sensation for the pilot, potentially giving rise to a pronounced feeling of continuing the turn or initiating a turn in the opposite direction, despite the aircraft having leveled out. The disparity between the pilot's vestibular perception and the actual flight conditions, as indicated by the instruments, poses a significant challenge to maintaining spatial orientation.

An additional element that may influence the intensity of the illusion, or the pilot's ability to maintain control, is the introduction of a task that diverts the pilot's focus from the spatial orientation instruments during the rapid deceleration phase. Notably, this phase of the experiment did not aim to replicate the Coriolis illusion; hence, inducing head movement was deemed inappropriate. Instead, an instruction to

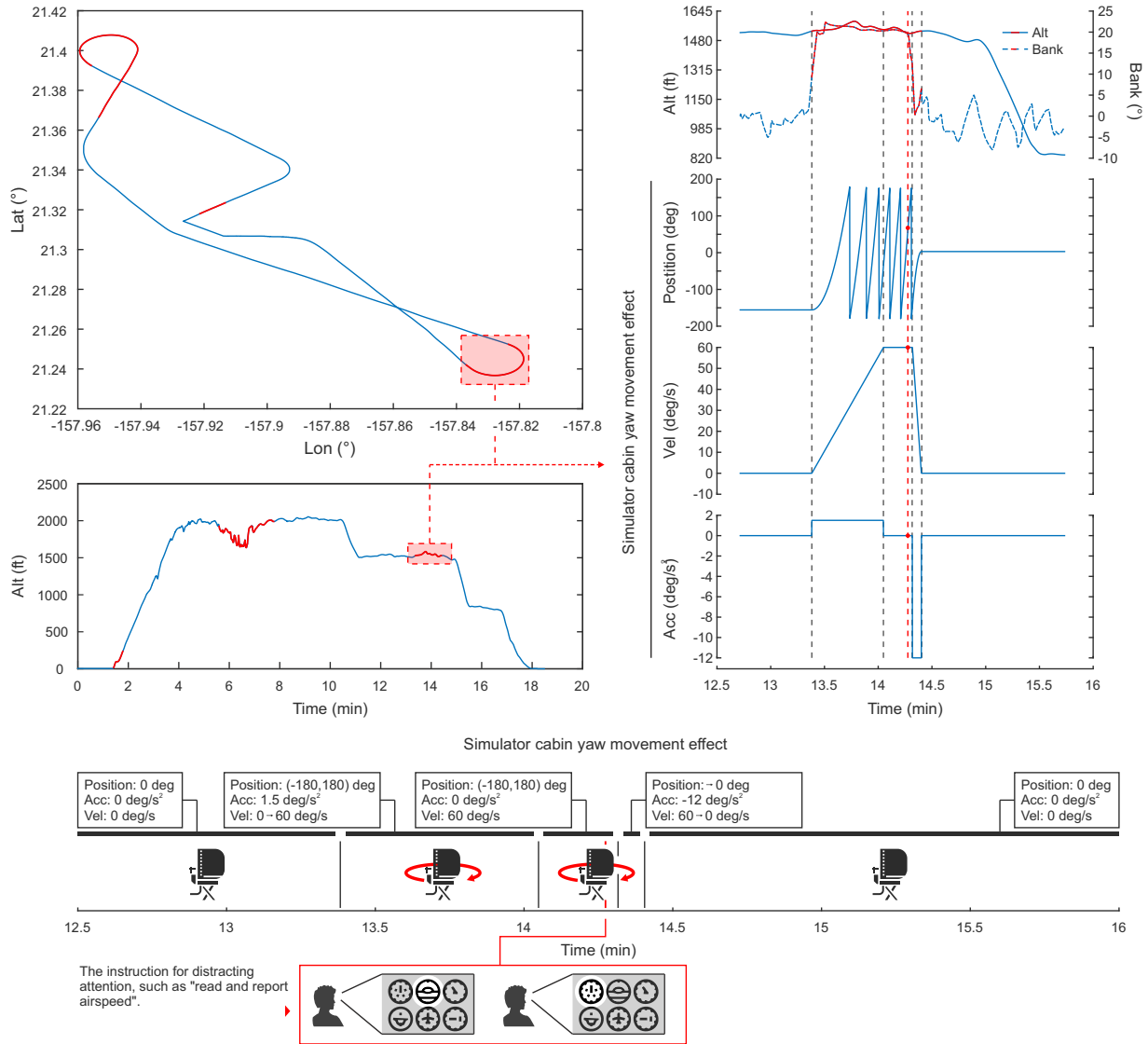


Figure 6: Principle of inducing the Coriolis illusion.

”report airspeed” was found to be effective during the experiment. This directive ensures that, amidst the rapid deceleration and while leveling the aircraft, the pilot’s attention is momentarily redirected to the airspeed indicator, further complicating the challenge of spatial orientation.

The concept described above is schematically illustrated in Fig. 7, for second flight profile.

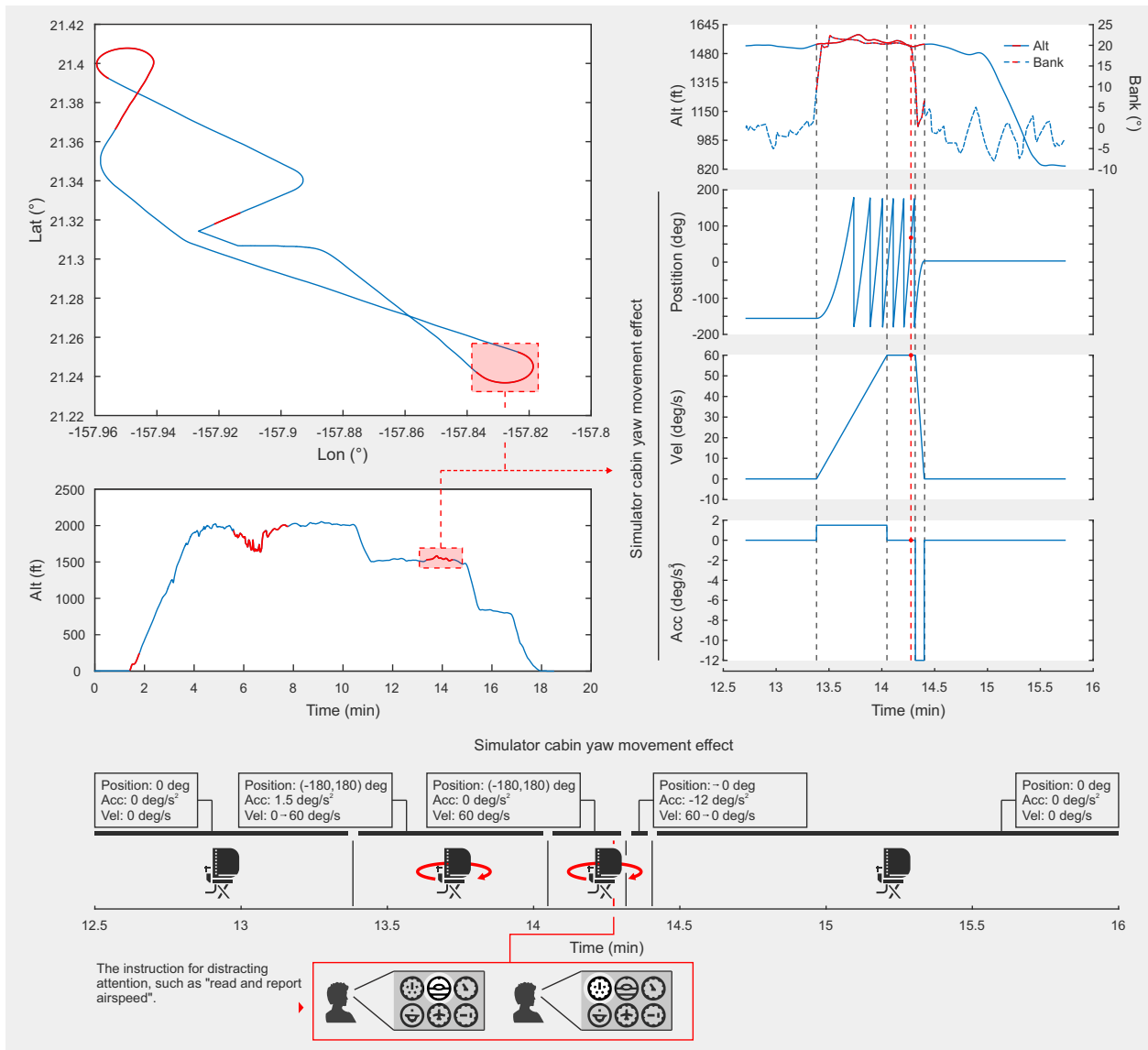


Figure 7: Principle of inducing the Somatogravil illusion.

Structured interview

As well as in Stage 1, the subjects were reporting their experience from simulated flights through structured interviews. After both flights using the first profile, the subjects were asked the following questions:

- Q1:** Somatogravic illusion – intensity, realness, did you recognised it?
- Q2:** Coriolis illusion – intensity, realness, did you recognised it?
- Q3:** Somatogravil illusion – intensity, realness, did you recognised it?
- Q4:** Did you feel something else? What and when?

Q5: Any further notes?

The same questions were also asked after both flights of the second profile. However, the interview was further extended:

Q1: Somatogravic illusion – intensity, realness, did you recognised it?

Q2: Coriolis illusion – intensity, realness, did you recognised it?

Q3: Somatogyral illusion – intensity, realness, did you recognised it?

Q4: Did you feel something else? What and when?

Q5: Any further notes?

Q6: Do you feel that you handled illusions better considering your previous experience?

Q7: Would you implement such a simulator session into training?


After the interview concluded, the collection of all data was also terminated, and the subject was disconnected from all devices and sensors.

2.3 Physiological measurements

To monitor the subjects' psychophysiological condition, two sets of signals were collected. Firstly, cardiac activity, which was considered the most important indicator of psychophysiological state. Secondly, brain activity, providing supplementary information. Both signals were collected throughout the entire measurements, including stabilometry testing. For both signals, 5-minute reference recordings were collected at the beginning of each measurement, see Figs. 1 and 4.

2.3.1 Cardiac activity

Monitoring of cardiac activity is nowadays widely used for estimating the psychophysiological state of personnel. The most common technique relies on heart rate variability (HRV) analysis, which, according to standards, includes analysis in the time domain, frequency domain, geometrical analysis, and non-linear analysis. The basis for HRV analysis is a vector of a person's RR (NN) intervals. The RR intervals could be derived either from pulse rate (heart rate) or from an electrocardiogram (ECG), depending on the measurement technique.

 The RR intervals represent the time elapsed between two consecutive R-waves in an ECG curve. As they indicate the time interval between two heartbeats, they can be calculated from heart rate and vice versa. For analysis, non-standard beats, such as ectopic beats, should be filtered out of the signal, and only NN (normal-to-normal) intervals should be used. In practice, these two terms are commonly interchanged. In this work, all the RR intervals vectors are filtered, and therefore only NN intervals are used. To maintain standard terminology regarding HRV parameters, the abbreviation RR is sometimes used even though NN intervals are analyzed.

For the purpose of this project, ECG data were collected and subsequent HRV parameters were derived as described in Section 2.6.2. The ECG data were collected during both stages of the project. However, the Stage 1 data were not evaluated. The reason is that Stage 1 served to set up and test the experimental design using feedback from the instructors. Therefore, the instructors were aware of the flight profile and details of the procedure, making the data biased and unnecessary. As the experimental procedure was tested and tuned during this stage, all data were collected to test and prepare the whole procedure. Additionally, including all testing and measurement of signals during Stage 1 (see Fig. 1) significantly helped the project team to become acquainted with the entire measurement protocol and with quality time planning for Stage 2, thus avoiding unnecessary time delays.

As for the Stage 2, the ECG data were collected throughout the entire measurement period, including both the beginning and end references, each lasting 5 minutes. The reference data are necessary to limit interindividual variability among subjects. Reference measurements were collected during rest, with subjects sitting without engaging in any other activity. Additionally, ECG data were collected during stabilometry in between flights, as shown in Fig. 4. However, during this phase, subjects were moving, and therefore the collected data are affected by these movements. For these reasons, these signals were not evaluated as they do not provide valuable information.

While cardiac activity is widely used for the estimation of psychophysiological state, monitoring of brain activity was also included to provide possible deeper insight into the state of the subjects during the experimental testing.

2.3.2 Brain activity

As well as cardiac activity, also brain activity was collected in both Stages of the project. According to stated above, also brain activity results are presented only for the Stage 2. However, measurements done during the Stage 1 was also crucial for multiple reasons. Firstly, the dry-electrodes cap was firstly used. Unfortunately, during the Stage 1, the project team obtained multiple complains as for the comfortability of the cap. Also, the correct setup and connection were problematic, especially in subjects with longer hair. Moreover, it was probematic to combine this type of the cap with the headset of the simulator. Therefore, the new cap, using conductive gel, was bought and used during the experiment. This setup significantly prolonged experimental time, as the correct application of the gel is time consuming. Such a knowledge then help with setting up Stage 2 measurements.

Also during the Stage 2, there were significant issues regarding the electroencephalography (EEG) measurements. During the data collection and ongoing preprocessing, an error was identified in the collection of EEG data. Signals from some electrodes were not being recorded. Additionally, a high level of noise was identified in the acquired signals, stemming from headphone interference, likely also due to unevenly distributed pressure from the headphones (which the pilot wore during the flight). Other issues included the drying out of the gel or its leakage beyond the contact between the electrode and tissue, which in many cases resulted in cross-contamination of signals between electrodes. However, it is necessary to realize that for an experimental setup like this one, involving relatively long repeated measurements in an environment exposed to electromagnetic noise, it is not easy to measure and preprocess such signals.

The most serious issue, and therefore the apparent malfunction of the device, was attempted to be resolved by purchasing a new EEG cap. This was also done because problems with electrode saturation were occurring even during control testing. Examples of some poorly recorded signals are displayed in Figure 8.

However, the acquisition of a new cap did not resolve the issues to the extent we had expected. Therefore, it was decided to discontinue the EEG measurements, which in themselves represented a high time demand and declared discomfort by the subjects on multiple occasions. Some participants even refused the EEG during the repeated (second measurement), further degrading the usability and comparability of the data. Omitting EEG also reduced the time burden of measurements, which in some cases exceeded 3 hours (within the project, only claimable time is reported), due to the time-consuming process of fitting the EEG cap at the beginning of the measurement session, as well as its checking, adjustment, and the application of contact gel between flights.

However, this does not mean that EEG will not be reflected in the results at all. In each group of pilots, at least 10 quality recordings were obtained. The total number of recordings is 148, out of which 102 were identified as usable by the end of the year. However, this does not jeopardize the actual results of the project. The primary psychophysiological indicator remains the ECG, whose analysis can be used to estimate the state of the autonomic nervous system and the regulatory mechanisms associated with it, i.e., based on the regulation of heart rhythm by the autonomic nervous system, determine the body’s response to a specific vestibular illusion or potential loss of spatial orientation. EEG also remains as one of the evaluated physiological parameters, but it is more of an experimental nature.

In general, the measurement procedures were similar to those for cardiac activity. This means that 5-minute reference periods were obtained at the beginning and at the end of each session, while data were also collected during the executed flights, as shown in Fig- 4. Furthermore, data were collected between flights, but as with the cardiac activity, this was done simply to ensure the continuity of the measurements, although the data itself does not provide any significant information.

Collected data was further processed by a standard technique relying on the frequency analysis, which is further described in section 2.6.3.

2.4 Stabilometry and motion tracking

Vestibular illusions can lead to spatial disorientation in pilots, disrupting their perception of direction and movement. When pilots are exposed to conditions that induce these illusions, the process of sensory reweighting—where the brain adjusts the reliance on different sensory inputs for balance—can take some time. This adjustment period may contribute to the occurrence of further illusions and subsequent loss of spatial orientation. This specific issue, especially in relation to in-flight vestibular illusions, is not widely addressed in the literature. Therefore, the primary goal of related data collection and analysis is to investigate whether continuous exposure to vestibular illusions can lead to a condition known as “land sickness” or “mal de débarquement” syndrome in individuals.

Postural stability is traditionally obtained by stabilometric platform, providing 2D information regarding so called centre of pressure (COP). Experimentally, the motion tracking systems (MoCap) using inertial measurement units (IMUs) are used as they provide 3D information. However, in clinical practice, only

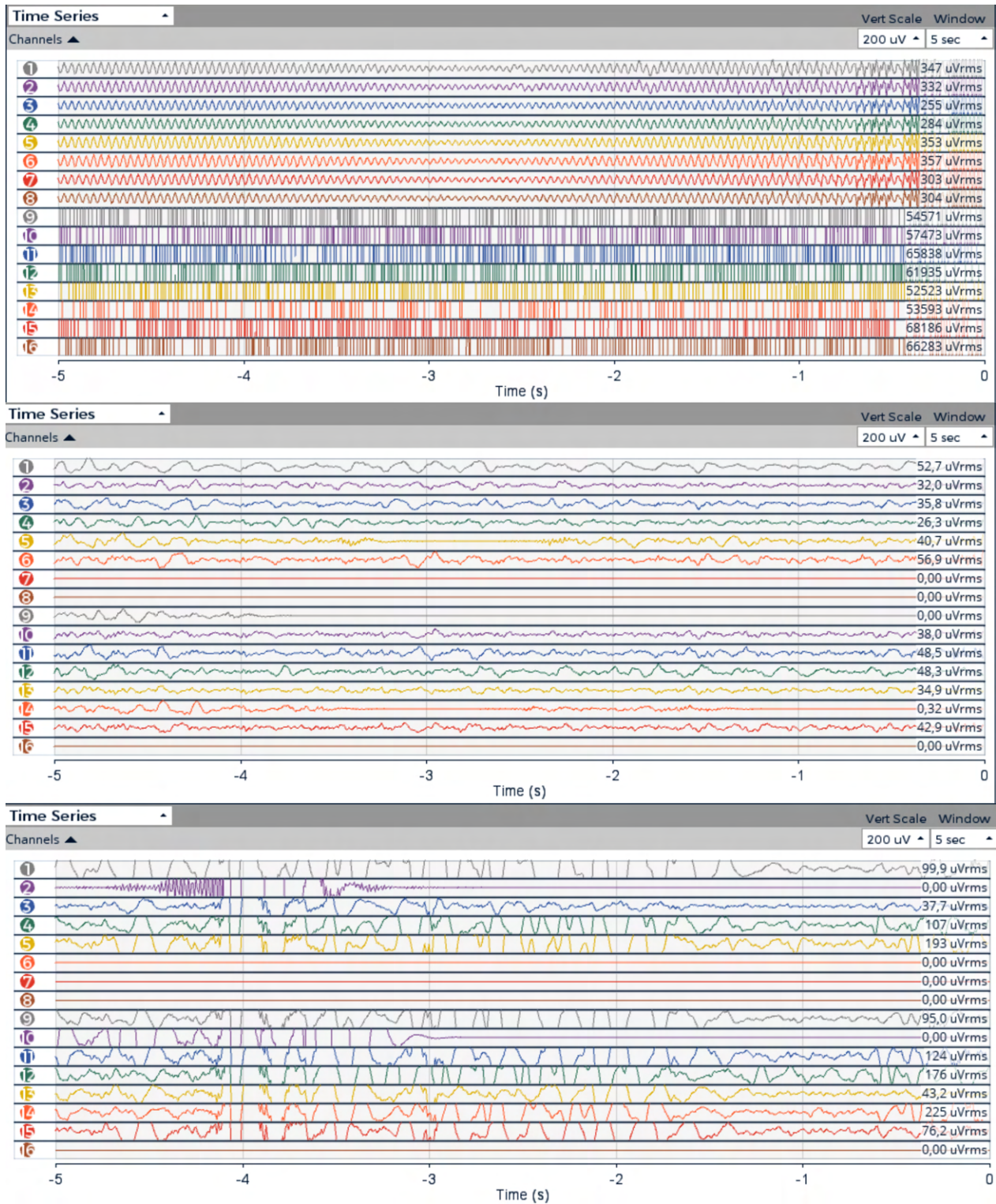


Figure 8: Example of EEG recordings with railed electrodes and noise.

platforms are used as the information provided is sufficient for stability measurements. In this project, to extend possible information obtained, also MoCap system with 7 IMUs was used. However, primary information is obtained using balance platform as this is standardized technique.

2.4.1 Postural stability

In the context of stability testing, it is common to test with changes in visual and surface conditions [2, 3]. Stability is often visually compensated for – for this reason, reducing visual stimuli (closing the subject’s eyes) is appropriate [4]. During a calm stand on a solid surface, posture correction occurs through small movements – known as postural sway [5]. These movements are controlled by the sensory and motor system – especially by mechanoreceptors in the feet [6], which provide the body with information about contact pressure on the surface [7]. To increase the sensitivity of the test, a foam pad is used, which reduces this regulation and makes stability disorders more visible [8]. The common examination consists of four measurements that combine the mentioned visual and surface conditions and is called the Romberg Test [9]. The duration of the test should, according to recommendations, be chosen to be at least 30 seconds, most often 60 seconds [10]. However, it has been proven that when measuring the COP at different test durations, chosen in the range of 30–300 seconds, the same results are reported [11].

To adhere to standard procedure, the Romberg test was also employed in this project. Consequently, each stabilometry test consisted of 4 conditions in the following order: firm surface with eyes open (FiS EO), firm surface with eyes closed (FiS EC), foam surface with eyes open (FoS EO), and foam surface with eyes closed (FoS EC). Each tested condition lasted for 33 seconds; however, the initial 3 seconds were not included in the analysis to allow the participant to adjust to the condition, ensuring a more accurate measurement. The shortest feasible duration was chosen to minimize the effect of time between the first and last condition.

Stability data were obtained during both stages of the project, and, as with the cases described previously, the Stage 1 data are not presented, as this information was deemed neither interesting nor necessary in the context of the project. In Stage 2, the data were collected three times. Initially, a reference measurement was conducted before any flight. Subsequent measurements were taken immediately after each flight, as soon as possible following the end of the simulation.

During the testing, the subject stood on a stabilometric platform with hands freely hanging, in an upright position. For the conditions with eyes open, subjects focused on a mark on the wall, which was positioned at eye level and located 2 meters from the platform. In the case of conditions with eyes closed, the subject maintained this position.

Core of the test used, assesses balance and proprioceptive function by requiring an individual to stand on firm and foam surfaces with eyes open or closed, emphasizing the reliance on vestibular and proprioceptive cues over visual ones. Information on postural stability can indicate how long it takes for the vestibular system and sensory mechanisms to return to their normal state. Transitioning from the simulator cabin to the stabilometric platform took about 2 minutes, a duration determined by the need to measure postural stability outside the simulator. This time also served as a research threshold to explore the hypothesis that after exiting a flight simulator, pilots might experience postural instability or balance difficulties due to the vestibular illusions experienced during the simulation. The human balance system depends on inputs from the vestibular, visual, and proprioceptive systems. Exposure to vestibular illusions in a simulator can trigger

a reweighting process in the brain to maintain balance. While adaptive in the simulation context, this may lead to temporary postural instability when the individual returns to a normal environment as the brain recalibrates the balance of sensory inputs.

2.4.2 Motion tracking

Following the stabilometric measurement, motion tracking was also done using MoCap system with IMUs. The motion tracking was done during stabilometry testing as well as during flights. However, the method of gyroaccelerometry is not standardized and used in clinical practice and was chosen to provide possible deeper insight into stability and movement when exposed to vestibular illusions.

For data collection, each IMU was positioned on the subject's body at predefined locations and secured with medical tape. The selected positions were both calves, both thighs, both arms, and the back in the lumbar area, see Fig. 9. Although a professional system was used for data collection, the project team experienced multiple issues with this measurement system.

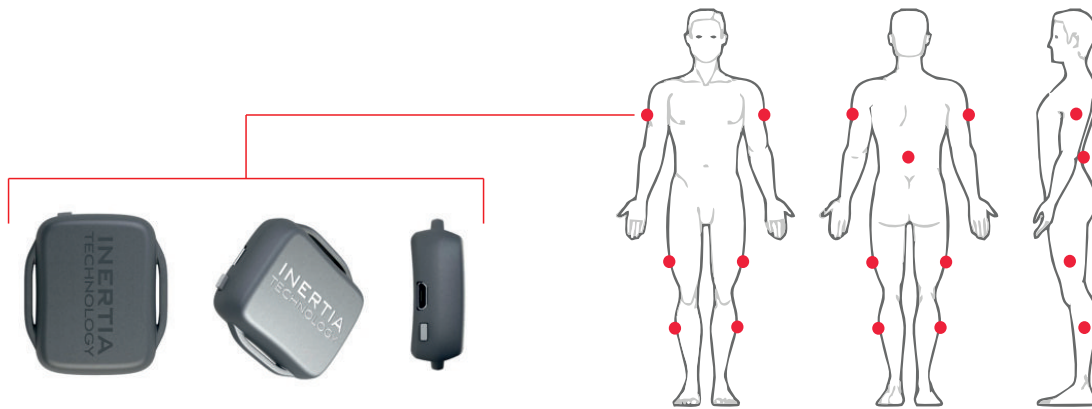


Figure 9: Illustration of the gyrosopic and accelerometric sensors used as part of the ProMove-mini MoCap system and the schematic placement of the accelerometric sensors.

The most significant problem encountered was with the connection between the IMUs and the central unit collecting data. The communication between the IMU and central unit, which is wireless, was unstable during several measurements. The project team identified this issue and attempted to resolve it with the system's manufacturer. Despite repairs made by the manufacturer, there were still obvious troubles with the connection. In some instances, the signal was lost even when the IMU and central unit were in next to each other.

As a workaround, data were saved into the internal memory of the IMUs and downloaded directly from there. However, further data processing revealed inconsistencies in signal length among the IMUs during a single collection session, with random parts of the signal missing. Despite efforts to use at least parts of the data that contained the complete signal, a significant number of poor-quality signals made the data non-representative.

Additionally, comfort issues arose with the subjects. In particular, taller subjects experienced discomfort from the lumbar IMU, leading to its removal and exclusion from testing. Also, several subjects refused to have

the IMUs fastened directly to their skin. Efforts were made to fasten the IMUs to clothing instead, as there were no other viable options for securing the IMUs without compromising the comfort of the participants. However, when IMUs were attached to clothing, they sometimes secured poorly and fell off during flights. Moreover, when subjects wore loose clothing, it was found as inappropriate to use this data as it was highly biased by the clothing's movement.

By the design of the experiment, the motion tracking data were not of high significance. While it is unfortunate that they cannot be used effectively, this situation is not crucial for the project and its goals, as standard stabilometry was performed using the platform. Despite the technical and practical challenges encountered with the supplementary motion tracking component, the integrity of the project's primary objectives remains intact, focusing on the core stabilometric measurements.

2.5 Equipment

For the purposes of the project, the spatial disorientation flight simulator GYRO IPT II was used. The simulator is shown in Fig. 10-A and it is a fully interactive and practical simulator designed to safely and affordably prepare pilots for flight illusions and spatial orientation in general. The simulator consists of a pilot cabin mounted on a sophisticated movable platform. This movable base has six degrees of freedom and is capable of accurately demonstrating aircraft movements and positions. The rotating platform located beneath the base allows continuous stable rotation independent of the cabin movement.

The cabin is designed for a single pilot only. The pilot is secured to the seat using a five-point harness system. The simulator's dashboard is configured to demonstrate the flight characteristics of multiple types of aircraft. The cabin also includes an interactive feedback control system, visualization system, instrument panel, and realistic sound effects. The view from the cabin to the outside is facilitated by a curved projection surface with a wide field of view. A generic model of the Zlín Z-142 aircraft, commonly used for training, was used in the project. The dashboard is depicted in Figure 10-B.

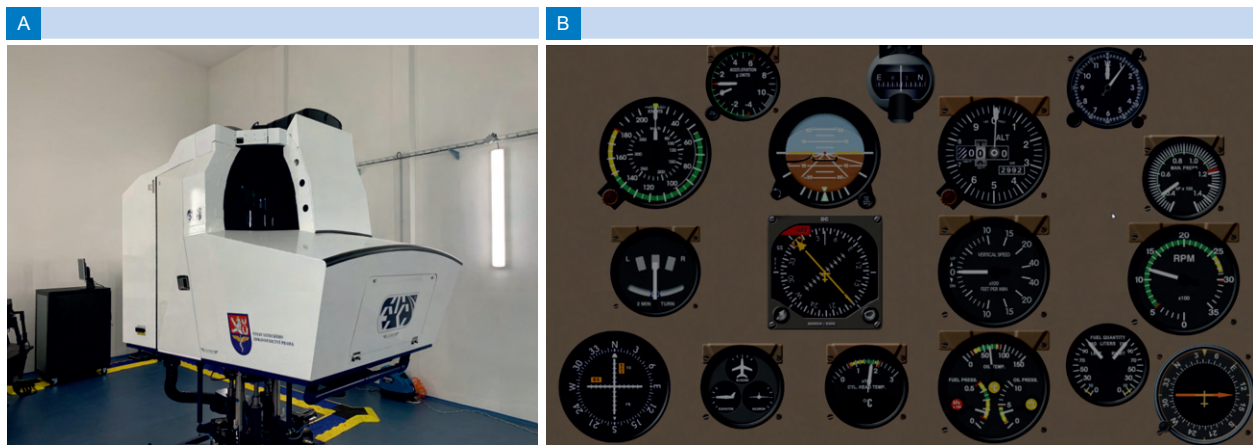


Figure 10: The Gyro IPT II simulator (A) with the dashboard of the Zlín-142 aircraft (B).

The simulator software is equipped with module for data collection. All flight data were recorded in csv format containing flight parameters as altitude, flight speed etc. Furthermore, the datasets contain all data

regarding simulator cabin position, velocity etc. as well as information regarding stick movements. Datasets contain time vector, starting at 0 s. The data collection starts when the subject presses a button for the start of the simulation. Real time is provided in the name of each file, corresponding to the 0 s. The data were collected with a sampling frequency of 125 Hz.

Furthermore, the cabin is equipped with CCTV cameras providing insight into the cabin during the flight. The CCTV system offers four channels: a map displaying the cabin's position, simulated scenery, an overhead view of the simulation, and a frontal view of the pilot. Surveillance videos were collected for all flights in the form of video files (in the .mkv format).

The cardiac activity data in the form of ECG, or the amplitude values of electrical voltage over time, were then obtained using the VLV Lab system developed at the Joint Department of FBME CTU and the First Faculty of Medicine, Charles University in Prague, which is primarily designed for experiments requiring continuous and accurate recording of biological and technical signals. In its basic configuration, the device includes, among other signals, ECG as well. For the purposes of the project, a single-lead ECG was utilized, along with disposable silver chloride electrodes placed in the chest area.

The system generates .txt files containing a time vector in Unix time, raw and filtered signals, and markers. For further analysis, raw ECG data were used. Unix time was also taken from the datasets for further synchronization with other signals, especially EEG. As the device can measure multiple signals, temperature and acceleration data were collected and employed during the synchronization between ECG data and flight data, as described in section 2.6.2. The data were collected at a sampling frequency of 1 000 Hz.

The EEG data were collected using a system developed by OpenBCI. Specifically, this involved a 16-channel EEG system - the Cyton and Daisy measuring boards (OpenBCI, Brooklyn, NY, USA) and the Ultracortex Mark IV helmet (OpenBCI, Brooklyn, NY, USA), employing the international 10-20 system for electrode placement. As mentioned, this helmet was found to be uncomfortable for users and impractical for experiment setup, leading to its replacement in Stage 1 with the OpenBCI EEG Electrode Cap, a standard textile EEG cap that uses conductive gel. The cap also includes 16 electrodes arranged according to the 10-20 system.

Data were recorded at the highest possible sampling frequency - 125 Hz. The system then generates .csv files containing timestamps in both datetime format and Unix time, as well as raw data from all 16 leads. This data was then examined (see section 2.6.3), while the time vectors were used in synchronizing with ECG.

For the stabilometric measurements, an affordable solution in the form of a commercial balance board was used. Although primarily used for rehabilitation medicine in medical applications, this platform has recently been evaluated for static posturography [12, 13], and its reliability for stabilometry has been confirmed [14]. Therefore, the Nintendo Wii Balance Board (Nintendo Co., Ltd., Kyoto, Japan) was chosen for data collection. The balance board provides stabilometric data as .txt files, with a sampling frequency of 100 Hz.

Lastly, the motion data were obtained using seven IMUs connected to a central unit via USB to a computer. These were ProMove-mini sensors with the Basic Inertia Gateway central unit (Inertia Technology B.V., Enschede, NL). The data are recorded at a sampling frequency of 200 Hz.

2.6 Data processing

2.6.1 Flight data

The flight data collection was conducted for each flight profile and setup (with and without illusions). Therefore, four flight records were created for each subject. The flight data encompassed comprehensive information on flight parameters such as altitude and various types of speed, aircraft pitch angles, geographic coordinates, performance and navigation characteristics, etc., as well as simulator cabin motion data including inclinations around individual axes, angular velocities, and rotational accelerations, among others. In total, the flight data comprised 158 features sampled at a frequency of 125 Hz.

The preparation of data for the final evaluation primarily consisted of defining flight segments corresponding to the segment where an illusion would be / was actually induced.

The dataset was initially imported into a structured format, where key variables such as time, longitude, latitude, heading, bank angle, and altitude were meticulously extracted.

The segmentation of the data ensued, orchestrated around predefined conditions that encapsulated various flight profiles and maneuvers. These conditions, articulated through mathematical inequalities, aimed at pinpointing specific altitudes, headings, and geographic positions relative to landmarks, notably VOR stations. The conditions were akin to setting thresholds, i.e.

$$Condition_i = Variable \geq Threshold_i, \quad (1)$$

guiding the segmentation to isolate segments indicative of distinct flight phases or maneuvers. These conditions were known based on specifically stated conditions for the given profiles, which are listed in the appendices of this report.

Detecting specific flight maneuvers and conditions was meticulously executed by identifying segments where the flight data satisfied predefined conditions subsequent to certain events or time markers. This involved a mathematical formulation to ascertain the indices of data points meeting these conditions, expressed as

$$Index_j = \min\{k > StartIndex | Condition_j \text{ is true for data point } k\} \quad (2)$$

where $Index_j$ denotes the index of the first data point fulfilling the j -th condition post a specified start index.

Geographic positioning and navigation formed a cornerstone of the analysis, especially in evaluating adherence to the designated flight path. The methodology employed mathematical constructs to delineate circular regions around navigational aids and assess the flight path's intersection with these regions. This was accomplished by calculating the aircraft's relative position and utilizing geometric principles to determine compliance with navigational requirements.

This principal processing was carried out on all data to obtain indexes corresponding to individual flight segments. This was particularly important for flights without illusions, where it was necessary to approximate these segments for the purposes of conducting further analysis. Examples of such identified indexes are shown in Fig. 11.

In flights with illusions, the segments during which an illusion was induced were identified directly from information about cabin accelerations and velocities in respective axes (see Fig.5-7). The demarcation of these

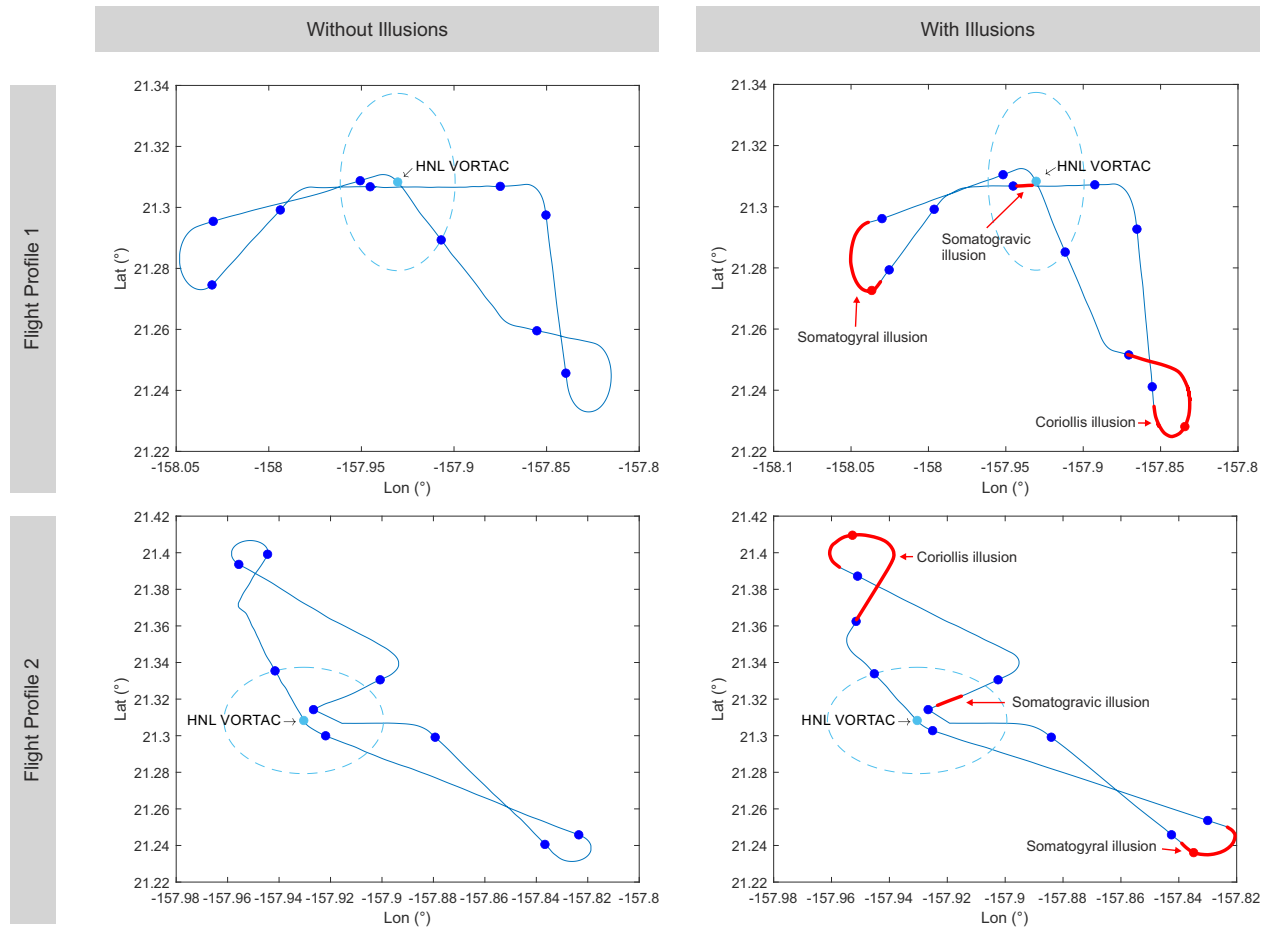


Figure 11: Flight profiles with identified points where the pilot received a specific instruction and marking of the exact segments in which a flight illusion was induced. Red points in the flight segments with induced illusion represent a command to turn the head (coriolis illusion) or to report flight speed (somatogyral illusion).

illusions was determined by examining variations in the specified metrics, marking the onset and cessation of illusion periods. This nuanced approach allowed for a detailed exploration of the periods within the flight data where perceptual distortions were likely to have impacted pilot actions or aircraft behavior.

For creating the dataset for further processing, individual segments corresponding to flight segments where a specific illusion was induced were extracted and then adjusted to a uniform length. To adjust to a uniform length, characteristic points in the individual segments corresponding to a specific illusion were identified. Specifically, this involved identifying the point $ISgr$, which was defined as the first point where Pitch $\geq 5^\circ$ in the flight segment corresponding to the somatogravic illusion (respectively, takeoff). Within the segment corresponding to the Coriolis illusion (first turn), the point ICo was identified, corresponding to the command to turn the head. Finally, in the case of the flight segment characteristic of the somatogyral illusion, the point $ISgy$ was identified, corresponding to the time when the instruction "report airspeed" was given.

Based on this, it was possible to systematically extract time series of a fixed length from the recorded flights. This extraction process ensured uniformity across all datasets, with each time series representing the period during which the respective illusion was in effect.

By focusing on specifically defined segments, the dataset encapsulates controlled scenarios where the impact of various flight illusions, including the somatogravic, Coriolis, and somatogyral illusions, on pilots' control abilities can be precisely analyzed. This methodological approach facilitates the creation of a dataset that is not only highly relevant to the project's objectives but also standardized across different simulation runs. This standardization provides a solid foundation for subsequent steps such as normalization, Dynamic Time Warping (DTW) analysis, and classification efforts, thereby enhancing the overall evaluation of the respective illusions.

In the preprocessing stage, particularly for altitude, bank angle, stick pitch and roll angle data collected from pilots during flight sequences simulated in a flight simulator, the primary objective was normalization. This step aimed to enable fair comparisons across different pilots and conditions by mitigating variations in absolute values. To enhance the dataset's accuracy, entries with missing values, which signified completely absent measurements for certain sequences, were excluded from further analysis.

For the measurements normalization, we utilized L2 normalization. This method scales the data such that the sum of the squares of the values in each time series is equal to 1. Consequently, this approach ensures that the analysis emphasizes the relative changes in respective parameters, rather than the absolute values, thus allowing for direct comparison of data from different pilots under varying conditions.

The process of L2 normalization is mathematically described as follows:

$$x_{\text{norm}} = \frac{x}{\|x\|_2} \quad (3)$$

where x represents an individual altitude time series, and $\|x\|_2$, the L2 norm of the time series, is computed as the square root of the sum of the squared values:

$$\|x\|_2 = \sqrt{\sum_{i=1}^n x_i^2} \quad (4)$$

This procedure ensures that each time series is normalized to a unit norm, which is crucial for conducting an unbiased comparison across all measured sequences corresponding to respective illusions.

Following the normalization phase, Dynamic Time Warping (DTW) was applied to evaluate the similarity among the flight sequences of different pilots. DTW is particularly suited for analyzing temporal sequences that may exhibit variations in timing or speed, thereby offering a nuanced perspective on the differences in pilots' control behaviors under the influence of flight illusions.

The application of DTW resulted in the generation of a comprehensive distance matrix, encapsulating the pairwise DTW distances between the time series of each pilot. This matrix serves as a critical component for subsequent classification and analysis, enabling us to identify patterns and clusters among pilots based on their control responses.

To compute the DTW distances, the following formula was used:

$$D_{\text{DTW}}(A, B) = \min \left(\sqrt{\sum_{i=1}^n \sum_{j=1}^m (a_i - b_j)^2} \right) \quad (5)$$

where A and B represent two different time series of specific parameter, a_i and b_j are the parameter measurements at time points i and j within each series, respectively, and n and m are the lengths of the two time series. The DTW algorithm optimally aligns these time series to minimize the cumulative distance between them, thus reflecting the true similarity in their patterns.

Following the computation of Dynamic Time Warping (DTW) distances, we proceeded to employ hierarchical clustering using the Ward’s method on the resultant distance matrix. Hierarchical clustering is a statistical technique used to group objects into clusters based on their similarities, where each object can be a data point or a group of data points. The Ward’s method, in particular, is a criterion applied within the hierarchical clustering framework that seeks to minimize the variance within each cluster. This method is especially effective for identifying distinct patterns and natural groupings in complex datasets.

The process begins with each altitude time series being considered as a separate cluster. At each step of the algorithm, the pair of clusters that leads to the minimum increase in total within-cluster variance after merging is combined. This incremental approach to merging clusters continues iteratively, reducing the number of clusters at each step until all the data points form a single cluster or until a specified number of clusters is reached. The increase in total within-cluster variance, which Ward’s method aims to minimize, is calculated using the squared Euclidean distance between the clusters.

Mathematically, the criterion for choosing the pair of clusters to merge at each step can be expressed as follows:

$$\Delta(\text{Ward}) = \sum_{i=1}^n \sum_{j=1}^m (a_i - b_j)^2 \quad (6)$$

where a_i and b_j represent the elements of the two clusters being considered for merging, and n and m are the sizes of the two clusters, respectively. The objective is to find the pair of clusters that, when merged, results in the smallest possible increase in ΔWard , thereby ensuring the homogeneity of the clusters.

The hierarchical nature of the clustering allows for the construction of a dendrogram, a tree-like diagram that visualizes the sequences of merges or splits. The dendrogram provides a comprehensive overview of the clustering process and the hierarchical relationships between the clusters. It serves as a valuable tool for analyzing the clustering results, facilitating the identification of the optimal number of clusters by examining the heights of the merges.

Applying hierarchical clustering with Ward’s method to the DTW distance matrix enables us to discern the underlying structure in the pilots’ altitude control behaviors during flight sequences affected by flight illusions. By grouping the time series into clusters based on their DTW distances, we can identify patterns of similarity and difference among the pilots’ responses to the illusions, offering insights into the various strategies employed to counteract the effects of somatogravic, Coriolis, and somatogyral illusions. This approach enhances our understanding of pilot behavior in simulated flight scenarios.

In addition to hierarchical clustering, Principal Component Analysis (PCA) was utilized to determine whether the observed flight parameter forms characteristic clusters that could correspond to profiles with and without illusions, or possibly distinguish between pilots’ groups. PCA is a statistical technique used to reduce the dimensionality of a dataset while retaining as much variability as possible. This is achieved by

transforming the original variables into a new set of variables, the principal components (PCs), which are orthogonal to each other and capture the maximum variance in the data.

PCA serves as a complementary analysis to hierarchical clustering, providing a broader understanding of the data’s structure. It aids in identifying key variables that contribute to the differences between flights with and without illusions and between different pilots’ groups, thereby enhancing the overall analysis of flight behavior under varied conditions.

2.6.2 Cardiac activity

Fistly, corresponding data for each subject, profile and setup were identified based on time measurement (saved in one table) and time time information included in all of the files. For that reason cell arrays containing all of the separate files for each data types were created, e.g. EEGFullFiles containing information about all EEG files, ECGFullFiles containing information about all ECG files etc. Also, EnterMatrix table was created, containing the indexes of files corresponding to specific measurements. The structure of EnterMatrix is depicted in Table 2. The Phase column contains 5 levels, where 1 is measurement prior flights, 2 is first flight (without illusions), 3 is measurement between flights, 4 is second flight (with illusions) and 5 is measurement after both flights. This means, that if EnterMatrix contains index 96 for specific subject, profile and phase in ECG column, corresponding dataset is in row 96 in ECGFullFiles cell array.

Table 2: The structure of the EnterMatrix – table containing indexes of separate files corresponding to specific measurements.

Subject	Profile	Phase	Flight	ECG	EEG	FiS EO	FiS EC	FoS EO	FoS EC
1	1	1	NaN						
1	1	2							
1	1	3	NaN						
1	1	4							
1	1	5	NaN						
1	2	1	NaN						
⋮	⋮	⋮							
1	2	5	NaN						
2	1	1	NaN						
⋮	⋮	⋮							
2	2	5	NaN						
⋮	⋮	⋮							
114	2	5	NaN						

Note: Only phase 2 and 4 corresponds to the flight. Therefore, for phases 1,3 and 5, the flight data were unavailable and thus NaN (not a number) value is placed into table

The cardiac activity data collection was conducted for each flight profile and setup (with and without illusions). Furthermore, the reference measurement were collected before and after each session. Therefore, 8 records were obtained for each subject. Data preprocessing primarily includes the time synchronization of data files, filtering of biosignals in terms of noise suppression, and the extraction of NN (normal-to-normal) intervals from ECG records for the purposes of further analysis.

The evaluation of the ECG was done in the time intervals corresponding to the part of flight in which specific illusion was induced and in respective parts of flight during the flight without illusion. For that, time stamps were obtained from evaluated flight data marking beginning and ending of each illusion (or the corresponding flight part in flight without the illusions). However, to use them, time synchronization between 2 types of data had to be done, as both were collected on different computers. Unfortunately, the flight data did not contain a vector with real time. However, the start of the measurement in datetime format was included in the filename. Nevertheless, the computer at the simulator control station and the computer used to collect the other data had different system times. Additionally, due to the transitions between winter and summer time, as well as multiple maintenance instances, there was no stable time shift between these two devices.

Two approaches of data measurement were used. The first approach involved measuring the initial 72 subjects in such a way that each of the 8 collected signals was recorded separately, necessitating time synchronization for each dataset corresponding to the flight. In the second approach (subjects 73–114), the continuous measurement of ECG and EEG signals were done through whole session and thus only one synchronization was needed. This approach was chosen to facilitate the time synchronization of data as which emerged from processing of the data. For that reason, software was then developed that allows the measurement operators to enter time stamps throughout the entire implemented measurement, see figure 12. This provided easier data selection with respect to the activities being conducted, such as posturographic measurement, or estimating the time segment of the flight. Thus, the development of the software made data navigation more efficient and also improved the orientation of the staff during the measurement.

For safety reasons, measurements had to be conducted in a closed simulator, leading to the initiation of other data recording before the simulation itself. Therefore, some form of marker had to be introduced into the collected data to synchronize all the signals, in both approaches. A time stamp was inserted into the data in the form of a unique artifact in the record of electrical heart activity (by pressing a measuring electrode). For the purpose of recording ECG, a polysomnograph was used, among other things, containing also a small accelerometer with an integrated temperature sensor. This was further used to create a backup marker, in the form of an artifact in this sensor (which is otherwise unused throughout the measurement) – an increase in temperature (the subject holds the sensor in their palm, leading to a sharp increase in temperature from a stable room level), where the beginning of the increase corresponds to the marker, see Fig. 13.

The marker had to be identified in separate datasets, one by one. As the team had an overview of all time transitions throughout the years of the project’s realization, episodes with the same time shifts between the two devices were identified. Therefore, the time shifts for the signals were calculated and then compared with other time shifts in the same episode. Since the maximum differences in these episodes were in the order of seconds, all time shifts for each episode were averaged and applied to datasets corresponding to that episode. This method was chosen to minimize errors regarding marker placement. Although subjects

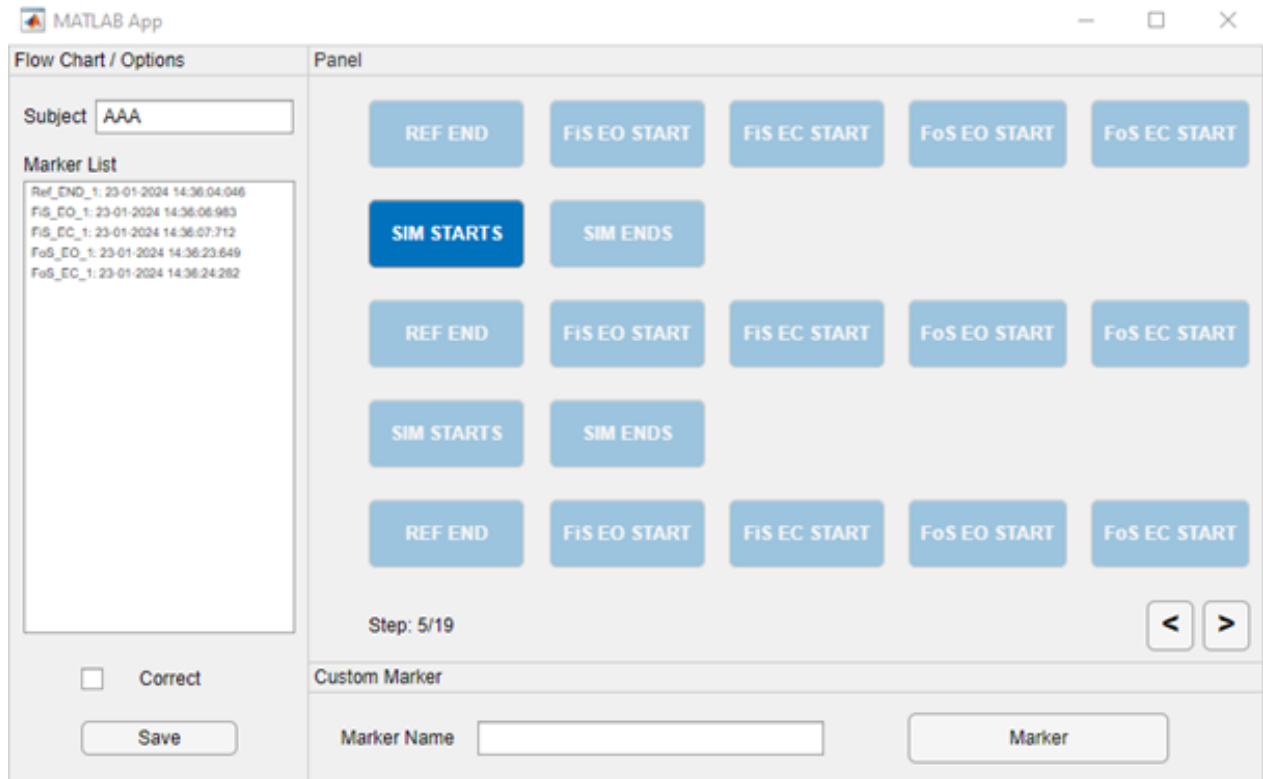


Figure 12: Software využitý při měření.

were instructed to start the simulation (i.e., the starting time is marked in the name of Flight data) and insert the marker simultaneously, the coordination of some subjects was not precise. Additionally, holding the electrode and temperature sensor was done for a brief period (a few seconds), leading to these minor time shift differences. Averaging all time shifts for the entire episode helped to limit this error. Moreover, evaluated data were always at least 3-minutes long (as further discussed), making the error regarding marker coordination minimal and insignificant. Furthermore, in case, the marker was not visible, averaged time shift between times on both computes for corresponding episode could be used.

During the first approach of data collection, markers had to be found in each dataset corresponding to Flight data. In the case of reference measurements, it is not necessary, as these are conducted independently of each other. When taking into account the second measurement approach including markers via custom app and session-long datasets, Only one marker had to be used as time was resynchronizes for whole dataset. On the other hand, to ensure the precision of time synchronisation, both markers were always found so the averaged time shifts were even more precise.

After the identification of the time shifts for each dataset, timestamps in ECG datasets were corrected by this shift. After that, it could be directly compared with flight data using markers of evaluated sections of the flights. However, when those sections were identified, also original ECG Unix times markers of those sections were saved to be further used in EEG data. Using Unix time brought small challenge in periods

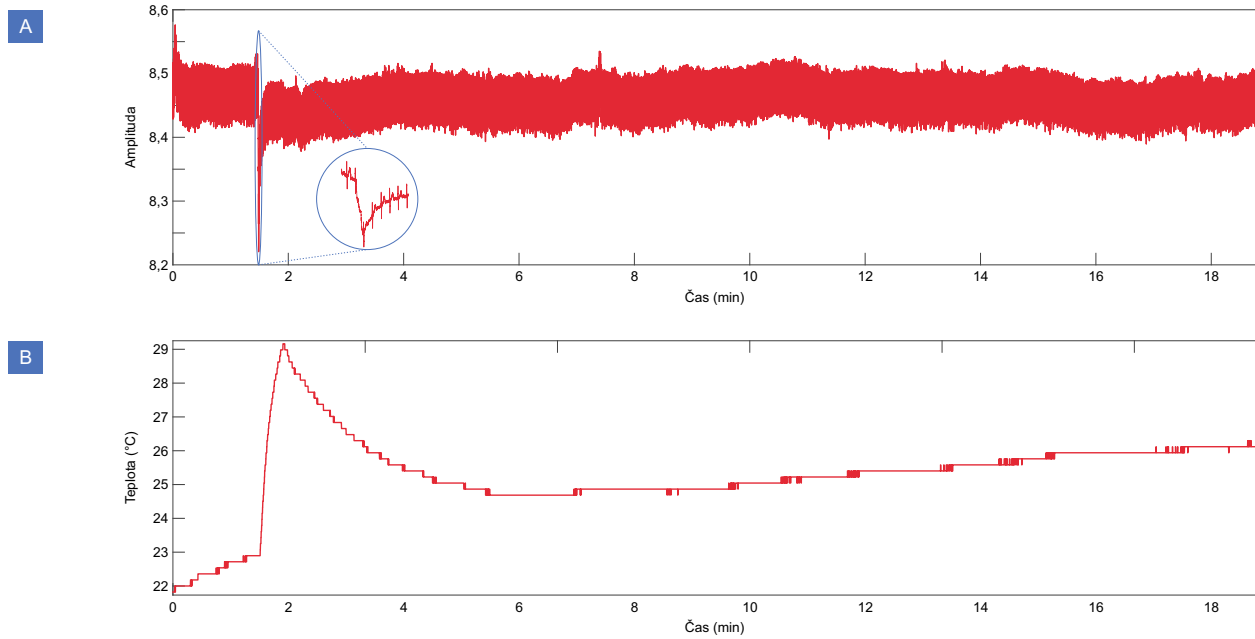


Figure 13: Creating a marker in physiological data. A) The record of electrical heart activity with an emphasized detail of the artifact. B) The temperature record with a synchronous artifact.

of transitions between winter and summer time in Czech Republic. Those transitions were identified and further corrected.

The primary synchronization and data cutting into specific segments for further evaluation had to be done twice, firstly for the first approach with separate data collection, secondly for the second approach with continuous measurement. After time synchronization and data cutting, further preprocessing and processing of data was done.

Preprocessing then also includes the mentioned filtering, primarily aimed at removing electrical noise (notch filter type) and, for example, motion artifacts through several filters. Also, detection of NN intervals was done during this phase of data processing.

Several approaches exist for this detection, primarily based on filtering. One of the most well-known techniques is the Pan-Tompkins method, which relies on filtering techniques. The first step is a band-pass filter (5–15 Hz) that emphasizes the QRS complex and suppresses noise or baseline drift. The filter is typically implemented as two filters—a low-pass and a high-pass. The next step involves using a five-point derivative filter with a defined transfer function and subsequently squaring the signal (second power is used) to emphasize R-waves. The final step is integration in a moving window. These steps are aimed at noise suppression, emphasizing QRS complexes or R-waves, and obtaining characteristics of these waves, such as slope.

Subsequently, a set of decision criteria is implemented for the correct detection of individual R-waves. The first step is the detection of primary peaks, i.e., areas where the signal shifts from rising to falling. It is also defined that another peak cannot be detected in less than 200 ms, corresponding to the refractory phase. Another decision rule is thresholding, based on the signal's characteristics and defining the minimum

amplitude of the peak with respect to the given signal. After each detected R-peak, the threshold value is adjusted. The algorithm also retrospectively checks the processed signal for potential detection of undetected R-waves based on the average of 8 selected RR intervals. The final step of the algorithm is to protect against unintended detection of T-waves, based on the slope of the detected peak and the peak preceding it if the peak is detected within 360 ms from the previous one. Details of the described algorithm can be found in the literature. The output of the algorithm is the localization of individual R-waves, from which RR intervals are subsequently calculated. From a practical standpoint, the signal thus obtained is often further processed into what are known as NN intervals.

From the perspective of detecting RR intervals, the obtained signal is often adjusted for atypical values, such as ectopic (sudden) heartbeats. After eliminating such beats or intervals from the records, the remaining intervals are often referred to as NN (normal-normal) intervals. It is standard practice for the subsequent analysis to be based on NN intervals; therefore, ectopic beats are routinely detected and removed from the records. There are several methods for detecting ectopic beats, with the analytical software implementing a method based on filtering through a median filter defined as:

$$D(n) = \frac{|x(n) - \text{med}(x)|}{1.483 \cdot \text{med}\{|x(n) - \text{med}(x)|\}}, \quad (7)$$

where x is the filtered signal, $n = 1, \dots, N$, and N is the length of the signal. If a value τ is defined, then

$$D(n) \geq \tau \quad (8)$$

indicates an ectopic heartbeat. The recommended threshold value is $\tau = 4$. Waves detected as ectopic are replaced using the median method in a centered window of a defined number of neighboring values, according to the equation

$$x'(n) = \text{med}\{x(n+m) : |m| \leq \frac{w_m - 1}{2}\}, \quad (9)$$

where x' is the series of NN intervals, w_m is the number of neighbors ($m = 1 \cdot w_m$), excluding neighbors identified as ectopic. The number of neighbors is chosen to be $w_m = 5$.

This adjustment yields NN intervals. However, in common practice, RR and NN intervals are used interchangeably, and practically no distinction is made between NN and RR intervals. From the obtained RR intervals, it is further possible to calculate the heart rate (HR), where a heart rate of 60 bpm (beats per minute) corresponds to an RR interval of 1000 ms. These signals are then further analyzed using a battery of methods—analysis in the time domain, frequency domain, time-frequency domain, and through nonlinear analysis.

2.6.2.1 Time domain analysis

From the perspective of standard analysis, the first method is time domain analysis. Time domain analysis mainly includes parameters based on descriptive statistics. These primarily encompass standard deviations, averages, and extremes (or ranges of values) of the observed signal, i.e., the series of RR (or NN intervals) and heart rate. Beyond basic statistics, heart rate variability is also described through additional parameters, such as the frequency of intervals that are a certain distance apart or parameters obtained through geometric

analysis. In terms of the length of records, three types of variability are defined: 24-hour HRV, short-term variability (ST—short-term, records shorter than 24 hours but longer than 5 minutes), and ultra-short-term heart rate variability (UST—ultra short-term, records shorter than 5 minutes). Considering the settings of the own experiment, or the length of the evaluated segments, this study is oriented towards UST, and in this context, the calculated parameters were also chosen. The output of own analytical system is 8 parameters, see Table 3. The input data necessary for analysis is the vector of NN intervals and the value x for calculating pNN x (in milliseconds).

Table 3: Time domain analysis parameters used in this project.

Parameter	Description
meanNN	Average length of NN (RR) intervals.
SDNN	Standard deviation of NN (RR) intervals.
RMSSD	Root mean square of successive RR (NN) interval differences.
meanHR	Average heart rate.
SDHR	Standard deviation of heart rate.
minHR	Minimum heart rate
maxHR	Maximum heart rate
pNN x *	Percentage of NN x , where NN x is a number of successive NN (RR) intervals differing by more than x .

*50 ms is typically chosen as the time.

Frequency domain analysis

The time domain analysis is the supplement by the frequency domain analysis. Standard frequency analysis primarily relies on Fourier transform. However, most Fourier approaches require equidistantly sampled data, which is not the case for RR (NN) interval series, as each interval has a different duration and thus, the time gap between two samples varies. In practice, two approaches are used to address this issue. The first approach depends on data interpolation, i.e., resampling the data to ensure equidistant sampling. The second approach employs methods developed for non-uniformly sampled data, typically the Lomb-Scargle periodogram, which belongs to the Fourier methods and is based on the Fourier transform but also integrates other methods, such as the least squares method, and can be derived from Bayesian probability theory. For these reasons, the Lomb-Scargle periodogram represents the main tool in the frequency analysis of non-equidistantly sampled signals.

The periodogram is a statistical tool used to identify significant periodic components, or significant frequencies in the analyzed series, thus it can provide information about the periodic components of time series. This method allows observation of the spectrum and is primarily used to calculate the estimate of spectral power components. The principle of this method is to transform individual elements of the time series into forms where the trigonometric functions sine and cosine appear.

The Lomb-Scargle periodogram, or least squares spectral analysis, provides a way to estimate the frequency spectrum and was developed for the mentioned adjustment of irregularly sampled data. The Lomb-Scargle periodogram is one of the methods for estimating the so-called Power Spectral Density (PSD) in an irregularly sampled signal, such as the time series of instantaneous heart rate (or RR/NN intervals), which is naturally distributed into irregular intervals.

In the calculation, x_j is the time series of data measured at times t_j , where $j = 1 \dots N$ and N is the number of data points. The average value is denoted as \bar{x} and the variance as σ^2 . The Lomb normalized periodogram $P(T)$ for the period T indicates the probable periodicity and is defined as:

$$P(T) = \frac{1}{\sigma^2} \left\{ \frac{\left[\sum_{j=1}^N (x_j - \bar{x}) \cos \frac{2\pi(t_j - \tau)}{T} \right]^2}{\sum_{j=1}^N \cos^2 \frac{2\pi(t_j - \tau)}{T}} + \frac{\left[\sum_{j=1}^N (x_j - \bar{x}) \sin \frac{2\pi(t_j - \tau)}{T} \right]^2}{\sum_{j=1}^N \sin^2 \frac{2\pi(t_j - \tau)}{T}} \right\}, \quad (10)$$

where the constant τ is implicitly defined by the formula:

$$\tan \frac{4\pi\tau}{T} = \frac{\sum_{j=1}^N \sin \left(\frac{4\pi t_j}{T} \right)}{\sum_{j=1}^N \cos \left(\frac{4\pi t_j}{T} \right)}. \quad (11)$$

For the null hypothesis, it is assumed that the values x_j are independent Gaussian random noise and $P(T)$ has an exponential probability distribution with UNIT MEAN. The significance level (p-value) of any peak is given by the relation:

$$p \equiv 1 - (1 - e^{-P(T)})^M, \quad (12)$$

where $M \approx N$.

With regard to the heart activity analysis, whether as a diagnostic tool or for instance, for psychophysiological state estimation, there are mentioned standards for the evaluation/interpretation of heart activity records. Specifically, the analysis of RR intervals in the frequency domain is accepted as a relatively high-quality tool for estimating the state of the ANS (Autonomic Nervous System). In this context, 4 frequency bands are defined (of which 2 are most commonly used), within which power is observed. The low-frequency band (LF, 0.04–0.15 Hz) and the high-frequency band (HF, 0.15–0.4 Hz) are considered most interesting. It is generally accepted that an increase in power in the LF band reflects higher sympathetic activity, and the HF band higher parasympathetic activity. The LF/HF ratio is then viewed as key, where an increase in this ratio indicates higher sympathetic engagement, thus higher stress/load.

By performing frequency analysis using own software tool with implement described methods, both absolute and normalized power in the individual spectral bands are obtained. For the purposes of the project, a total of 6 parameters are acquired as described in Table 4. Note that excluding ULF and VLF band was needed regarding the signal length.

Non-linear methods

From the perspective of nonlinear methods, the Poincaré plot, and sample entropy methods were selected based on the standards of HRV analysis and the signal length. Nonlinear methods primarily originate from

Table 4: Frequency analysis parameters available used in the project.

Parameter	Description
LF	Power in the low frequency band (0.04–0.15 Hz).
HF	Power in the high frequency band (0.15–0.4 Hz).
LF/HF	Ratio of powers in the low and high frequency bands.
Total	Total power of the frequency spectrum.
nLF	Normalized power in the low frequency band (0.04–0.15 Hz) relative to the total spectrum power
nHF	Normalized power in the high frequency band (0.15–0.4 Hz) relative to the total spectrum power

chaos theory and provide additional insights compared to traditional methods in the time/frequency domain. Their use in the case of biological signals seems particularly appropriate, given the nature of these signals. Biological signals are nonlinear, nonstationary, dynamic, and complex [15], and thus the use of nonlinear methods presupposes a new perspective on the data.

The first method is the Poincaré plot (or return map) method. One of the advantages of using the Poincaré plot is its high resilience to extreme values and artifacts in the signal. The method can be used for evaluating both short-term and long-term records, and although in terms of quantification it involves relatively simple statistical techniques, it has been proven that nonlinear characteristics of the signal are also reflected within the quantification parameters [16].

The Poincaré plot itself is a graphical method based on plotting a data vector against its time-delayed copy. Thus, two vectors are defined:

$$RRi_n = (x_1, x_2, \dots, x_{N-1}), \quad (13)$$

$$RRi_{n+1} = (x_2, x_3, \dots, x_N). \quad (14)$$

For an easier understanding and quantification of the Poincaré plot, an ellipse is drawn in the graph, whose major axis is in the direction of the line of identity ($x=y$), whose center is placed at the point given by

$$SD1 = \sqrt{Var(x_1)}, \quad (15)$$

$$SD2 = \sqrt{Var(x_2)}, \quad (16)$$

where $Var(x)$ is the variance of x and x_1, x_2 are defined as [17]:

$$x1 = \frac{RRi_n - RRi_{n+1}}{\sqrt{2}}, \quad (17)$$

$$x_2 = \frac{RRi_n + RRi_{n+1}}{\sqrt{2}}, \quad (18)$$

respectively, as a rotation of RRi_n and RRi_{n+1} by $\pi/4$, i.e.,

$$\begin{bmatrix} x_1 \\ x_2 \end{bmatrix} = \begin{bmatrix} \cos(\frac{\pi}{4}) & -\sin(\frac{\pi}{4}) \\ \sin(\frac{\pi}{4}) & \cos(\frac{\pi}{4}) \end{bmatrix} \begin{bmatrix} RRi_n \\ RRi_{n+1} \end{bmatrix} \quad (19)$$

Traditionally calculated parameters include the sizes of the axes, i.e., SD1 and SD2, their ratio (SD1/SD2), and the ellipse area [17], which are also outputs of the analytical software. SD1 defines the width of the ellipse, reflecting short-term changes and is identical to RMSSD. SD2 defines the length of the ellipse, reflecting long-term changes and correlates with power in LF. The SD1/SD2 ratio then correlates with LF/HF and reflects autonomic balance, where an increasing ratio indicates greater sympathetic engagement [18].

The second type of nonlinear analysis used is sample entropy. It is a quantifier of signal complexity. Sample entropy represents an algorithm for estimating entropy based on probability and was specifically developed for HRV analysis as an improvement over approximate entropy, addressing some of its limitations. It is defined as the negative logarithm of the conditional probability that two randomly chosen sequences of length m will remain similar at $m + 1$ points, based on a defined distance criterion, with sequences considered similar if their distance is less than r , both at m and $m + 1$ points. Self-matches are not included in the probability calculation. If the resulting sample entropy is equal to zero, the subsequent segments are identical. Conversely, an increasing entropy value indicates higher signal complexity [19]. The input for the analysis is the series of NN intervals, the dimension m , and the distance r , with the recommended values for HRV analysis being $m = 2$ and $r = 0.2 \times SD$ (SD – standard deviation). The output is the value of sample entropy (sampEN).

Using the approach described, total of 8 time-domain HRV parameters, 6 frequency domain HRV parameter, and 5 non-linear HRV pparameters are obtained for each evaluated data segment. This means, that for each evaluated flight, total of 3×19 parameters is obtained as each flights consist of 3 evaluated periods. Those were further statistically analyzed.

2.6.3 Brain activity

Considering the fact that the records from both ECG and EEG contain real-time data (in the form of Unix or standard local time) and acknowledging that these data were measured through a single PC, all signals are subsequently time-synchronized as part of the data preprocessing, with the synchronization based on that of the ECG. Hence, the time indices marking the start and end of each evaluated period (illusion) with the original ECG Unix time were utilized to segment the EEG data.

Following this process, each of the signals was further preprocessed by filtering. The most significant artifact is interference from the electrical network; for these reasons, a band-pass filter of 0.5–40 Hz is used. Subsequently, the signal is transformed into the frequency domain via Fast Fourier Transform, and the area under the curve in specified frequency bands is calculated.

As the EEG signal itself is considerably complex, containing a multitude of waves and artifacts, some types of waves are defined forming these specific frequency bands. This means that there exist basic so-called

EEG rhythms. There are four fundamental rhythms, each specific in amplitude and frequency, and it is further defined under what conditions (alertness, sleep, eyes closed/open, etc.), and in which area of the skull these rhythms occur. Moreover, there are many waves that do not typically occur in a healthy individual. The initial intention was to use these bands. However, subsequent processing showed that using smaller bands was more appropriate, with the goal of finding frequencies based on which it would be possible to distinguish between individual measurements.

Given that the objective was to identify attributes that could differentiate between flight with illusions and without and further to distinguish between both profiles, finer bands were created than those traditionally used. The entire frequency spectrum was thus divided into small frequency bands with a width of 0.1 Hz. The power within these 0.1 Hz bands was then calculated. This approach resulted in 624 attributes (powers in 0.1-Hz bands) for each of the 16 electrodes used. The resulting 9984 data points for each measurement of each subject were further used for subsequent statistical analysis.

2.6.4 Stabilometry

Posturography, in general, is a method used to measure (and subsequently evaluate) postural stability during upright standing using a force platform [20]. In static posturography (stabilometry), the position (and displacement) of the point on the platform, where the resultant of the reaction forces acts, known as the center of pressure (COP), is measured. COP closely approximates, in static posturography, the projection of the body's center of gravity onto the support surface [21]. From a biomechanical perspective, COP displacement is a measure of the energy expended to maintain balance [10], and static posturography is objective and reliable in determining static balance [20].

Force platforms are flat plates that measure the reaction forces generated by a standing (or moving) body on the platform [22]. A stabilometric platform is a device designed to measure forces in three orthogonal axes and moments around the associated axes. The platform is equipped with piezoelectric sensors or load cells that measure deformation depending on its magnitude and direction of application. Knowing the platform's geometry and sensor placement allows for the calculation of the magnitude of the applied forces and moments. The COP position can be displayed in the Antero-Posterior (AP) and Medio-Lateral (ML) direction.

Stabilometric platforms are one of the most commonly used methods for measuring stability disturbances. They are common in clinical practice, with many manufacturers producing them. The simplest technologies are financially accessible, such as Nintendo platforms sold with gaming consoles which was used in this project.

Quantitative assessment involves several traditional parameters called stability indexes [23]. Evaluation is done in the time domain, and using geometry methods. In the time domain, the parameters are further divided into two groups: parameters in 1D and parameters in 2D. Evaluation using geometric methods is possible only in 2D.

Time domain analysis

The output from the stabilometric platform consists of instantaneous Center of Pressure (COP) data, i.e., two time series (in the AP and ML directions) – stabilograms. Posturography is a clinically used method that

has several traditional assessment parameters. Among these parameters is the evaluation of stabilograms in the time domain. The basic parameter of the COP trajectory is the mean value, specifically the arithmetic average \bar{x} :

$$meanAP = \frac{1}{n} \sum_{i=1}^n = COP_{i_{AP}}, \text{ and} \quad (20)$$

$$meanML = \frac{1}{n} \sum_{i=1}^n = COP_{i_{ML}}, \quad (21)$$

where (COP_1, \dots, COP_n) are COP data for respective direction collected over 30 s and $n = 30\,000$ representing the number of samples, which depends on the length of the measurement (30 s) and the sampling frequency (100 Hz). The zero value for both directions is placed at the center of the platform. Along with the mean value, a measure of variability is also obtained – the standard deviation:

$$sdAP = \sqrt{\frac{1}{n} \sum_{i=1}^n (COP_{i_{AP}} - meanAP)^2}, \text{ and} \quad (22)$$

$$sdML = \sqrt{\frac{1}{n} \sum_{i=1}^n (COP_{i_{ML}} - meanML)^2}. \quad (23)$$

The set of statistical parameters of the datasets is expanded by extreme values, i.e. minimum ($minAP$, $minML$) and maximum ($maxAP$, $maxML$) values for respective directions. However, often the individual values of the extremes are not as interesting as their difference. It means that those parameters are interesting in individual evaluation or in specific clinical cases, i.e. unilateral vestibular surgery etc. However, in the case of this project, the binominal distribution can occur due to the fact, that some of subject has one dominant side. The same issue is then with mean values for both direction. As such a phenomenon was observed in the data, those parameters are inappropriate for the evaluation in the context of the project and therefore other parameters are used.

Extreme values provide an interval within which the values of the time series moved throughout the entire measurement and are represented by a single parameter, the range of motion (ROM):

$$romAP = maxAP - minAP, \text{ and} \quad (24)$$

$$romML = maxML - minML. \quad (25)$$

In described time analysis, only a single time series of data is evaluated. To evaluate the development of a certain variable in 2D, these methods are not well applicable. Therefore, the indices based on dynamical properties are also employed. Namely, mean ($meanVEL$) and maximal ($maxVEL$) velocity, and mean ($meanACC$) and maximal ($maxACC$) acceleration. The velocity vector is then computed as:

$$v_i = \sqrt{(COP_{i+1_{ML}} - COP_{i_{ML}})^2 + (COP_{i+1_{AP}} - COP_{i_{AP}})^2} \cdot fs, \quad (26)$$

where $i = 1 \dots n - 1$ and n represents the number of samples (30 000), while fs is the sampling frequency (100 Hz). From the velocity vectors, the acceleration vectors are calculated as:

$$acc_i = (v_{i+1} - v_i) \cdot fs, \quad (27)$$

where $i = 1 \dots n - 2$ and n represents the number of samples (30 000). After obtaining the velocity and acceleration vectors, the maximal and mean values are derived and used for further analysis as stability indexes. The 2D evaluation is then complemented by total trajectory length (TL) of COP data as:

$$TL = \sum_{i=1}^{n-1} \sqrt{(COP_{i+1_{ML}} - COP_{i_{ML}})^2 + (COP_{i+1_{AP}} - COP_{i_{AP}})^2}, \quad (28)$$

where $i = 1 \dots n - 1$ and n represents the number of samples (30 000). To extend the 2D evaluation, methods based on the characteristics of selected geometric elements are used. Commonly used, not only in posturography, are confidence ellipses and convex hulls. These methods also enable the assessment of position in the transverse plane, i.e., in 2D.

Geometric method analysis

The first method involves evaluation using a confidence ellipse (CE), most commonly with a 95% confidence level. When assessing stability, this is one of the commonly used methods, wherein the area of this ellipse is primarily calculated, along with the size of its semi-axes and its orientation. The size of the CE depends on the dispersion, with the calculation derived from the covariance matrix. A 2×2 covariance matrix is obtained by calculating the covariances between variables x (ML direction) and y (AP direction), representing their mutual variance [24]:

$$\sigma_{xy}^2 = \frac{1}{n} \sum_{i=1}^n (x_i - \bar{x}) \cdot (y_i - \bar{y}), \quad (29)$$

where n is the number of values, \bar{x} is the mean value of variable x , and \bar{y} is the mean value of variable y . The resulting covariance matrix M is shaped as [24]:

$$M_{CE} = \begin{bmatrix} \sigma_{xx}^2 & \sigma_{xy}^2 \\ \sigma_{yx}^2 & \sigma_{yy}^2 \end{bmatrix} \quad (30)$$

Based on the covariance matrix, the CE is then plotted (see Fig. 14), from which its characteristics are computed. For this study, the CE area (areaCE), orientation of the ellipse (phiCE), length of major (majorCE) and minor (minorCE) half-axes and their ratio (ratioCE) are used. However, the phiCE, as well as means and extreme values in specific directions, is inappropriate in this case, as binomial distributions are observed and therefore it's eliminated from further analysis.

The use of convex hulls (CH) in assessing postural stability is primarily within the scope of research. CH is defined as the smallest convex set, which is precisely the set where, if we connect any two arbitrary points with a line segment, then this segment will always lie inside the set. From this definition, it is apparent that the CH encompasses all data points, see Fig. 14. CH includes outliers (random deviations) and extreme values. For this reason, the CH method is not typically implemented in the software provided by manufacturers of stabilometric platforms and thus is not widely used in clinical practice. The computation of CH, as well as the calculation of its area, is implemented in MATLAB as the function *convexHull*.

Within this study, the area of convex hull (areaCH) is evaluated. The area is computed using Delaunay triangulation, where the area bounded by the CH is divided into the smallest number of triangles, each of

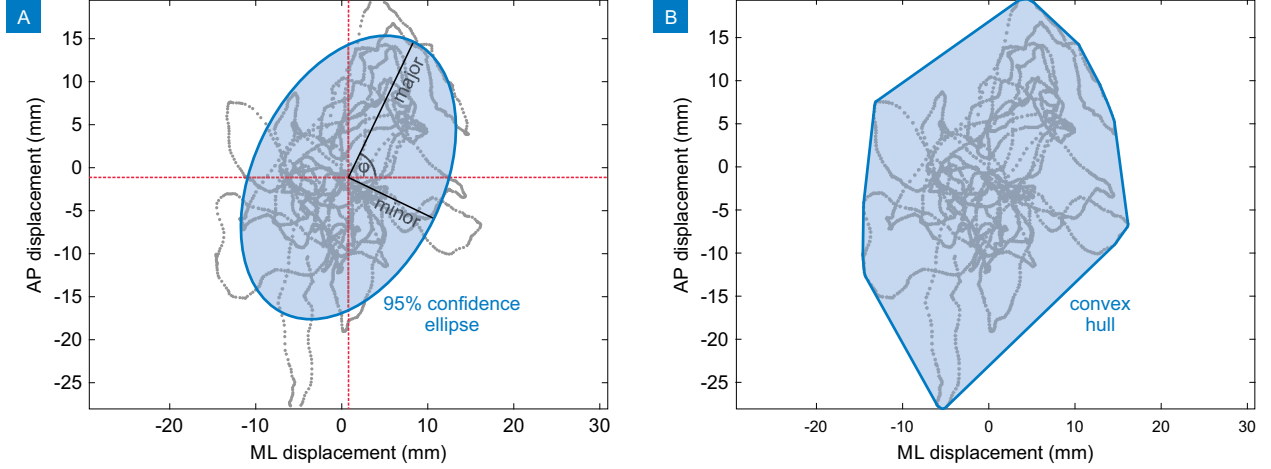


Figure 14: Example of statokinesiograms with applied geometrical methods, 95% confidence ellipse (A) and convex hull (B).

which does not contain any of the points (meaning that the points of the convex set are the vertices of these triangles) [25].

2.7 Statistical analysis

For the physiology signals, the normalization was needed to suppress interindividual variability as much as possible. As only one reference value is needed for this process, only pre-flight reference was used. The normalization was done for each subject, profile and parameter of each data type (ECG, EEG) separately. The normalisation was done by standard method of percentage normalization, i.e. value X is normalized as:

$$X_{norm_{S,P,I,IL,PAR}} = \frac{X_{S,P,I,IL,PAR} - X_{S,P,-1,IL,PAR}}{X_{S,P,-1,IL,PAR}} \cdot 100, \quad (31)$$

where S denotes subject No., $P \in \{1; 2\}$ and denotes profile, $I \in \{-1; 0; 1\}$ where -1 indicates reference value, 0 indicates value obtained in flight without illusions, 1 indicates value obtained in flight with illusion, $IL \in \{1; 2; 3\}$ where 1 is somatogravic illusion, 2 is Coriolis illusion and 3 is somatogyral illusion, and PAR denoting specific parameter, e.g. meanNN, LF, etc.

By this, all the values are shown as positive (increase) or negative (decrease) percentual change of reference value. Those are then used for subsequent statistical analysis.

2.7.1 Cardiac activity

In total, 19 normalized HRV parameters were used for statistical analysis. For each subject, total 12 segments were evaluated, as there were 3 illusions (somatogravic, Coriolis, somatogyral), 2 flight conditions (without/with illusions) and 2 profiles (with approx. 1 week time gap between each other). The structure of final dataset is therefore present in Table 5.

In the evaluation of HRV parameters across varied conditions regarding illusion presence and profile, a repeated measures Analysis of Variance (rANOVA) was used and conducted via MATLAB. This choice

Table 5: The structure of the data used for statistical analysis containing heart rate variability parameters.

Group	Subject	Profile	Illusion	IllusionType	meanNN	...	sampEn
	1	1	0	1			
	1	1	0	2			
	1	1	0	3			
	1	1	1	1			
	1	1	1	2			
	1	1	1	3			
	1	2	0	1			
	⋮	⋮	⋮	⋮			
	1	2	1	3			
	2	1	0	1			
	⋮	⋮	⋮	⋮			
	2	2	1	3			
	⋮	⋮	⋮	⋮			
	114	2	1	3

Note: Illusion indicates flight (0) without or (1) with illusion and IllusionType indicates (1) somatogyral, (2) Coriolis and (3) somatogravic illusion.

was predicated on the method’s aptness for data derived from identical subjects under disparate conditions, thereby facilitating a nuanced investigation into the ramifications of flight simulation exercises, inclusive of vestibular illusion simulations, on cardiac activity.

The dataset, initially arrayed with each row signifying a measurement and subsequent columns delineating diverse variables, was systematically imported (see to Table 5). To align with rANOVA prerequisites, an extensive data reorganization was undertaken. This entailed aligning each subject’s measurements across all conditions in a row-wise fashion, a crucial step for the precise evaluation of within-subject effects across the experiment’s various group, measurement sessions (profile), and setup conditions.

A within-subject design table clearly outlined the experimental parameters: two distinct profiles (denoting separate days) and two simulated flights (first flight profile without vestibular illusions, and flight incorporating simulated vestibular illusions). This structural framework was essential in defining the within-subject factors for the rANOVA, facilitating a comprehensive analysis of HRV under the influence of the specified experimental conditions.

The rANOVA model is mathematically encapsulated as follows. Given a response variable Y corresponding to each subject i under varying conditions c (encompassing phase combinations, measurement sessions, and setups), the model is delineated as:

$$Y_{ic} = \mu + \alpha_i + \tau_c + (\alpha\tau)_{ic} + \epsilon_{ic} \quad (32)$$

wherein Y_{ic} denotes the measured response for subject i under condition c ; μ represents the overall mean response; α_i signifies the subject-specific effect (random effect); τ_c denotes the fixed effect of condition c ; $(\alpha\tau)_{ic}$ indicates the interaction effect between subject and condition; ϵ_{ic} is the random error term for each measurement, presumed to follow a normal distribution with mean 0 and variance σ^2 .

The rANOVA was then performed which tested for main effects and interactions between the phases of the experiment, measurement sessions, and subject group as it is expected, that there would be difference in reaction between different levels of experience. This approach provided insights into the statistical significance of the observed effects, allowing us to determine whether the flight simulation exercises and the induced vestibular illusions had measurable impacts on the subjects' psychophysiological state by the means of cardiac activity.

The fitting of the repeated measures model and the subsequent rANOVA is aimed at testing the significance of the main effects and interactions among the experimental conditions. This is achieved by examining the F-statistics and corresponding p-values for each effect in the model.

The F-statistic for a given effect is calculated as:

$$F = \frac{MS_{effect}}{MS_{error}} \quad (33)$$

where MS_{effect} is the mean square for the effect being tested, and MS_{error} is the mean square error. A significant F-statistic (typically, $p < 0.05$) indicates that the effect or interaction has a significant impact on the response variable. As the compound symmetry assumption was not satisfied, the p-value with lower bound adjustment (pValueLB) was used, representing the most conservative p-value.

Our diligent analysis of the rANOVA outcomes, encompassing F-statistics and p-values, unraveled the nuanced interplay of effects and interactions within the experimental framework. This scrutiny offered profound insights into the complexities of human balance control, alongside the consequential effects of flight simulation experiences on vestibular functionality and postural stability, thereby enriching our understanding of human factors in aviation safety and performance.

2.7.2 Brain activity

Given the nature and size of the data, the processing of EEG signals was conditioned on dimensionality reduction through Principal Component Analysis (PCA). The main objective was to determine whether PCA would reveal natural patterns in the data that distinguish between individual measurements, based on the frequency analysis of brain activity under each electrode. Assuming the use of all variables, or features, as coordinates for plotting the target variable (measurement) into a scatter plot, it is presumed that such projection would create distinguishable clusters of points. However, the main problem with this approach is that the space for plotting such a scatter plot would be 9984-dimensional, and data clustering would work under the assumption that each feature would describe a certain part of the variability in the data, and that there would be no high degree of collinearity, etc.

Based on the above, an approach using PCA for dimensionality reduction was chosen to enable the identification of dependencies in the data, transform the data based on the knowledge of these dependencies, and quantify the importance of these dependencies.

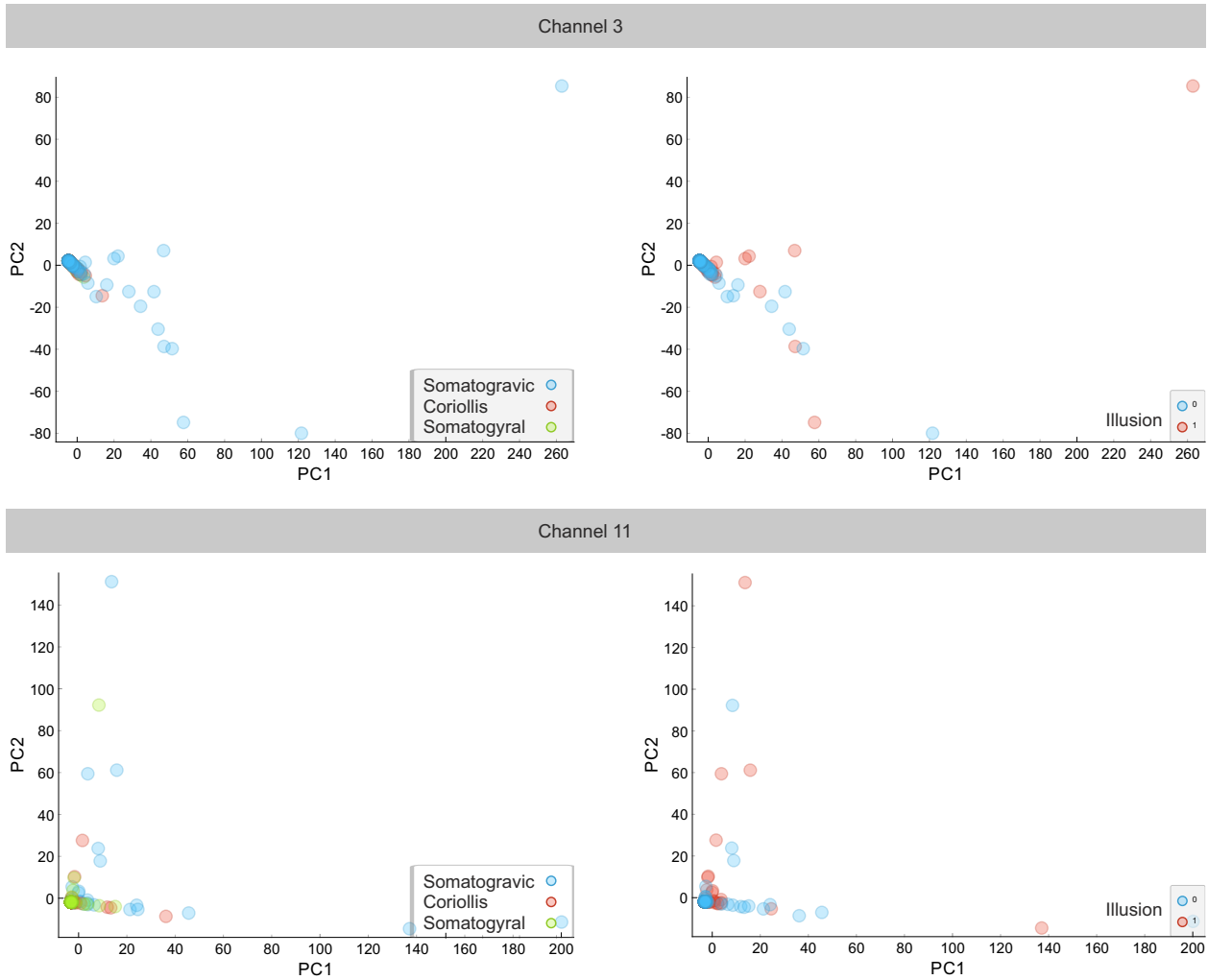


Figure 15: An example of inconclusiveness in the discriminative ability of types of illusions or flight segments with illusions based on EEG data.

As mentioned in the description of the processed data, the input dataset consisted of 9,984 attributes, each representing the power in a 0.1 Hz band for every channel, with a total of 16 channels being used. These attributes were used as inputs into PCA for each of the four measurements (2 profiles \times 2 illusion conditions). The data unfortunately did not form any clusters. An illustration of the PCA analysis and its results is shown in Fig. 15.

From the obtained data, we can infer that the measurement of EEG was influenced by significant noise. It appears plausible that the measurement of such a signal is not convenient, as the simulator cabin is full of electromagnetic noise. This could also be a reason for the poor quality of the motion tracking data. Furthermore, regarding EEG measurements, the fact that pilots have to wear headphones could significantly influence the measured signals. Unfortunately, due to technical limitations, it was impossible to maintain proper communication between the pilot and the controller without the headset.

As the data did not show any potential for further analysis, they are not included in the results section of the project.

2.7.3 Stabilometry

The statistical approach to stabilometry is similar to the one of ECG data. However, before describing the statistical evaluation of posturographic data, it seems appropriate to describe the resulting dataset, as the nature of the data subsequently determines the analysis itself.

This dataset presents stabilometric measurements of subjects undergoing a series of tests before and after flight simulator exercises. The exercises were designed to assess the impact of vestibular illusions on postural stability. Measurements were taken at three stages: before the flight simulation exercise, after executing a flight profile without vestibular illusions, and after a flight profile with simulated vestibular illusions. These stages are referred to as Measurements 1, 3, and 5, respectively. The entire setup was repeated across two different days, designated as Phases 1 and 2.

Within the stabilometric assessments, participants were tested under four conditions as part of the Romberg’s test: standing on a firm surface with eyes open (EO FiS), standing on a firm surface with eyes closed (EC FiS), standing on a foam surface with eyes open (EO FoS), and standing on a foam surface with eyes closed (EC FoS). This setup allowed for a comprehensive evaluation of each subject’s balance and postural stability under varying sensory conditions.

The dataset records multiple metrics for each measurement, range of motion, sway path length, and various parameters related to velocity and acceleration as described in section 2.6.4. These metrics could provide insight into the participants’ balance control mechanisms and their adaptation to the different test conditions.

In evaluating stabilometric measurements under various conditions before and after flight simulator exercises, we employed a repeated measures Analysis of Variance (rANOVA) conducted using MATLAB. This choice was based on the same assumptions as in the case of ECG, i.e. the suitability of the method for analyzing data from the same subjects under different conditions, thus enabling a detailed investigation into the effects of flight simulation exercises, including vestibular illusion simulations, on postural stability.

The dataset, initially arrayed with each row signifying a measurement and subsequent columns delineating diverse variables, was systematically imported (see to Table 6). To align with rANOVA prerequisites, an extensive data reorganization was undertaken. This entailed aligning each subject’s measurements across all conditions in a row-wise fashion, a crucial step for the precise evaluation of within-subject effects across the experiment’s various phases, measurement sessions, and setup conditions.

A within-subject design table clearly outlined the experimental parameters: two distinct phases (denoting separate days), three measurement sessions (pre-flight, post-first flight profile devoid of vestibular illusions, and post-second flight profile incorporating simulated vestibular illusions), alongside four setup conditions (EO FiS, EC FiS, EO FoS, EC FoS). This structural framework was essential in defining the within-subject factors for the rANOVA, facilitating a comprehensive analysis of postural stability under the influence of the specified experimental conditions.

The rANOVA was then performed which tested for main effects and interactions between the phases of the experiment, measurement sessions, and setup conditions. This approach provided insights into the statistical

Table 6: The structure of the data used for statistical analysis containing stability parameters.

Subject	Phase	Measurement	Setup	romML	...	meanACC
1	1	1	EO FiS			
1	1	1	EC FiS			
1	1	1	EO FoS			
1	1	1	EC FoS			
1	1	3	EO FiS			
1	1	3	EC FiS			
⋮	⋮	⋮	⋮			
1	1	5	EC FoS			
2	1	1	EO FiS			
⋮	⋮	⋮	⋮			
2	2	5	EC FiS			
⋮	⋮	⋮	⋮			
114	2	5	EC FoS

significance of the observed effects, allowing us to determine whether the flight simulation exercises and the induced vestibular illusions had measurable impacts on the subjects' postural stability.

As well as with the ECG, p-value with lower bound adjustment (pValueLB) was used. Our thorough analysis of the repeated measures ANOVA outcomes, including F-statistics and p-values, revealed the complex interplay of effects and interactions within the experimental framework. This careful examination provided deep insights into the complexities of human balance control, as well as the significant effects of flight simulation experiences on vestibular function and postural stability. Consequently, this has enhanced our understanding of human factors in aviation safety and performance.

2.7.4 Structured interviews

The structured interviews were primarily focused on the subjective feeling of illusion intensity, the subjective feeling of improvement, and whether such training should be implemented into the training programs. As the subjects answered on the scale from 1 to 10. To have more clear presentations and interpretation of the results, prior the statistical analysis, the data were rescaled into scale from 1 to 5.

The evaluation of the reported intensity was based on the Sign test. This testing method was chosen for several reasons. Firstly, the dataset represents paired data, which must be considered. Furthermore, the data do not fulfill the requirements for a standard distribution. Also, the data are categorical. Taking into account these circumstances, the Sign test proved to be the most suitable, as it can be used for data meeting all the aforementioned requirements. Testing was conducted at a significance level of $\alpha = 0.05$.

3 Results

3.1 Structured interview

Structured interviews served as subjective indicators of the perceived intensity of specific illusion. For the purpose of evaluation, the scoring of intensity is ranked from 1 (subject did not feel illusion at all) to 5 (very strong feeling of illusion). Frequency of the answers between all subjects for specific illusions is depicted in Fig. 16.

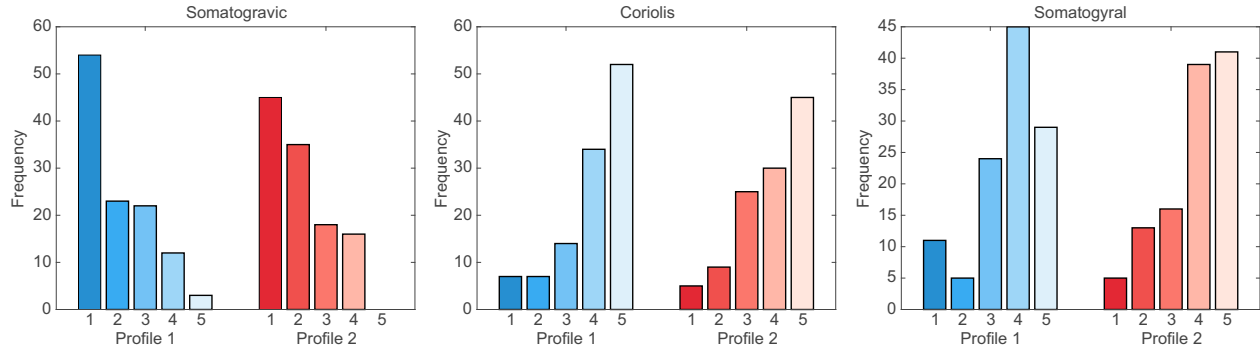


Figure 16: Frequency of subjective illusion intensity.

From the results is obvious that subjects mostly did not feel somatogravic illusion while coriolis illusion was usually marked as strongest one, inducing feelings of dizziness and nausea. Similar symptoms were also reported in the case of the somatogyral illusion. Moreover, tunnel vision was frequently mentioned in relation to these two illusions. Mean intensities for specific subject groups are then presented in Table 7. It is apparent that an improvement in subjective feelings between two profiles was observed mostly with the Coriolis illusion. The statistical analysis using the sign test did not reveal statistically significant differences between both profiles for any group or for the overall evaluation, as all p-values were greater than 0.05.

Table 7: Overview of mean intensities across subject groups.

Profile	Illusion type	Mean	SD	Mean Gr. 1	Mean Gr. 2	Mean Gr. 3	Mean Gr. 4
1	Somatogravic	2.01	1.16	2.07	2.04	2.10	1.83
2	Somatogravic	2.04	1.06	1.87	2.08	2.21	2.03
1	Coriolis M1	4.03	1.18	3.90	4.12	4.34	3.77
2	Coriolis M2	3.89	1.15	3.83	3.80	4.21	3.70
1	Somatogyral M1	3.67	1.19	3.50	3.64	3.83	3.70
2	Somatogyral M2	3.86	1.16	3.40	3.92	3.97	4.17

However, most of the subjects reported improvement in Profile 2, specifically 80 subjects. They usually reported, the even though feeling were still strong and unpleasant, they know how to better cope in the situation and that they were more focused on instruments as they understand what is happening with their body. Other 34 subjects did not feel any improvement, while 8 of those were from Gr. 1, 5 from Gr. 2,

7 from Gr. 3 and 14 from Gr. 4. When discussing implementation into training, 110 subjects supported implementation into training as they feel the experience is beneficial as they experience the specific feeling which can't be experienced during theoretical training. Other 3 subjects would not recommend implementation into training while 1 subject did not responded/was undecided.

3.2 Flight data

3.2.1 Somatogravic illusion

In this analysis, the focus was primarily on the flight parameter of altitude and the Stick Pitch angle. This was because these two parameters can demonstrate both the effect of illusions on flight control and how such illusions influence pilot intervention. Within the chosen methodology, the initial step involved performing Principal Component Analysis (PCA) on the normalized data. The temporal progression of altitude for each measurement in both raw and normalized forms is displayed in Fig. 17.

The explained variance ratio for the first two principal components in the dataset, which characterizes the propagation of altitude among different pilots, is as follows: Principal Component 1 explains approximately 64.03% of the variance, and Principal Component 2 explains an additional 20.14% of the variance. Together, the first two principal components account for about 84.17% of the total variance in the normalized altitude time series data.

This substantial portion of variance captured by the first two principal components suggests that they effectively represent the bulk of the information in the original high-dimensional data. Through these components, we can observe the most critical patterns and variations in the pilots' take-off altitude profiles, now simplified into a more manageable two-dimensional form. This described variability is primarily related to the occurrence or induction of illusions. The reduced data dimensionality can relatively well distinguish flights during which illusions were induced, as seen in Fig. 17. No further natural clustering was observed, for example, in the context of groups or profiles.

The loading plot in Fig. 17 then indicates that the primary influence on the formation of these clusters is the altitude trajectory within the range of 1500-2500 samples (considering a threshold value of 0.01). These values primarily affect PC1, which defines the axis according to which the data are clustered. This is also evident from the visualization of average altitude trajectories during takeoff, where this particular segment can be considered significantly different when comparing takeoff without and with induced illusion. It is also evident from the presentation that inducing an illusion results in a loss of altitude, compared to a takeoff without illusion, which has a linear character.

For a more precise evaluation of the occurrence of the somatogravic illusion effect on the observed population, classification was performed using hierarchical clustering, which was preceded by the calculation of a distance matrix using Dynamic Time Warping. Using this unsupervised method, it's observable that 169 out of 228 cases were correctly classified as takeoffs influenced by the illusion, and 168 out of 228 were classified as takeoffs not influenced by the illusion. It's important to note that this highly discriminative classification division is characteristic of the data itself, which speaks for itself.

Based on the findings presented, it is evident that the somatogravic illusion adversely impacts ascent, leading pilots to descend when experiencing this illusion.

To compare resilience to this illusion, classifications for the first and second profiles were analyzed. The analytical approach was identical to that used in the global case presented above.

When dividing the data into the first and second profiles (Fig. 18 and Fig. 19), slight differences can be observed in the execution of takeoff in the context of the reaction to the illusion.

Partial results for the first profile are similar to the previous overall assessment. Dimensionality reduction using PCA divides the dataset into two characteristic clusters described by the first two principal components. As in the previous case, principal component 1 accounts for 64% of the variability in the data, and principal component 2 accounts for 20% of the variability. Charakteristické zhlukovanie dát opäť prislúcha prítomnosti somatogravickej ilúzie. Interpretácia loadings, je obdobná ako pri hodnotení všetkých leťov.

In the classification, it is observable that 90 out of 114 takeoff trajectories correctly belong to those without illusions. Conversely, cluster C1 accurately identifies 83 out of 114 takeoffs during which the somatogavic illusion was induced. The temporal profiles of altitude at takeoff again indicate a significant decrease in altitude in cases where the illusion was induced.

In contrast, the second session that the pilots underwent shows a slight improvement. Observing Fig. 19, it's possible to notice a greater overlap of confidence intervals when looking at the averaged altitude trajectory for flights with and without the illusion. This naturally means that there is a smaller Euclidean distance between the individual time series. This is reflected in hierarchical clustering, where an increase in the number of false positive classifications can be observed. This means that takeoffs categorized as "with illusion" are considered to be flights without illusion. In this case, 60 out of 114 characteristic takeoffs were identified as those with the illusion. Then, 89 out of 114 flights without illusion correctly fall into cluster C2.

The analysis mentioned above took into account the final effect of inducing the illusion. The next step was to explore whether this effect originates from a reflexive push on the control stick. The principle of the analysis remains consistent in this scenario, given the uniformity in presentation.

The suppression of the control stick (negative amplitude values) can be observed immediately after the initiation of the synthetic cabin lift (approximately 3.2 seconds after initiation), which was an act to simulate the somatogavic illusion (see Fig. 20). It is also noticeable that the push of the control stick is immediately compensated by a counter-movement.

However, dimensionality reduction did not confirm that such a difference, in relation to takeoffs without illusions, distinctively divided the dataset as it did in the case of altitude. The total variability described by the first two components is approximately 50%.

Nonetheless, the loading plot indicates that individual components are influenced by temporal components corresponding to the segments in which these movements are executed. As seen from the presented trajectories, control stick deviations are quite variable within the observed population, which is likely the reason why PCA is not conclusive.

Nevertheless, when examining the classification based on the distance matrix, it can be observed that the characteristic cluster C2 is able to classify 159 out of 228 takeoffs during which the illusion was induced. Of course, in this case, there is likely a considerable variability in activity on the control stick, leading to a significant number of false positive and negative classifications. This ambiguity is similarly observed in the analysis of profiles, which are not presented in this report.

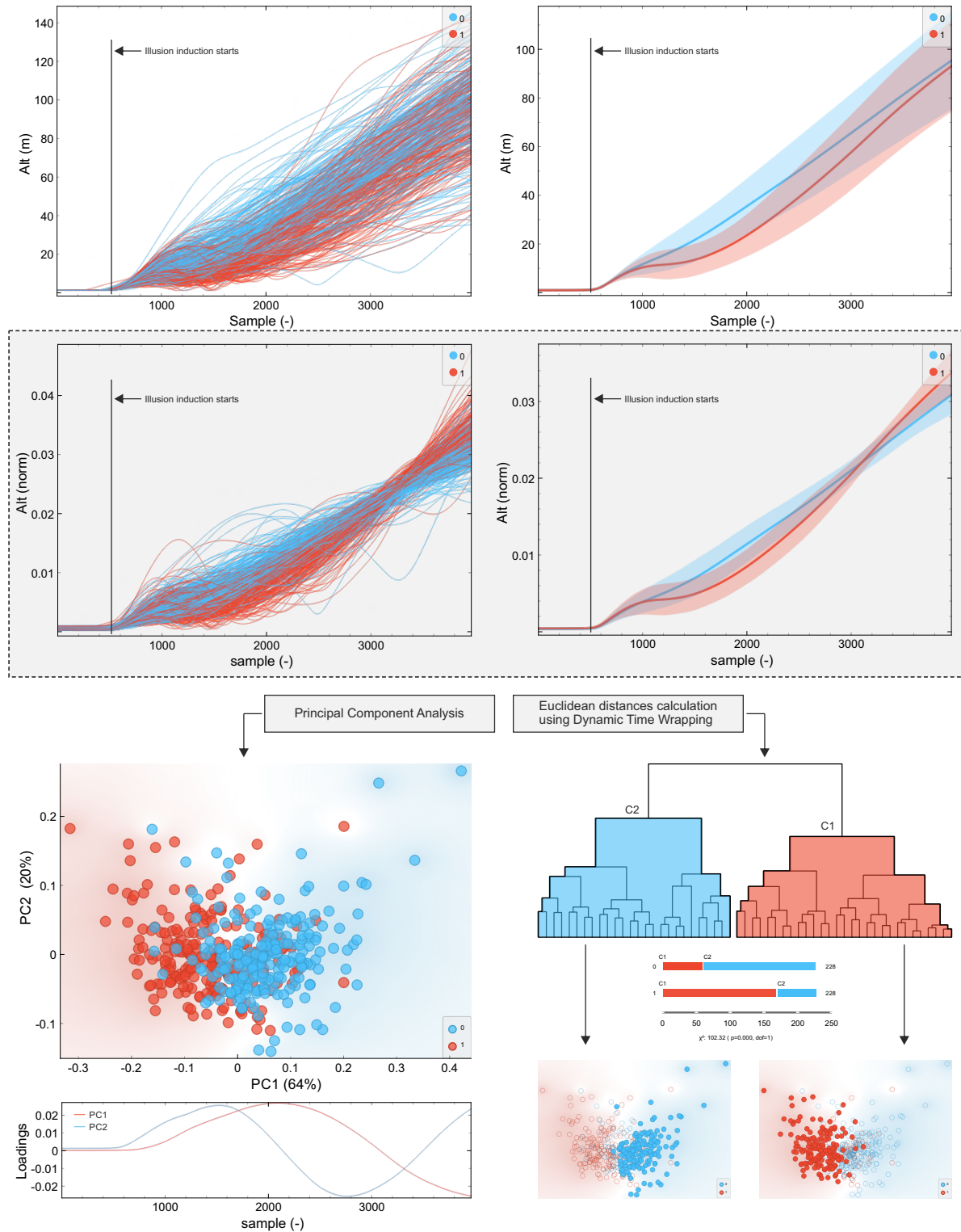


Figure 17: Results of the analysis and classification for investigating the impact of somatogravic illusion on altitude. 0 - without illusion, 1 - with illusion.

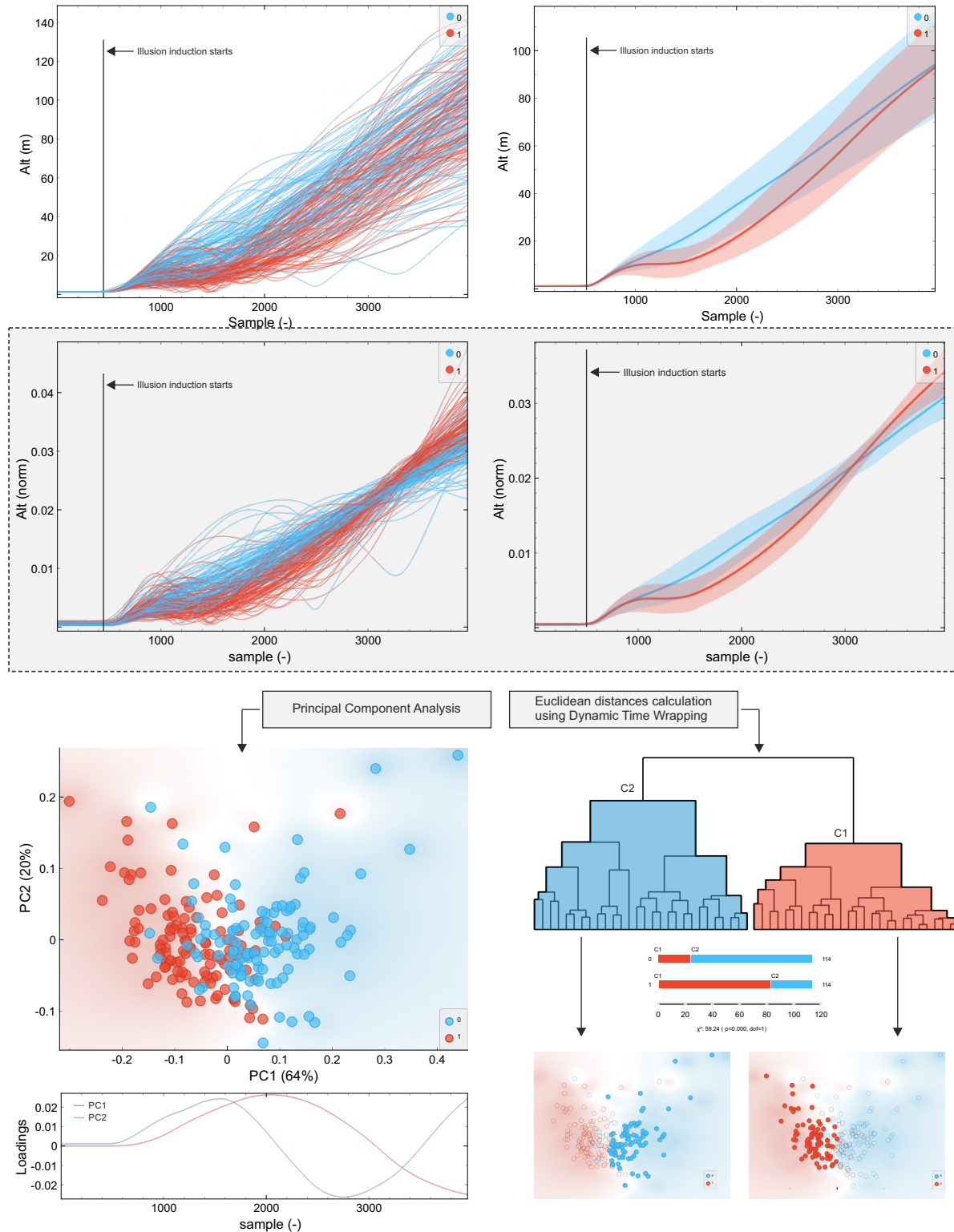


Figure 18: Results of the analysis and classification for investigating the impact of somatogravic illusion on altitude in first flight session. 0 - without illusions, 1 - with illusion.

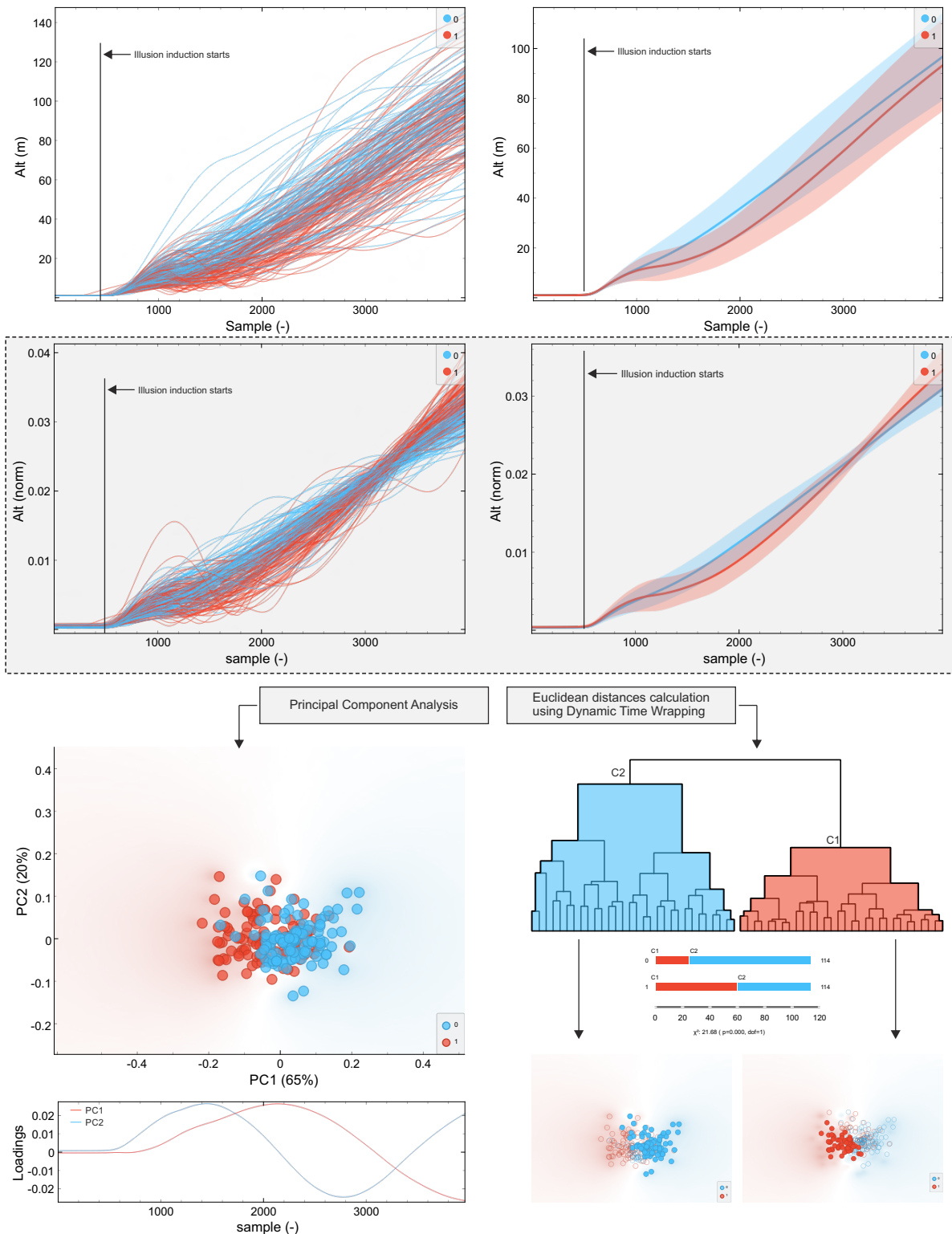


Figure 19: Results of the analysis and classification for investigating the impact of somatogravic illusion on altitude in second flight session. 0 - without illusions, 1 - with illusion.

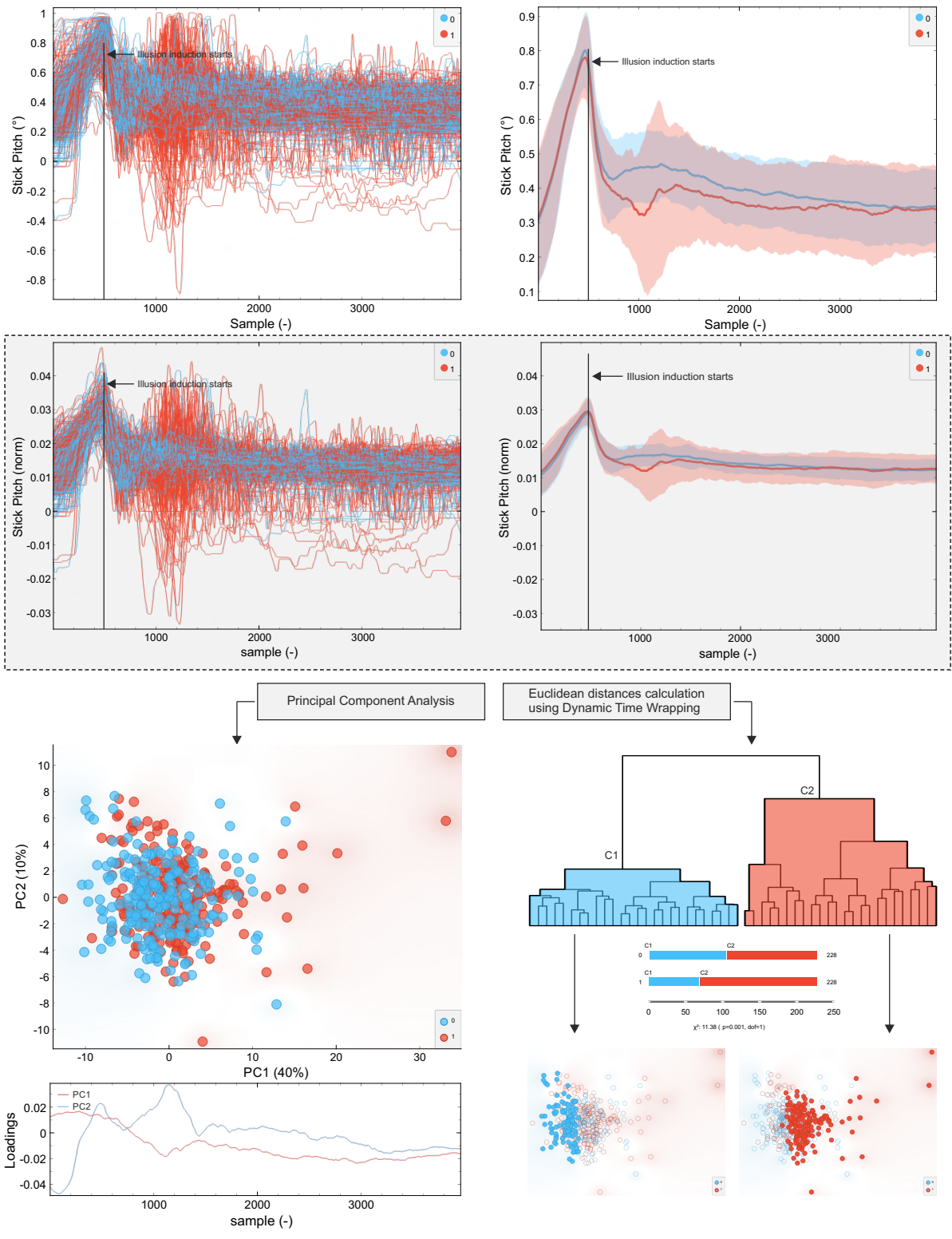


Figure 20: Results of the analysis and classification for investigating the impact of somatogravic illusion on stick pitch. 0 - without illusions, 1 - with illusion.

To ensure the clarity and focus of this report, we've opted not to include inconclusive analyses, particularly those concerning pilot groups. This decision was made to avoid introducing complexity that might obscure the report's findings. It's important to note that our review of the data did not uncover substantial evidence to suggest significant differences in reactions among pilot groups based on their experience levels.

Furthermore, in this section, we have limited our presentation to the most critical flight parameter, i.e., Altitude. Parameters such as flight speed were set the same for all subjects, and its variability would be affected by changes in altitude, as would be the case with vertical speed.

What can be generalized from the analysis of the somatogravic illusion in relation to flight data is that it is possible to induce the somatogravic illusion through simulation. The induction of the somatogravic illusion can lead to a negative change in altitude, likely caused by pulling on the control stick. It can also be argued that a single (even if only simulated) experience can have a positive impact on understanding the mechanics and effects of this illusion, thereby positively altering pilot behavior and enhancing their resilience.

3.2.2 Coriolis Illusion

The analysis of flight segments corresponding to the Coriolis illusion did not show a significant change in piloting among the observed subjects. No difference was found in the execution of maneuvers between the different groups. Maneuvers in both the first and the second flight profiles were performed uniformly regardless of the presence of the illusion. No characteristic deviations in bank angle, altitude, or specific patterns in the manipulation of the control stick were found.

Various approaches were used for the analysis. As in the previous case, unsupervised methods were employed. In an effort to determine if the presence of the illusion is detectable in the data, supervised methods such as LSTM, gradient boosting, etc., were also utilized. Proving the absence of a significant effect is a challenging task, as it always raises the question of whether the maximum effort was made and all possibilities for analysis were exhausted, whether the analysis was performed correctly, or whether the data are of the required quality. In this context, the research team did their utmost. The trends of selected parameters over time, for all measurements of the Coriolis illusion, are shown in Fig. 21 and 22.

The principle used to induce the Coriolis illusion, involving head rotation, can evoke different perceptions of spatial orientation in individual subjects. This may be one of the reasons why dealing with this illusion represents a relatively variable approach based on the variable experience among pilots and their variable reactions. This illusion was subjectively rated as the most intense, causing a feeling comparable to dizziness. This high intensity of experience, resulting from the influence on the vestibular apparatus, may also be one of the reasons why pilots were able to identify that something was happening, and thereby cope with this illusion.

Given the clear evidence that the Coriolis illusion was both intentionally induced and demonstratively present within the experimental framework, we maintain a strong stance that the absence of a measurable effect on piloting skills should not detract from the value of incorporating this form of training into standard pilot training programs. The rationale behind this assertion lies not merely in the manifestation of the illusion itself but in the intrinsic benefits derived from pilots' exposure to such phenomena. Engaging with the Coriolis illusion, even in the absence of observable impacts on flight maneuver execution, plays a pivotal role in cultivating a pilot's adaptability and resilience to spatial disorientation.

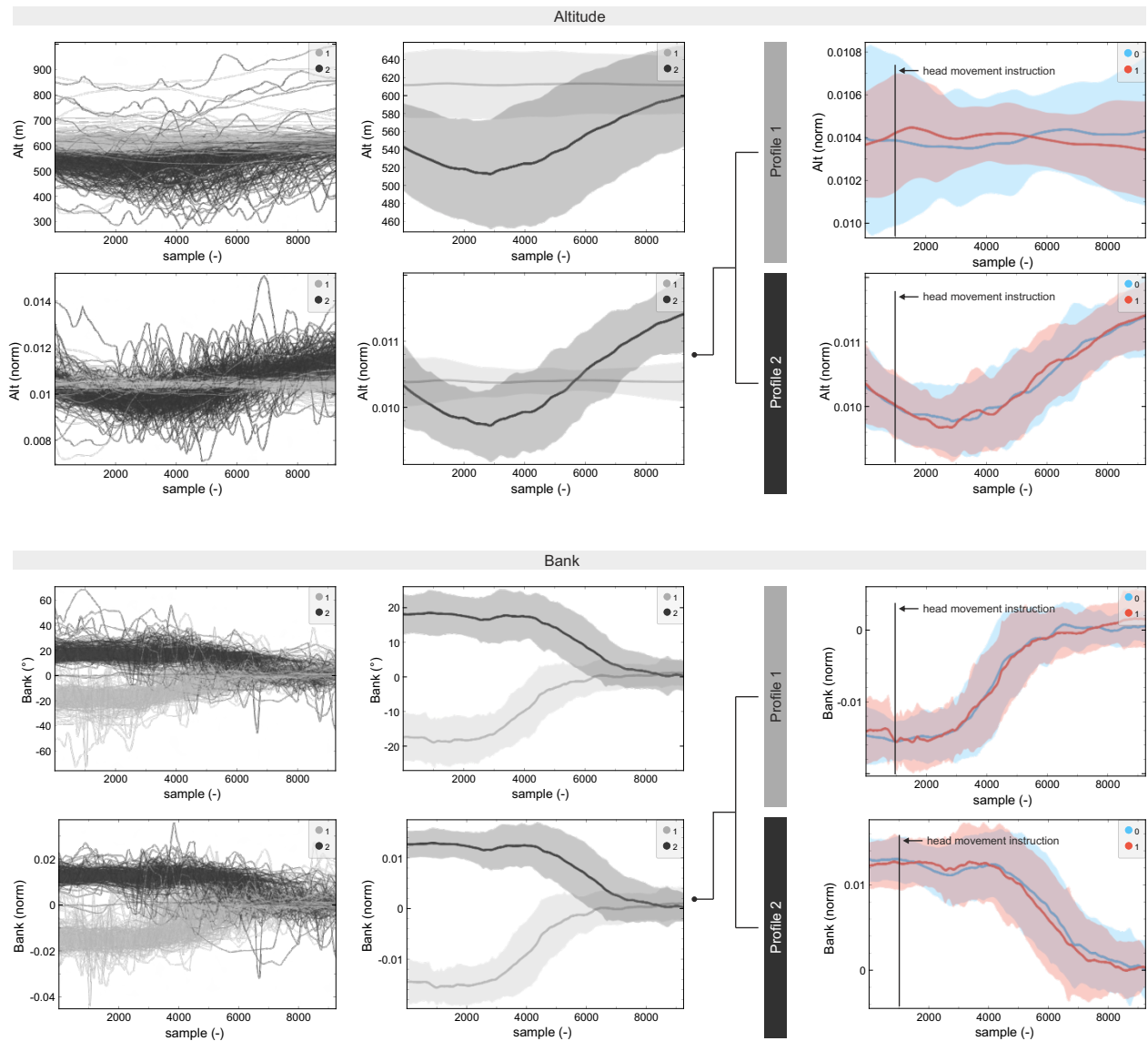


Figure 21: Trends of altitude and bank angle in the flight segment corresponding to the Coriolis illusion. The graphs present both raw and normalized data in both overall and averaged forms, with a distinction of the profile and detail on the trend of these parameters in a specific profile in relation to flights without and with the illusion (0 - without illusions, 1 - with illusion).

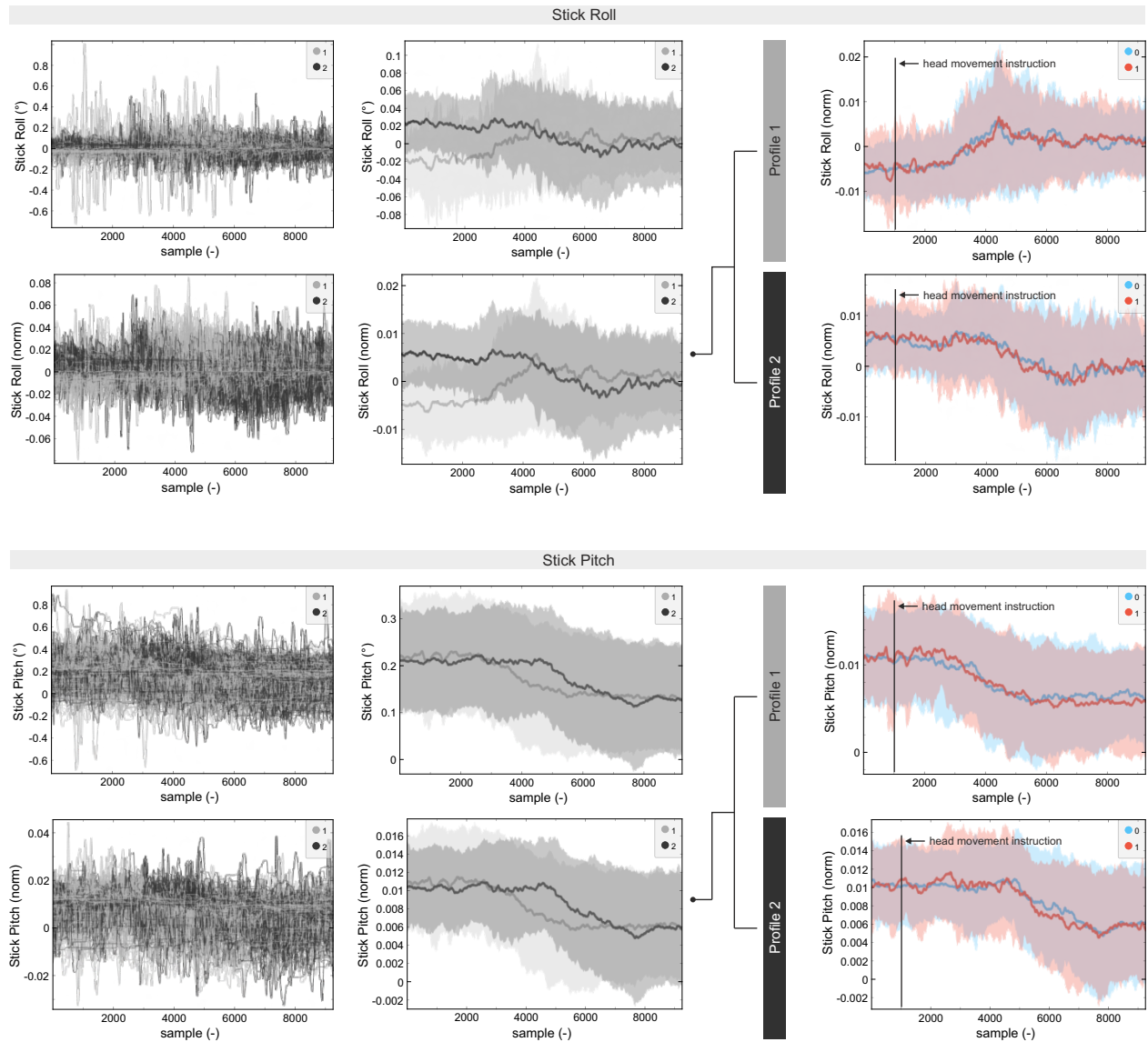


Figure 22: Trends of Stick Pitch and Roll angle in the flight segment corresponding to the Coriolis illusion. The graphs present both raw and normalized data in both overall and averaged forms, with a distinction of the profile and detail on the trend of these parameters in a specific profile in relation to flights without and with the illusion (0 - without illusions, 1 - with illusion).

3.2.3 Somatogravic Illusion

In evaluating the somatogyral illusion, we employed techniques such as dimensionality reduction, the application of Discrete Wavelet Transform (DWT), and clustering on parameters like Altitude, Bank, Stick Roll, Stick Pitch, Vertical Speed, and Heading. Despite these efforts, dimensionality reduction using Principal Component Analysis (PCA) failed to naturally segment the dataset into clusters that could significantly distinguish between pilot groups or between profiles with and without the illusion. Consequently, our presentation will adopt a similar approach to that used for the Coriolis illusion. Therefore, the time progression of the same parameters is depicted in Fig. 23 and 24.

The results reinforce the observation that executing maneuvers, whether in the presence or absence of the illusion, does not exhibit distinct characteristic features. Nonetheless, this particular illusion is uniquely induced by rapidly halting the simulator's rotation from $60^\circ/\text{s}$ within 5 seconds. This action triggers movement in the endolymph, causing pilots to feel as though they are continuing to turn. It was hypothesized that after this rapid deceleration, performed while leveling the aircraft for horizontal flight, pilots would naturally correct towards the opposite bank. This deceleration occurs roughly 7 seconds after the "report air speed" instruction, around the 2000th sample in Fig. 23 and 24. At this juncture, it's noticeable that flights subjected to this illusion prompted pilots to adjust their banking. This adjustment is visible both in terms of the aircraft's actual bank and the Stick Roll's movement. It's also apparent that this pattern persists across both the first and second profiles.

However, the confidence interval of the population mean, which informs this trend, overlaps with the confidence interval of averaged values from illusion-free flights. Thus, these findings pose a challenge for statistical analysis due to various factors such as pilot reaction speed to errors, quick adaptation to the artificial horizon, and the magnitude of the executed deviation, among others.

As an illustrative example, Figures 23 and 24 feature a case study of a pilot from group 3 (post-IFR training) who completely lost control due to this illusion. Intriguingly, this occurred during the execution of the second profile, despite prior experience with this illusion, highlighting the unpredictable nature of spatial disorientation.

This scenario again underscores the unpredictable nature of spatial disorientation and the critical need for comprehensive training in disorientation simulators. Currently, such training is not mandated by regulation nor widely adopted by flight schools, a gap that poses a significant risk to flight safety. The empirical evidence provided by our study and similar research highlights the essential role of simulator-based disorientation training in preparing pilots to recognize, understand, and effectively counteract spatial disorientation. Incorporating this training into standard pilot education programs could significantly enhance pilots' resilience to disorientation, ultimately leading to safer skies. The aviation industry must consider these findings and adapt its training protocols accordingly, prioritizing the incorporation of disorientation simulation as a fundamental component of pilot training curricula.

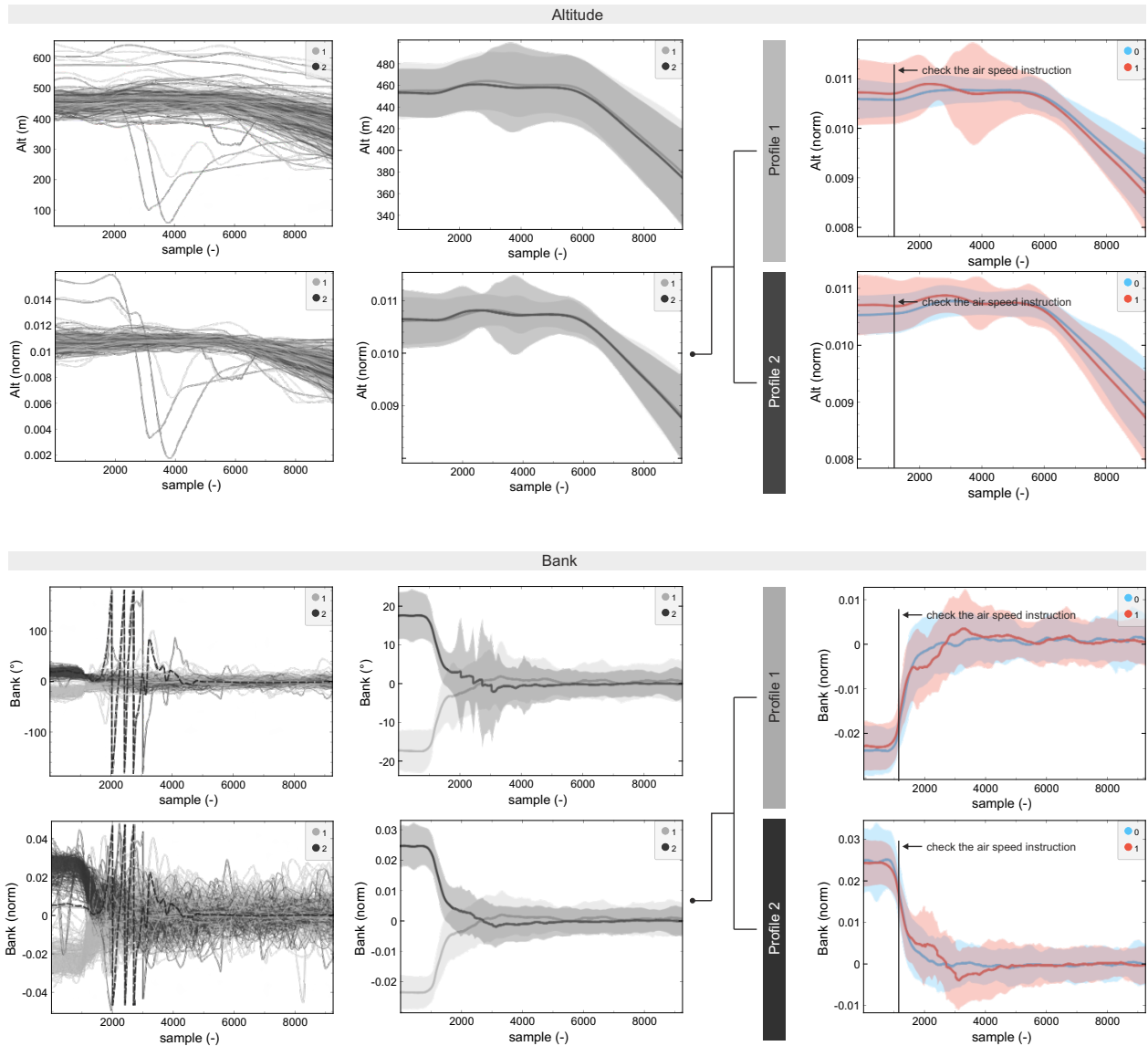


Figure 23: Trends of altitude and bank angle in the flight segment corresponding to the Somatogyral illusion. The graphs present both raw and normalized data in both overall and averaged forms, with a distinction of the profile and detail on the trend of these parameters in a specific profile in relation to flights without and with the illusion (0 - without illusions, 1 - with illusion).

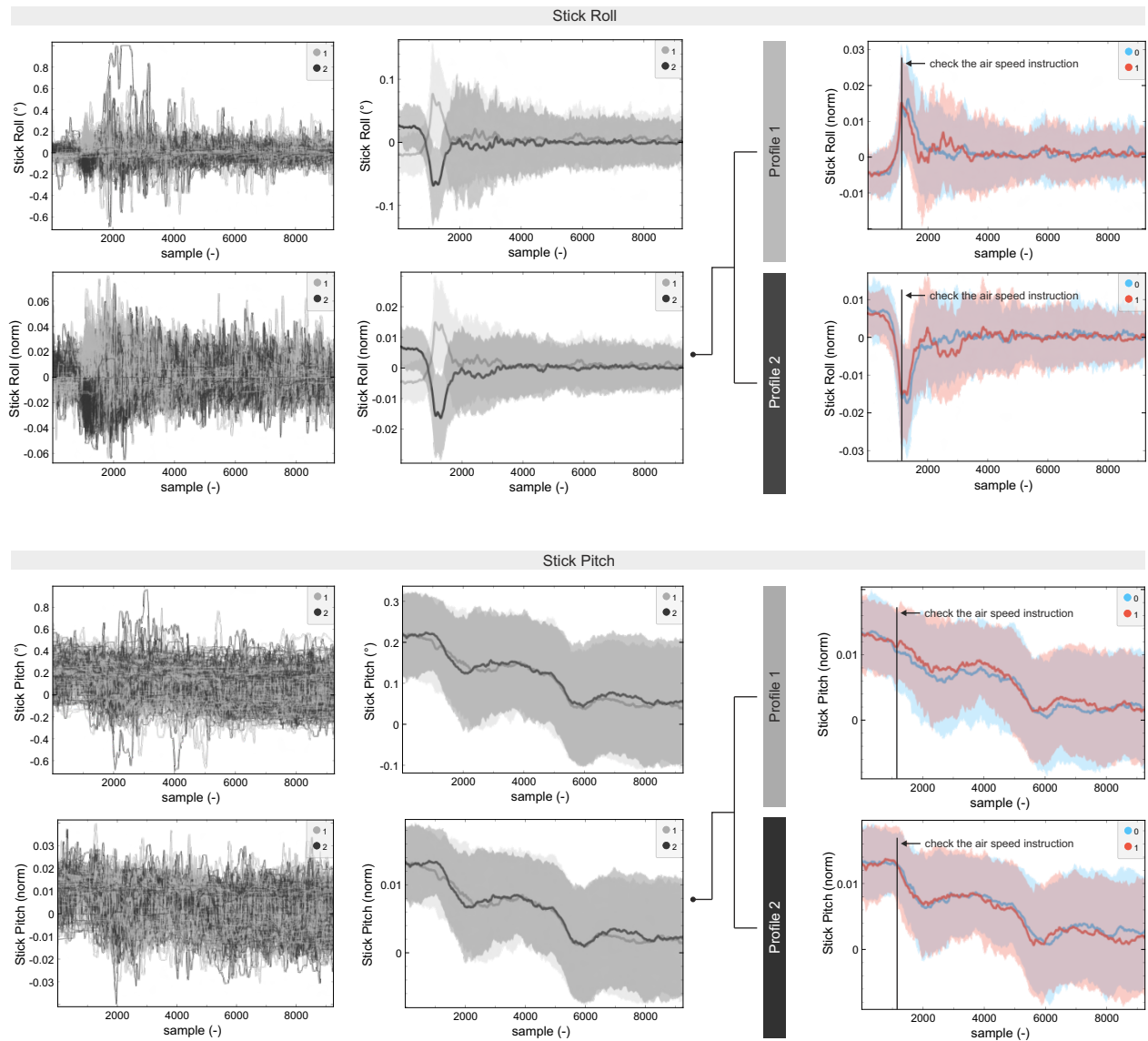


Figure 24: Trends of Stick Pitch and Roll angle in the flight segment corresponding to the Somatogyral illusion. The graphs present both raw and normalized data in both overall and averaged forms, with a distinction of the profile and detail on the trend of these parameters in a specific profile in relation to flights without and with the illusion (0 - without illusions, 1 - with illusion).

3.3 Cardiac activity

The calculated HRV parameters were evaluated by rANOVA for each parameter and specific illusion. Statistically significant results are primarily highlighted. Given the extensive nature of the results, due to numerous observed conditions, various parameters, and multiple interactions, we focus on presenting primary general trends to provide a comprehensive overview of main results, especially in the case of post-hoc analysis which would in whole form consisted of almost 350 extensive tables.

3.3.1 Somatogravic illusion

The analysis of the mean normal to normal (NN) interval (meanNN) during the somatogravic illusion showed significant differences for individual flight profiles ($F = 5.04$, $p\text{ValueLB} = 0.027$) and illusions conditions ($F = 71.69$, $p\text{ValueLB} = 5.11\text{e-}13$). A significant interaction effect of meanNN was also observed between profile and illusion ($F = 5.87$, $p\text{ValueLB} = 0.017$), and among all three within-subject factors group – profile – illusion ($F = 4.58$, $p\text{ValueLB} = 0.005$). For the standard deviation of the NN interval during the given illusion (SDNN), a statistically significant impact was identified only for profiles ($F = 5.78$, $p\text{ValueLB} = 0.018$) and illusions ($F = 4.42$, $p\text{ValueLB} = 0.038$). The analysis of RMSSD during the somatogravic illusion (RMSSD) and the percentage of NN50 (pNN50) again confirmed significant differences for illusion conditions ($F = 13.68$, $p\text{ValueLB} = 3.76\text{e-}4$), respectively ($F = 16.71$, $p\text{ValueLB} = 1\text{e-}4$). The heart rate (HR) analysis during the somatogravic illusion demonstrated significant differences for the illusion condition in the mean value (meanHR) ($F = 19.82$, $p\text{ValueLB} = 2.48\text{e-}5$) and the minimum HR (minHR) ($F = 9.37$, $p\text{ValueLB} = 2.93\text{e-}3$). In the case of meanHR, an interaction effect was also observed among all three within-subject factors ($F = 3.22$, $p\text{ValueLB} = 0.026$). For the standard deviation of HR (SDHR), a significant interaction effect was found between profile and illusion ($F = 4.19$, $p\text{ValueLB} = 0.044$). No significant difference was observed in the maximum HR (maxHR) among within-subject factors or their interactions.

Statistically significant variations were identified in the low-frequency band of heart rhythm (LF) for individual profiles ($F = 9.44$, $p\text{ValueLB} = 2.81\text{e-}3$) and illusion condition ($F = 4.9$, $p\text{ValueLB} = 0.029$), as well as in the interaction among all three within-subject factors ($F = 2.8$, $p\text{ValueLB} = 0.044$). In the high-frequency band of heart rhythm (HF) and the ratio of LF to HF power during the somatogravic illusion (LF/HF), no significant differences were observed among within-subject factors or their interactions. The total power of frequency components (Total) recorded a statistically significant difference in the case of profiles ($F = 4.08$, $p\text{ValueLB} = 0.046$). The frequency analysis of heart rate variability at normalized low frequency (nLF) and high frequency (nHF) bands showed statistically significant differences for the illusion condition ($F = 10.18$, $p\text{ValueLB} = 1.96\text{e-}3$) and ($F = 6.33$, $p\text{ValueLB} = 0.014$), respectively. In the case of nLF, a difference was also identified in the mutual interaction of all three within-subject factors ($F = 4.11$, $p\text{ValueLB} = 8.91\text{e-}3$).

According to the Poincaré plot, statistically significant differences were identified in the variability of NN intervals during the somatogravic illusion in the direction perpendicular to the line of identity on the Poincaré plot (SD1) based on the illusion conditions ($F = 13.71$, $p\text{ValueLB} = 3.72\text{e-}4$). The analysis of variability of NN intervals in the direction parallel to the line of identity (SD2) showed variability by the profile factor ($F = 6.31$, $p\text{ValueLB} = 0.014$). The analysis of the ratios of SD1 to SD2 (SD1/SD2) confirmed significant

differences also for the factor of illusion conditions ($F = 23.43$, $p\text{ValueLB} = 5.48e-6$) and the interaction of all three factors with each other ($F = 3.72$, $p\text{ValueLB} = 0.014$). The analysis of the area covered by points on the Poincaré plot (Area) observed no significant difference among within-subject factors or their interactions.

The last observed parameter, sample entropy (SampEnt), demonstrated statistically significant differences in the mutual interaction of all three factors with each other ($F = 2.73$, $p\text{ValueLB} = 0.049$).

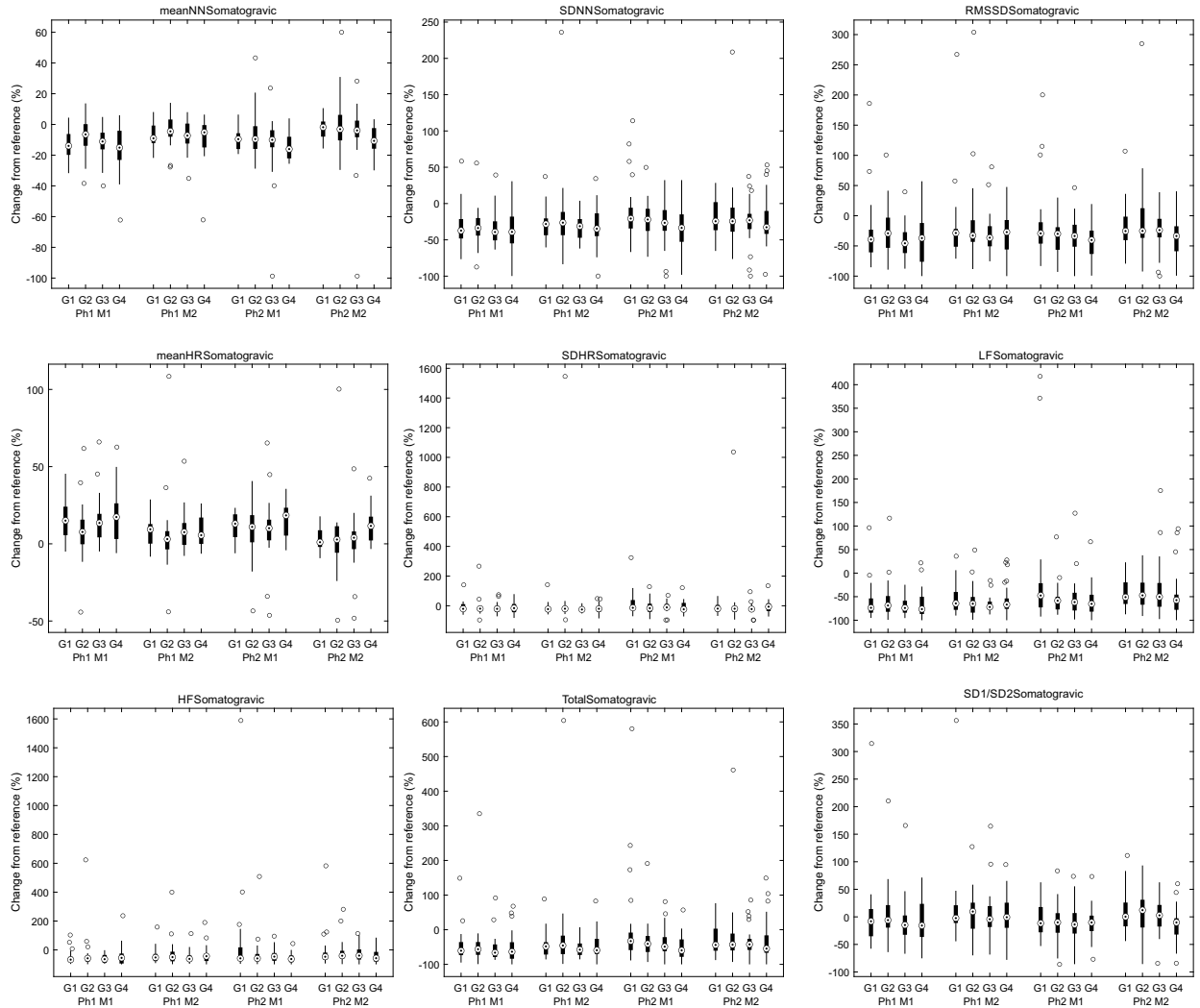


Figure 25: Graphical representation of data distribution in selected heart rate variability parameters for somatogravic illusion. Note that G1–G4 marks Group, Ph represents Profile and M represents flight without (0) and with (1) illusions.

The post-hoc analysis across different factors reveals that the illusion significantly influences meanNN, with a notable difference between the conditions without illusions and with illusions, suggesting a strong illusion effect. Conversely, group differences were not statistically significant, indicating a uniform response across groups. Profile differences showed significance, highlighting the impact of profile on meanNN, especially between Profile 1 and Profile 2. Within the flight with illusions, a significant difference was observed between

profiles, indicating that the effect of illusion varies with the profile. When looking at the data trend, see Fig. 25, it is obvious, that in both profiles there is increase in meanNN in flights with illusions. It indicates lower load on subject which corresponds with the fact that subjects were not aware of the presence of the illusion. Results are further supported by higher variability in case of flights with illusions by the means of SDNN. For the SDNN, significant findings emerged related to the effects of illusion and profile, while group differences remained nonsignificant. The distinction between two flight conditions was notably significant, as well as differences between Profile 1 and Profile 2.

The consistency across groups, however, suggests that the subjects reaction is similar regardless experience which is also supported by subjective evaluation. The RMSSD as well as meanHR and SDHR provides similar results. However, in the case of HR parameters, Profile interaction is non-significant. The data trend is however consistent with previous, see Fig. 25. When looking into other time domain analysis parameters, also those support these findings, as they do not show any significant interactions (minHR) or point out the significant difference between flights without illusions and with them.

Frequency analysis support previously discussed results as obvious also from consistent trends in the data, Fig. 25. Generally, difference between illusion conditions are observed. Also, in some cases, interaction between profile and illusion condition is observed, e.g. for LF for all possible combinations. Also, the Total parameters shows differences between profiles, however there is no interaction regarding illusion conditions. Furthermore, analysis through Pointcaré plot supports influence of illusions condition while increase of SD1/SD2 indicates lower load in case of the flight with illusion.

Across all parameters analyzed, a consistent and compelling narrative emerges with regard to the role of illusion conditions. Although not all groups significant in all of the parameters, the importance of the parameter illusion, i.e. conditions of flight without illusions versus those with illusions, is obvious. The analysis consistently underscore the illusion conditions as a significant factor affecting the Somatogravic effect, suggesting that the presence or absence of illusions has a profound impact on psychophysiological state of the subjects. The data reveal that regardless of the specificities of the groups or profiles involved, the illusion conditions (such as those simulating different flight conditions) consistently stands out as a critical influencer.

To summarize, a consistent trend is observed across HRV parameters, mostly based on time domain analysis which shows strongest results, suggesting a reduced load during the second flight of each session. This makes sense as the subjects mostly did not feel any illusion, while being less overloaded because they already knew what would be happening during the flight and were familiar with the simulator's reactions.

3.3.2 Coriolis illusion

The analysis of the mean normal to normal (NN) intervals (meanNN) during the Coriolis illusion revealed significant differences for all three factors individually: groups of pilots ($F = 4.6$, $pValueLB = 0.00489$), flight profiles ($F = 4.14$, $pValueLB = 0.045$), and illusions conditions ($F = 32$, $pValueLB = 1.88e-7$); and in the interactions between profile and illusion factors ($F = 35.18$, $pValueLB = 5.79e-8$) as well as among all three within-subject factors ($F = 3.89$, $pValueLB = 0.011$). The standard deviation of the NN interval during the Coriolis illusion (SDNN) demonstrated a statistically significant effect for the illusion factor ($F = 4.24$, $pValueLB = 0.042$). The RMSSD analysis for the given illusion conditions (RMSSD) did not confirm

any statistically significant difference among within-subject factors or their interactions. The time domain analysis of heart rate showed significant differences in the interaction between profile and illusion conditions in cases of mean value (meanHR) ($F = 17.11$, $p\text{ValueLB} = 8.03e-5$) and maximum value (maxHR) ($F = 3.96$, $p\text{ValueLB} = 0.049$). In the case of meanHR, an interaction effect was also observed among all three within-subject factors ($F = 3.18$, $p\text{ValueLB} = 0.028$) as well as separately for the illusion conditions factor ($F = 9.61$, $p\text{ValueLB} = 0.00261$). No significant differences were observed in the minimum HR value (minHR) or the standard deviation of HR (SDHR) among within-subject factors or their mutual interactions.

Frequency analysis of heart rate variability identified significant p-value differences in low-frequency band (LF) for profile factors ($F = 6.75$, $p\text{ValueLB} = 0.012$) and illusion condition ($F = 5.72$, $p\text{ValueLB} = 0.019$). In high-frequency band of heart rhythm (HF), the ratio of LF to HF frequencies (LF/HF), and the total power of frequency components during the Coriolis illusion (Total), no significant differences were observed among within-subject factors or their interactions. The frequency analysis of heart rate variability in normalized low frequency (nLF) showed statistically significant differences for the profile factor ($F = 6.21$, $p\text{ValueLB} = 0.015$) and interaction between group factors depending on the illusion conditions, i.e. flight without or with illusion ($F = 3.76$, $p\text{ValueLB} = 0.014$). In the case of normalized value for high-frequency band (nHF), differences were observed in the illusion factor ($F = 3.99$, $p\text{ValueLB} = 0.049$) and interaction among all three within-subject factors group – profile – illusion ($F = 3.06$, $p\text{ValueLB} = 0.032$).

The analysis of heart rate variability through the Poincaré diagram revealed only one case of significant factor differences, specifically in the variability of NN intervals in the direction parallel to the line of identity (SD2) for the illusion factor ($F = 4.23$, $p\text{ValueLB} = 0.043$). In cases of variability of NN intervals in the direction perpendicular to the line of identity on the Poincaré plot (SD1), the ratios of SD1 to SD2 (SD1/SD2), and the area of the region formed by points on the Poincaré plot (Area), no significant differences were observed among within-subject factors or their interactions.

No significant differences were detected in the sample entropy (SampEnt) among within-subject factors or their interactions either.

The posthoc analysis of the meanNN parameter across various factors — groups, illusions, profiles, and their interactions—has revealed multiple relationships and effects. Particularly notable is the significant impact of the illusion conditions on this parameter. The comparison between two specific illusion conditions shows a statistically significant difference in the meanNN. This finding suggests that the type of illusion condition significantly affects the parameter, underscoring the parameter’s sensitivity to changes in the illusion condition. While the analysis of other factors such as group and profile differences, as well as their interactions, did not consistently show statistically significant results, the clear impact of the illusion factor stands out. This highlights the nuanced nature of the parameter’s behavior, suggesting that while some factors may not individually lead to significant differences, the type of illusion conditions is a crucial determinant of the parameter’s values. However, also in this case, there is obvious trend (see Fig 26) similar to one in somatogravic illusion.

This indicates, that subject felt less of the load during the flight with illusions. Interestingly enough, the trend also suggest increase in values between profiles, suggesting less load during second profile. However, those are significant only for Group 1. The results are also supported by SDNN parameter. However, statistically significant influence os illusion conditions is shown only in case of Group 2. Similar results are

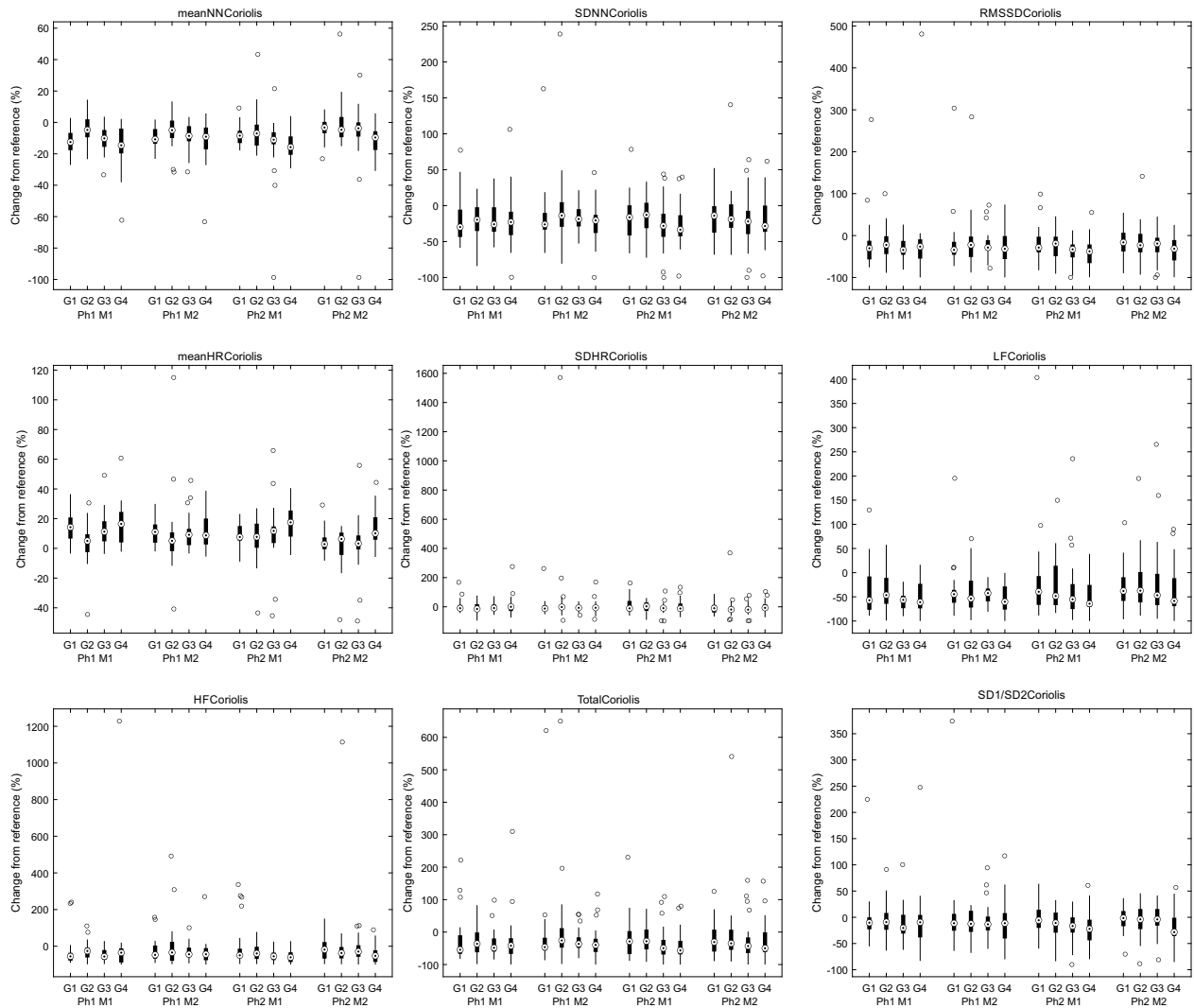


Figure 26: Graphical representation of data distribution in selected heart rate variability parameters for Coriolis illusion. Note that G1–G4 marks Group, Ph represents Profile and M represents flight without (0) and with (1) illusions.

then obtained for the meanHR parameter as well as SD2 of Pointcaré plot. Interestingly, frequency analysis indicated differences between 2 profiles in flight with illusions by the means of LF parameter.

In summary, when looking at the parameters' distributions, it is obvious the similar trend is across all of them following the trend in somatogravic illusion. Based on the rAnova and post-hoc analysis, the main effect is again cause by illusions conditions. Also in here, not in all parameters significant for all groups shows that effect. While the differences in illusion conditions were expected, the trend of values of separate parameters are opposite to what was expected. Therefore, also in the case of Coriolis illusion, the subjects seems to be more relaxed in the case of the flight with illusion. While we know from subjective evaluation and reports on subjects' feelings that Coriolis illusion was highly challenging, it seems that habituation effect was stronger

regarding physiological signals or cardiac activity, respectively. Also, it is possible, that while manifestation of illusion was strong, the subjects were aware of presence of non-standard situation and focused on the flight performance, as flight data indicated.

3.3.3 Somatogyral illusion

The analysis of the mean normal to normal (NN) interval during the somatogyral illusion (meanNN) revealed significant differences in p-values for all three factors individually and in their interactions ($F = 3.26$, $pValueLB = 0.025$). The pValueLB values were significant for groups of pilots ($F = 3.27$, $pValueLB = 0.025$), flight profiles ($F = 14.62$, $pValueLB = 2.44e-4$), and illusions conditions ($F = 29.87$, $pValueLB = 4.25e-7$). From the standard deviation of the NN interval during the illusion (SDNN) and the RMSSD analysis during the somatogyral illusion (RMSSD), significant differences were confirmed only in the factor of the illusion conditions ($F = 10.8$, $pValueLB = 1.46e-3$) and ($F = 25.86$, $pValueLB = 2.05e-6$), respectively. The time domain analysis of heart rate during the somatogyral illusion showed statistically significant differences only in the mean HR value (meanHR) for factors of profile ($F = 11.72$, $pValueLB = 9.39e-4$) and illusion conditions ($F = 16.32$, $pValueLB = 1.14e-4$); and in the interaction between the factors of group of pilots and profile ($F = 2.72$, $pValueLB = 0.049$). No significant differences were observed in the standard deviation of HR (SDHR), minimum HR value (minHR), and maximum HR value (maxHR) among within-subject factors or their interactions.

Frequency analysis of heart rhythm, both in low frequency (LF) and high frequency (HF) bands, showed statistically significant differences in the illusions conditions ($F = 12.96$, $pValueLB = 5.26e-4$) and ($F = 5.95$, $pValueLB = 0.017$), respectively. The total power of frequency components (Total) also noted a statistically significant difference in the case of profiles ($F = 6.76$, $pValueLB = 0.011$). Other components of frequency analysis, such as the ratio of LF to HF frequencies during the somatogyral illusion (LF/HF) and the frequency analysis of heart rate variability at normalized low frequency (nLF) and high frequency (nHF), did not show any statistically significant differences among within-subject factors or their interactions.

A trend of statistically significant differences in the illusion factor was observed throughout the statistical measure of variability of R-R intervals according to the Poincaré plot. The variability of NN in the direction perpendicular to the line of identity on the Poincaré plot (SD1) was ($F = 25.88$, $pValueLB = 2.04e-6$), in the direction parallel to the line of identity (SD2) the value was ($F = 9.14$, $pValueLB = 3.28e-3$), for the ratios of SD1 to SD2 (SD1/SD2) it was ($F = 14.59$, $pValueLB = 2.49e-4$), and for the analysis of the area of the region (Area) the value was ($F = 11.61$, $pValueLB = 9.92e-4$). No other significant differences were identified in within-subject factors or their interactions in all the above methods.

The sample entropy (SampEnt) did not show any significant difference among within-subject factors or their interactions.

The post-hoc analysis revealed strong effect of illusion conditions in all groups except for Gr. 2 in case of meanNN. Groups 1 and 3 furthermore shows differences between the two profiles. When looking at the distribution of this parameter, see Fig. 27, the same trend as with previous two illusions is observed. This means that subject seems to be more relaxed during second flights of the measurement. It also important to note, that taking into account differences between profiles, the Profile 1 seems to be more challenging than

Profile 2 indicating improvement. Strong effect of illusion conditions is also observed in SDNN and RMSSD parameter. MeanHR than shows same results as SDNN.

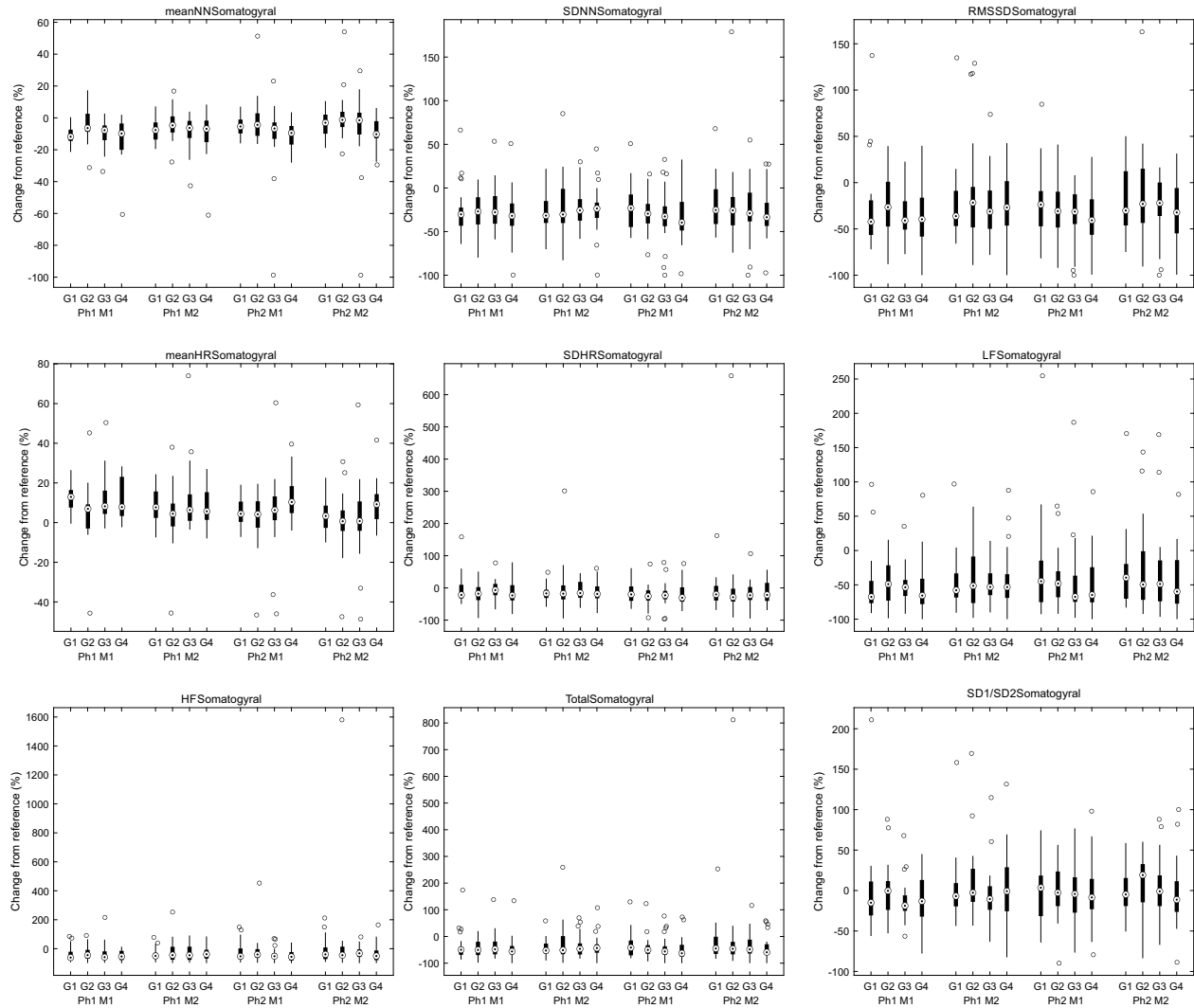


Figure 27: Graphical representation of data distribution in selected heart rate variability parameters for somatogyral illusion. Note that G1–G4 marks Group, Ph represents Profile and M represents flight without (0) and with (1) illusions.

Frequency analysis supports the strong effects of illusion conditions, as LF, HF and Total manifested differences regarding two flight conditions. Same effect is then observed in the POintcaré plot parameters, the SD1 and SD1/SD2, for Gr. 2 then also in the Area of the ellipse.

For the summary, the effects observed in the case of somatogyral illusion seems to be consistent with Coriolis illusion. The predominant effect of the illusion conditions is observed in most of the subject groups. Once again, the opposite trend than expected is observed, as it seems, that during second flights (flights with

illusions) were subjects more relaxed. On the other hand the non-standard situations does not have to as stressful when in simulated environment and habituation could be predominant.

Overall, the results across all illusion from HRV are mostly consistent as it seems, than only illusion conditions seems to influence evaluated parameters. This does not mean, that any other significant differences were not observed, but it was not systemic or consistent, usually manifesting in one group. The result thus do not indicate significant differences in psychophysiological condition of subjects regarding the level of experience or profile.

3.4 Postulography

The analysis identified a statistically significant effect on the range of ML (romML) displacement across different phases ($F = 10.57$, $pValueLB = 0.0015$) and setups ($F = 181.40$, $pValueLB = 8.84e-25$) of the experiment. A statistically significant variation in romML was also found in the interaction between measurements and setups ($F = 4.20$, $pValueLB = 0.0428$). Additional significant differences were observed for the standard deviation of ML (sdML) displacement across different phases ($F = 10.99$, $pValueLB = 0.00125$) and setups ($F = 384.04$, $pValueLB = 3.43e-37$). Significant bidirectional interactions include differences between phase and setup ($F = 5.69$, $pValueLB = 0.0189$) as well as between measurement and setup ($F = 5.58$, $pValueLB = 0.020$).

Statistically significant variations were identified in the range of AP displacement across different phases ($F = 5.57$, $pValueLB = 0.0201$) and setups ($F = 383.92$, $pValueLB = 3.48e-37$) of the experiment, as well as in the interaction between measurements and setups ($F = 6.30$, $pValueLB = 0.0135$). Significant differences were also observed for the standard deviation of AP displacement (sdAP) in different phases ($F = 4.48$, $pValueLB = 0.0367$) and setups ($F = 293.36$, $pValueLB = 1.96e-32$).

The analysis of the area of the confidence ellipse (areaCE) and the values of the minor axis of the confidence ellipse (minorCE) revealed significant differences in two specific within-subject factors and their interactions. Specifically, significant differences were identified in areaCE, where the values for the experiment phase ($F = 16.42$, $pValueLB = 9.64e-05$) and setup ($F = 164.74$, $pValueLB = 2.17e-23$) showed significance. Similarly, the interaction between phase and setup ($F = 10.89$, $pValueLB = 0.00132$), as well as between measurement and setup ($F = 6.45$, $pValueLB = 0.0126$), demonstrated significant differences. Significant differences in minorCE were observed for phases ($F = 13.46$, $pValueLB = 0.00038$), setups ($F = 575.15$, $pValueLB = 7.63e-45$), as well as in the interaction between phase and setup ($F = 10.58$, $pValueLB = 0.00153$) and between measurement and setup ($F = 7.44$, $pValueLB = 0.00745$). The analysis of the major axis of the confidence ellipse (majorCE) revealed significant differences only in the mentioned within-subject factors: phase ($F = 5.51$, $pValueLB = 0.0207$) and setup ($F = 270.62$, $pValueLB = 4.53e-31$). Significant differences were also found in setup for the ratio of the confidence ellipse axes (ratioCE) ($F = 214.94$, $pValueLB = 2.39e-27$).

The evaluation of the convex hull area (areaCH) revealed significant differences that reflect the same within-subject factors and their interactions as in the case of the confidence ellipse area. Significant differences were found in the phases of the experiment ($F = 12.41$, $pValueLB = 0.00063$), setup ($F = 115.51$, $pValueLB = 1.03e-18$), as well as in the interaction between phase and setup ($F = 5.12$, $pValueLB = 0.0291$) and between measurement and setup ($F = 4.47$, $pValueLB = 0.039$).

In the case of the analysis of track length (TL), mean velocity (meanVEL), and mean acceleration (meanACC) on the stabilometric platform, significant differences were identified across all three within-subject factors, as well as in the interaction between the phase of the experiment and setup, and between measurement and setup. Specifically, significant differences were recorded in TL at phases ($F = 30.62$, $pValueLB = 2.25e-7$), measurement ($F = 30.77$, $pValueLB = 2.12e-7$), setup ($F = 284.66$, $pValueLB = 6.38e-32$); meanVEL at phases ($F = 30.62$, $pValueLB = 2.25e-7$), measurement ($F = 30.77$, $pValueLB = 2.12e-7$), setup ($F = 284.66$, $pValueLB = 6.38e-32$); and meanACC at phases ($F = 25.43$, $pValueLB = 1.88e-6$), measurement ($F = 35.77$, $pValueLB = 2.98e-8$), setup ($F = 211.18$, $pValueLB = 4.49e-27$). A significant interaction effect was found between the phase of the experiment and setup for TL ($F = 24.58$, $pValueLB = 2.70e-6$), meanVEL ($F = 24.58$, $pValueLB = 2.69e-6$), and meanACC ($F = 20.96$, $pValueLB = 1.47e-5$); as well as between measurement and setup for TL ($F = 30.38$, $pValueLB = 2.48e-07$), meanVEL ($F = 30.38$, $pValueLB = 2.48e-7$), and meanACC ($F = 33.47$, $pValueLB = 7.28e-8$).

For maximum velocity (maxVEL), significant differences were observed only in the case of two factors: phase of the experiment ($F = 5.03$, $pValueLB = 0.027$) and setup ($F = 90.62$, $pValueLB = 6.27e-16$), with differences noted in the interaction only between measurement and setup ($F = 7.55$, $pValueLB = 0.0071$). In the case of maximum acceleration (maxACC), differences were significant only within the phase and setup of the experiment ($F = 28.81$, $pValueLB = 4.67e-7$).

The post-hoc analysis revealed that it is possible to distinguish between the two profiles across most parameters, particularly when focusing on measurements using the foam surface. The analysis highlighted significant results relevant to the project setup in three parameters: first, in trajectory length (TL); second, in mean velocity (meanVEL); and third, in mean acceleration (meanACC), both of which directly influence the trajectory length. The analysis shows that, with few exceptions of measurements on the firm surface, it is possible to distinguish between the measurements, also taking into account the profiles. This means that based on these parameters, it is possible to distinguish among three measurements, i.e., before, during, and after flights in both profiles. However, when examining the data distribution, it is clear that subjects improve their balance across the measurements, as indicated by decreases in trajectory length, velocity, and acceleration, see Fig. 28. Given the hypothesis that vestibular illusions affect stability, an opposite trend would be expected.

The results thus indicated that vestibular illusions do not significantly influence subjects' postural stability, as no significant worsening of postural stability was manifested. The possible explanation for the observed improvement in stability could be multifaceted. The most probable explanation, however, is associated with a learning effect. The repeated measurements might introduce a learning effect, wherein subjects unconsciously learn to maintain better balance with each subsequent measurement, regardless of the vestibular illusions. This hypothesis is further supported when focusing on the differences between the two profiles. While post-hoc analysis shows there are significant differences between the profiles across the measurements, the data distributions suggest better stability in the case of the second profile, supporting the assumption that a learning effect is manifested.

Note, that only significant results are presented as full post-hoc analysis consist of 84 tables.

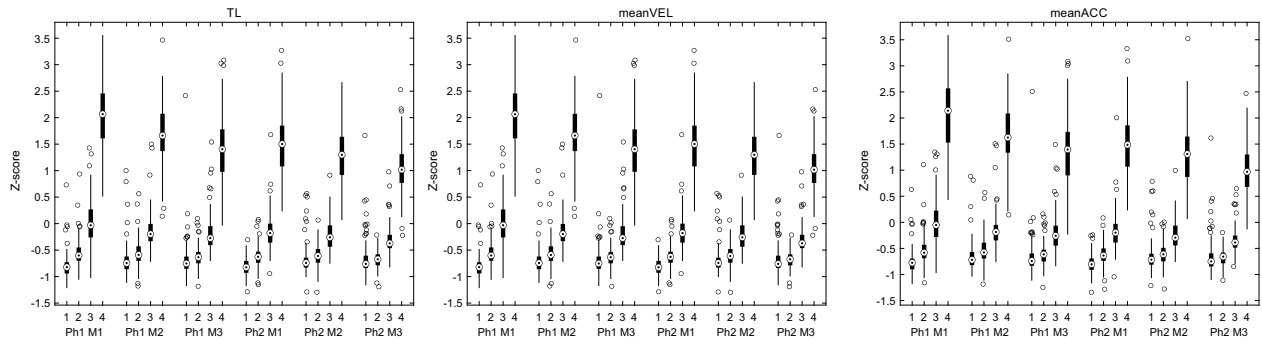


Figure 28: Graphical representation of data distribution in selected posturography parameters. Note that 1 – FiS EO, 2 – Fis EC, 3 – FoS EO, 4 – FoS EC. Ph represents Profile and M represents measurement before (1), between (2) and after (3) flights.

4 Conclusion

Drawing from the findings of this research report, we can deduce the following insights:

- Participants' subjective assessments indicate that the method developed for inducing vestibular illusions is effective and believable.
- The somatogravic illusion clearly affects pilot behavior by subconsciously causing them to push the control stick forward, leading to a decrease in altitude during takeoff. Notably, the impact of this illusion diminished after participants underwent their initial flight experience, where they encountered the illusion firsthand. Despite being perceived as the least intense and frequently unnoticed, the somatogravic illusion had the most profound impact on flight control.
- Participants described the Coriolis illusion as the most intense, likening its effects to dizziness. This illusion's influence on flight control did not follow a predictable pattern, with pilots' responses varying as much as they did in turns not influenced by the illusion. This variability implies that the participants could readily identify and respond to the discomfort induced by the illusion, likely adopting proactive measures in flight monitoring and control to preclude significant piloting errors. Hence, the sheer intensity of the Coriolis illusion may have acted as a deterrent to its full effect in this experimental context.
- Regarding the somatogyral illusion, a specific response pattern was noted where there was an unintended bank in the opposite direction to what was needed for leveling the aircraft. This response, while not as marked as the response to the somatogravic illusion, was nonetheless discernible.
- Based on the analysis of cardiac activity, it is evident that the psychophysiological state of subjects was different during flights with illusions and without them. Contrary to assumptions, however, higher workload levels were observed in flights without illusions. These flights always took place first. Therefore, it is possible that a habituation effect occurred, as the second flight was more familiar to the subjects, who also became accustomed to the simulator's environment. This was observed with all three illusions. In the case of the somatogyral illusion, this effect can be assumed since the subjects mostly did not register it. In the context of the Coriolis and somatogyral illusions, it can be inferred that due to the strong manifestation of these illusions, the unusual situation was recognized by the pilots and was not mentally demanding for them. This may also have been influenced by the fact that these were simulated flights and the subjects were not in any real danger.
- Based on the analysis of cardiac activity, it is evident that the psychophysiological state of subjects was different during flights with illusions and without them. Contrary to assumptions, however, higher workload levels were observed in flights without illusions. These flights always took place first. Therefore, it is possible that a habituation effect occurred, as the second flight was more familiar to the subjects, who also became accustomed to the simulator's environment. This was observed with all three illusions. In the case of the somatogyral illusion, this effect can be assumed since the subjects mostly did not register it. In the context of the Coriolis and somatogyral illusions, it can be inferred

that due to the strong manifestation of these illusions, the unusual situation was recognized by the pilots and was not mentally demanding for them. This may also have been influenced by the fact that these were simulated flights and the subjects were not in any real danger.

- Regarding postural stability, it can be stated that the effects of the illusions did not have a negative impact. On the contrary, a so-called learning effect can be observed, where the subjects' stability improved with subsequent measurements.

References

1. ASSOCIATION, World Medical et al. World Medical Association Declaration of Helsinki: ethical principles for medical research involving human subjects. *Jama*. 2013, vol. 310, no. 20, pp. 2191–2194.
2. HONEGGER, F.; SPIJKER, G. van; ALLUM, J. H. J. Coordination of the head with respect to the trunk and pelvis in the roll and pitch planes during quiet stance. *Neuroscience* [online]. 2012, vol. 213, pp. 62–71 [visited on 2016-05-16]. ISSN 03064522. Available from DOI: [10.1016/j.neuroscience.2012.04.017](https://doi.org/10.1016/j.neuroscience.2012.04.017).
3. KUTILEK, P.; SOCHA, V.; ČAKRT, O.; SCHLENKER, J.; BIZOVSKA, L. Trajectory length of pitch vs. roll: Technique for assessment of postural stability. *Acta Gymnica* [online]. 2015, vol. 45, no. 2, pp. 85–92 [visited on 2016-05-16]. ISSN 23364912, ISSN 23364920. Available from DOI: [10.5507/ag.2015.008](https://doi.org/10.5507/ag.2015.008).
4. BERGSON, E.; SATALOFF, R. T. Preoperative computerized dynamic posturography as a prognostic indicator of balance function in patients with acoustic neuroma. *Ear, Nose, & Throat Journal*. 2005, vol. 84, no. 3, pp. 154–156. ISSN 0145-5613.
5. HORAK, F. B.; NASHNER, L. M. Central programming of postural movements: adaptation to altered support-surface configurations. *Journal of Neurophysiology*. 1986-06, vol. 55, no. 6, pp. 1369–1381. ISSN 0022-3077.
6. MAGNUSSON, M.; ENBOM, H.; JOHANSSON, R.; PYYKKÖ, I. Significance of pressor input from the human feet in anterior-posterior postural control. The effect of hypothermia on vibration-induced body-sway. *Acta Oto-Laryngologica*. 1990, vol. 110, no. 3, pp. 182–188. ISSN 0001-6489.
7. PATEL, M.; FRANSSON, P. A.; LUSH, D.; GOMEZ, S. The effect of foam surface properties on postural stability assessment while standing. *Gait & Posture* [online]. 2008, vol. 28, no. 4, pp. 649–656 [visited on 2016-05-16]. ISSN 09666362. Available from DOI: [10.1016/j.gaitpost.2008.04.018](https://doi.org/10.1016/j.gaitpost.2008.04.018).
8. NURSE, M. A.; HULLIGER, M.; WAKELING, J. M.; NIGG, B. M.; STEFANYSHYN, D. J. Changing the texture of footwear can alter gait patterns. *Journal of Electromyography and Kinesiology: Official Journal of the International Society of Electrophysiological Kinesiology*. 2005, vol. 15, no. 5, pp. 496–506. ISSN 1050-6411. Available from DOI: [10.1016/j.jelekin.2004.12.003](https://doi.org/10.1016/j.jelekin.2004.12.003).
9. ČAKRT, O.; VYHNÁLEK, M.; SLABÝ, K.; FUNDA, T.; VUILLERME, N.; KOLÁŘ, P.; JEŘÁBEK, J. Balance rehabilitation therapy by tongue electro-tactile biofeedback in patients with degenerative cerebellar disease. *NeuroRehabilitation*. 2012, vol. 31, no. 4, pp. 429–434. ISSN 1878-6448. Available from DOI: [10.3233/NRE-2012-00813](https://doi.org/10.3233/NRE-2012-00813).
10. HOUDIJK, H.; FICKERT, R.; VELZEN, J. van; BENNEKOM, C. van. The energy cost for balance control during upright standing. *Gait & Posture* [online]. 2009, vol. 30, no. 2, pp. 150–154 [visited on 2016-05-16]. ISSN 09666362. Available from DOI: [10.1016/j.gaitpost.2009.05.009](https://doi.org/10.1016/j.gaitpost.2009.05.009).
11. SCHUBERT, P.; KIRCHNER, M.; SCHMIDTBLEICHER, D.; HAAS, C. T. About the structure of posturography: Sampling duration, parametrization, focus of attention (part I). *Journal of Biomedical Science and Engineering* [online]. 2012, vol. 05, no. 9, pp. 496–507 [visited on 2016-05-16]. ISSN 1937-6871, ISSN 1937-688X. Available from DOI: [10.4236/jbise.2012.59062](https://doi.org/10.4236/jbise.2012.59062).

12. CASTELLI, L.; STOCCHI, L.; PATRIGNANI, M.; SELBITTO, G.; GIULIANI, M.; PROSPERINI, L. We-Measure: Toward a low-cost portable posturography for patients with multiple sclerosis using the commercial Wii balance board. *Journal of the Neurological Sciences* [online]. 2015, vol. 359, no. 1, pp. 440–444 [visited on 2016-05-16]. ISSN 0022510X. Available from DOI: [10.1016/j.jns.2015.10.016](https://doi.org/10.1016/j.jns.2015.10.016).
13. LLORENS, R.; LATORRE, J.; NOÉ, E.; KESHNER, E. A. Posturography using the Wii Balance Board™. *Gait & Posture* [online]. 2016, vol. 43, pp. 228–232 [visited on 2016-05-16]. ISSN 09666362. Available from DOI: [10.1016/j.gaitpost.2015.10.002](https://doi.org/10.1016/j.gaitpost.2015.10.002).
14. NAGYMÁTÉ, Gergely; ORLOVITS, Zsanett; KISS, Rita M. Reliability analysis of a sensitive and independent stabilometry parameter set. *PLOS ONE*. 2018, vol. 13, no. 4, e0195995. ISSN 1932-6203. Available from DOI: [10.1371/journal.pone.0195995](https://doi.org/10.1371/journal.pone.0195995).
15. BISWAS, Uzzal; GOH, Choon-Hian; OOI, Sze-Yuan; LIM, Einly; REDMOND, Stephen James; LOVELL, Nigel Hamilton. Chapter 12 - Telemedicine systems to manage chronic disease. In: GODFREY, Alan; STUART, Sam (eds.). *Digital Health*. Academic Press, 2021, pp. 177–195. ISBN 978-0-12-818914-6. Available from DOI: <https://doi.org/10.1016/B978-0-12-818914-6.00020-X>.
16. HOSHI, Rosangela Akemi; PASTRE, Carlos Marcelo; VANDERLEI, Luiz Carlos Marques; GODOY, Moacir Fernandes. Poincaré plot indexes of heart rate variability: Relationships with other nonlinear variables. *Autonomic Neuroscience*. 2013, vol. 177, no. 2, pp. 271–274. Available from DOI: [10.1016/j.autneu.2013.05.004](https://doi.org/10.1016/j.autneu.2013.05.004).
17. PISKORSKI, Jarosław; GUZIK, Przemysław. Filtering poincare plots. *Computational methods in science and technology*. 2005, vol. 11, no. 1, pp. 39–48.
18. SHAFFER, Fred; GINSBERG, Jay P. An overview of heart rate variability metrics and norms. *Frontiers in public health*. 2017, p. 258.
19. ESTEBAN, Rebeca Goya. Heart rate variability characterization using entropy measures. *Faculdade de Engenharia da Universidade do Porto*. 2008.
20. FURMAN, J. M.; BALOH, R. W.; BARIN, K. Assessment: posturography. Report of the Therapeutics and Technology Assessment Subcommittee of the American Academy of Neurology. *Neurology*. 1993, vol. 43, no. 6, pp. 1261–1264. ISSN 0028-3878.
21. WINTER, D. A.; PATLA, A. E.; FRANK, J. S. Assessment of balance control in humans. *Medical Progress Through Technology*. 1990, vol. 16, no. 1, pp. 31–51. ISSN 0047-6552.
22. PROSPERINI, L.; POZZILLI, C. The Clinical Relevance of Force Platform Measures in Multiple Sclerosis: A Review. *Multiple Sclerosis International* [online]. 2013, vol. 2013, pp. 1–9 [visited on 2016-05-16]. ISSN 2090-2654, ISSN 2090-2662. Available from DOI: [10.1155/2013/756564](https://doi.org/10.1155/2013/756564).
23. BROWNE, J.; O'HARE, N. Development of a novel method for assessing balance: the quantitative posturography system. *Physiological Measurement*. 2000, vol. 21, no. 4, pp. 525–534. ISSN 0967-3334.
24. SCHUBERT, P.; KIRCHNER, M. Ellipse area calculations and their applicability in posturography. *Gait & Posture* [online]. 2014, vol. 39, no. 1, pp. 518–522 [visited on 2016-05-16]. ISSN 09666362. Available from DOI: [10.1016/j.gaitpost.2013.09.001](https://doi.org/10.1016/j.gaitpost.2013.09.001).

25. LEE, D. T.; SCHACHTER, B. J. Two algorithms for constructing a Delaunay triangulation. *International Journal of Computer and Information Sciences*. 1980, vol. 9, no. 3, pp. 219–242.

Appendices

Appendix 1 Flight profile 1 for Stage 1

Appendix 2 Flight profile 2 for Stage 1

Appendix 3 Flight profile 3 for Stage 1

Appendix 4 Flight profile 1 for Stage 2

Appendix 5 Flight profile 2 for Stage 2

Appendix 1

Flight profile 1 for Stage 1

PROFILE 1 for Stage 1

Voice Message

Start Time	30.00 s	Message Name	DF_1_1_1.wav
Duration	4.43 s	Volume	50
Message: "Oscar Kilo Romeo Alpha Lima, turn left heading 0 9 0"			

Voice Message

Start Time	90.00 s	Message Name	DF_1_1_2.wav
Duration	6.36 s	Volume	50
Message: "Oscar Alpha Lima, descend 2 thousand 5 hundred feet altitude, maintain five hundred feet per minute"			

Visibility

Start Time	166.00 s	Condition	Haze
Visibility Distance	17 mi	Top	600 ft
Brown Out	Disabled	WhiteOut	Disabled

Visibility

Start Time	169.00 s	Condition	Haze
Visibility Distance	13.5 mi	Top	600 ft
Brown Out	Disabled	White Out	Disabled

Voice Message

Start Time	170.00 s	Message Name	DF_1_1_3.wav
Duration	3.28 s	Volume	50
Message: "Oscar Alpha Lima, turn left heading 3 6 0"			

Visibility

Start Time	173.00 s	Condition	Haze
Visibility Distance	10 mi	Top	600 ft
Brown Out	Disabled	WhiteOut	Disabled

Middle Level Clouds

Start Time	176.00 s	Type	AltoCumulus
Coverage	02.VIII	Base	200 ft
Height	4000 ft	Slope	0 deg
Axis Heading	0 deg		

Middle Level Clouds

Start Time	181.00 s	Type	AltoCumulus
Coverage	4/8	Base	200 ft
Height	4000 ft	Slope	0 deg
Axis Heading	0 deg		

Middle Level Clouds

Start Time	184.00 s	Type	<i>AltoCumulus</i>
Coverage	4/8	Base	200 ft
Height	4000 ft	Slope	0 deg
Axis Heading	0 deg		

Visibility

Start Time	186.00 s	Condition	<i>Rain</i>
Visibility Distance	5 mi	Top	200 ft
Brown Out	<i>Disabled</i>	WhiteOut	<i>Disabled</i>

Middle Level Clouds

Start Time	188.00 s	Type	<i>AltoCumulus</i>
Coverage	5/8	Base	200 ft
Height	4000 ft	Slope	0 deg
Axis Heading	0 deg		

Middle Level Clouds

Start Time	192.00 s	Type	<i>AltoCumulus</i>
Coverage	08.VIII	Base	200 ft
Height	5000 ft	Slope	0 deg
Axis Heading	0 deg		

Voice Message

Start Time	234.00 s	Message Name	<i>DF_1_1_4.wav</i>
Duration	3.09 s	Volume	50
Message: "Oscar Alpha Lima, turn left heading 1 1 0"			

Condition

Start Time	237.00 s	Condition	Roll Angle < -5.00 deg
------------	----------	-----------	------------------------

Yaw

Start Time	238.00 s	Command Type	<i>Velocity</i>
Velocity	-60.00 deg/s	Acceleration	1.50 deg/s ²
Duration	40.00 s		

Condition

Start Time	279.00 s	Condition	Heading < 210.00 deg
------------	----------	-----------	----------------------

Voice Message

Start Time	285.00 s	Message Name	<i>DF_1_1_6.wav</i>
Duration	3.14 s	Volume	50
Message: "Oscar Alpha Lima, level off and fly present heading"			

Condition

Start Time	288.00 s	Condition	Roll Angle > -15.00 deg
------------	----------	-----------	-------------------------

Yaw

Start Time	289.00 s	Command Type	Velocity
Velocity	0.00 deg/s	Acceleration	12.00 deg/s ²
Duration	5.01 s		

Visibility

Start Time	310.00 s	Condition	Clear
Visibility Distance	5 mi	Top	800 ft
BrownOut	Disabled	WhiteOut	Disabled

Voice Message

Start Time	341.00 s	Message Name	DF_1_1_7.wav
Duration	6.36 s	Volume	50
Message: "Oscar Alpha Lima, climb altitude 3 thousand feet, maintain rate of climb 7 hundred feet per minute"			

Voice Message

Start Time	386.00 s	Message Name	DF_1_1_8.wav
Duration	3.40 s	Volume	50
Message: "Oscar Alpha Lima, turn left heading 0 3 0"			

Voice Message

Start Time	466.00 s	Message Name	DF_1_1_9.wav
Duration	5.27 s	Volume	50
Message: "Oscar Alpha Lima, make a right 3 60, maintain 45 degree bank turn"			

Voice Message

Start Time	531.00 s	Message Name	DF_1_1_10.wav
Duration	4.88 s	Volume	50
Message: "Oscar Alpha Lima, contact Honolulu Approach, 1 1 8 decimal 3"			

Voice Message

Start Time	564.00 s	Message Name	DF_1_1_11.wav
Duration	8.44 s	Volume	50
Message: "Oscar Kilo Romeo Alpha Lima, starting from this heading, make a right turn 20 degree banked level turn and hold the turn until I'll tell you to roll out"			

Condition

Start Time	573.00 s	Condition	Roll Angle > 5.00 deg
------------	----------	-----------	-----------------------

Roll

Start Time	574.00 s	Command Type	Position
Position	3.00 deg	Velocity	0.30 deg/s
Acceleration	0.30 deg/s ²	Duration	11.00 s

Yaw

Start Time	574.00 s	Command Type	Velocity
Velocity	16.00 deg/s	Acceleration	0.50 deg/s ²
Duration	32.00 s		

Condition

Start Time	607.00 s	Condition	Heading > 270.00 deg
------------	----------	-----------	----------------------

Voice Message

Start Time	608.00 s	Message Name	DF_1_1_12.wav
Duration	3.92 s	Volume	50
Message: "Oscar Alpha Lima, roll to wings level and maintain your heading"			

Condition

Start Time	612.00 s	Condition	Roll Angle < 15.00 deg
------------	----------	-----------	------------------------

Roll

Start Time	613.00 s	Command Type	Position
Position	-3.00 deg	Velocity	4.00 deg/s
Acceleration	10.00 deg/s ²	Duration	1.90 s

Yaw

Start Time	613.00 s	Command Type	Velocity
Velocity	0.00 deg/s	Acceleration	2.00 deg/s ²
Duration	8.00 s		

Roll

Start Time	614.90 s	Command Type	Position
Position	0.00 deg	Velocity	0.20 deg/s
Acceleration	0.10 deg/s ²	Duration	17.00 s

Voice Message

Start Time	706.00 s	Message Name	DF_1_1_13.wav
Duration	3.36 s	Volume	50
Message: "Oscar Alpha Lima, reduce speed to eight zero knots"			

Visibility

Start Time	717.00 s	Condition	Haze
Visibility Distance	10 mi	Top	600 ft
BrownOut	Disabled	WhiteOut	Disabled

Middle Level Clouds

Start Time	718.00 s	Type	AltoCumulus
Coverage	5/8	Base	200 ft
Height	4000 ft	Slope	0 deg
Axis Heading	0 deg		

Middle Level Clouds

Start Time	721.00 s	Type	AltoCumulus
Coverage	4/8	Base	200 ft
Height	4000 ft	Slope	0 deg
Axis Heading	0 deg		

Voice Message

Start Time	761.00 s	Message Name	DF_1_1_14.wav
Duration	6.35 s	Volume	50
Message: "Oscar Alpha Lima, turn left heading 1 4 0 and descend altitude 2 thousand 5 hundred feet "			

Voice Message

Start Time	841.00 s	Message Name	DF_1_1_15.wav
Duration	4.48 s	Volume	50
Message: "Oscar Alpha Lima, Contact Honolulu Tower 1 1 8 decimal 1"			

Voice Message

Start Time	871.00 s	Message Name	DF_1_1_16.wav
Duration	3.65 s	Volume	50
Message: "Oscar Alpha Lima, increase speed to one one zero knots "			

Voice Message

Start Time	920.00 s	Message Name	DF_1_1_17.wav
Duration	3.35 s	Volume	50
Message: "Oscar Alpha Lima, turn left heading 0 6 0"			

Voice Message

Start Time	975.00 s	Message Name	DF_1_1_18.wav
Duration	8.45 s	Volume	50
Message: "Oscar Alpha Lima, make a smooth 30 degrees banked turn"			

Condition

Start Time	980.00 s	Condition	Roll Angle > 10.00 deg
------------	----------	-----------	------------------------

Yaw

Start Time	981.00 s	Command Type	Velocity
Velocity	60.00 deg/s	Acceleration	2.00 deg/s ²
Duration	30.00 s		

Voice Message

Start Time	1002.00 s	Message Name	DF_1_1_19_5.wav
Duration	3.20 s	Volume	50
Message: "Oscar Alpha Lima, turn right heading 3 6 0"			

Condition

Start Time	1012.00 s	Condition	Heading > 220.00 deg
------------	-----------	-----------	----------------------

Voice Message

Start Time	1013.00 s	Message Name	DF_1_1_20.wav
Duration	3.73 s	Volume	50
Message: "Oscar Alpha Lima, can you check that the COM speaker is off?"			

Voice Message

Start Time	1017.00 s	Message Name	DF_1_1_21.wav
Duration	2.85 s	Volume	50
Message: "It is on the left side console towards the rear. "			

Condition

Start Time	1020.00 s	Condition	Heading > 5.00 deg
------------	-----------	-----------	--------------------

Condition

Start Time	1021.00 s	Condition	Roll Angle < 15.00 deg
------------	-----------	-----------	------------------------

Yaw

Start Time	1022.00 s	Command Type	Velocity
Velocity	0.00 deg/s	Acceleration	1.00 deg/s ²
Duration	60.00 s		

Voice Message

Start Time	1089.00 s	Message Name	DF_1_1_22.wav
Duration	3.44 s	Volume	50
Message: "Oscar Alpha Lima, turn left heading 2 0 0 "			

Voice Message

Start Time	1120.00 s	Message Name	DF_1_1_23.wav
Duration	6.85 s	Volume	50
Message: "Oscar Alpha Lima, descend altitude 1 thousand 6 hundred feet and maintain rate of descent 5 hundred feet per minute"			

Voice Message

Start Time	1340.00 s	Message Name	DF_1_1_24.wav
Duration	3.13 s	Volume	50
Message: "Oscar Alpha Lima, turn left heading 1 4 0"			

Visibility

Start Time	1390.00 s	Condition	Haze
Visibility Distance	7 mi	Top	600 ft
BrownOut	Disabled	WhiteOut	Disabled

Visibility

Start Time	1395.00 s	Condition	Haze
Visibility Distance	3.5 mi	Top	600 ft
BrownOut	Disabled	WhiteOut	Disabled

Visibility

Start Time	1400.00 s	Condition	Haze
Visibility Distance	1 mi	Top	600 ft
BrownOut	Disabled	WhiteOut	Disabled

Voice Message

Start Time	1400.00 s	Message Name	DF_1_1_25.wav
Duration	4.59 s	Volume	50
Message: "Oscar Alpha Lima, contact Honolulu approach 1 2 4 decimal 8"			

Voice Message

Start Time	1436.00 s	Message Name	DF_1_1_26.wav
Duration	7.23 s	Volume	50
Message: "Oscar Kilo Romeo Alpha Lima, descend altitude 5 hundred feet, at 6 5 knots, flaps full"			

Condition

Start Time	1443.00 s	Condition	Altitude (MSL) < 550.00 ft
------------	-----------	-----------	----------------------------

Condition

Start Time	1444.00 s	Condition	Airspeed < 70.00 knots
------------	-----------	-----------	------------------------

Voice Message

Start Time	1445.00 s	Message Name	DF_1_1_27.wav
Duration	4.71 s	Volume	50
Message: "Oscar Alpha Lima, Go around and climb straight ahead atitude 3 thousand feet "			

Condition

Start Time	1450.00 s	Condition	Airspeed > 70.00 knots
------------	-----------	-----------	------------------------

Pitch

Start Time	1451.00 s	Command Type	Position
Position	12.00 deg	Velocity	4.00 deg/s
Acceleration	1.30 deg/s ²	Duration	6.08 s

Pitch

Start Time	1457.10 s	Command Type	Position
Position	0.00 deg	Velocity	1.00 deg/s
Acceleration	0.30 deg/s ²	Duration	15.33 s

Profile End

Profile End Time	1800.00 s
------------------	-----------

Appendix 2

Flight profile 2 for Stage 1

PROFILE 2 for Stage 1

Voice Message

Start Time	27.00 s	Message Name	DF_2_1_1.wav
Duration	9.11 s	Volume	50
Message: "Oscar Kilo Romeo Alpha Lima, runway 2 6 cleared for take off, when airborne maintain runway heading and climb altitude three thousand feet "			

Condition

Start Time	36.00 s	Condition	Pitch Angle > 5.00 deg
------------	---------	-----------	------------------------

Pitch

Start Time	37.00 s	Command Type	Position
Position	12.00 deg	Velocity	4.00 deg/s
Acceleration	1.30 deg/s ²	Duration	6.08 s

Pitch

Start Time	43.10 s	Command Type	Position
Position	0.00 deg	Velocity	1.00 deg/s
Acceleration	0.30 deg/s ²	Duration	15.33 s

Visibility

Start Time	50.00 s	Condition	Haze
Visibility Distance	40 mi	Top	200 ft
BrownOut	Disabled	WhiteOut	Disabled

Condition

Start Time	59.00 s	Condition	Distance > 3.00 mile(s) from Lat : 21°
------------	---------	-----------	---

Voice Message

Start Time	60.00 s	Message Name	DF_2_1_2.wav
Duration	5.97 s	Volume	50
Message: "Oscar Alpha Lima contact honolulu approach frequency 1 2 4 decimal 8, good day"			

Middle Level Clouds

Start Time	70.00 s	Type	Stratocumulus
Coverage	3/8	Base	1000 ft
Height	5000 ft	Slope	0 deg
Axis Heading	0 deg		

Middle Level Clouds

Start Time	75.00 s	Type	Stratocumulus
Coverage	4/8	Base	1000 ft
Height	5000 ft	Slope	0 deg
Axis Heading	0 deg		

Middle Level Clouds

Start Time	80.00 s	Type	Stratocumulus
Coverage	5/8	Base	1000 ft
Height	5000 ft	Slope	0 deg
Axis Heading	0 deg		

Middle Level Clouds

Start Time	85.00 s	Type	Stratocumulus
Coverage	8/8	Base	1000 ft
Height	5000 ft	Slope	0 deg
Axis Heading	0 deg		

Voice Message

Start Time	86.00 s	Message Name	DF_2_1_2_5.wav
Duration	3.90 s	Volume	50
Message: "Oscar Kilo Romeo Alpha Lima, good day, radar contact"			

Condition

Start Time	90.00 s	Condition	Distance > 5.00 mile(s) from Lat : 21°
------------	---------	-----------	---

Voice Message

Start Time	91.00 s	Message Name	DF_2_1_3.wav
Duration	9.11 s	Volume	50
Message: "Oscar Alpha Lima turn left heading 1 4 0 and intercept radial 1 7 5 outbound Hotel November Lima V O R"			

Condition

Start Time	100.00 s	Condition	Heading < 180.00 deg
------------	----------	-----------	----------------------

Voice Message

Start Time	101.00 s	Message Name	DF_2_1_4.wav
Duration	4.26 s	Volume	50
Message: "Oscar Alpha Lima due to traffic turn left heading 0 4 0"			

Condition

Start Time	105.00 s	Condition	Heading < 55.00 deg
------------	----------	-----------	---------------------

Middle Level Clouds

Start Time	120.00 s	Type	Stratocumulus
Coverage	5/8	Base	1000 ft
Height	5000 ft	Slope	0 deg
Axis Heading	0 deg		

Low Level Clouds

Start Time	122.00 s	Type	AltoCumulus
Coverage	3/8	Base	100 ft
Height	1000 ft	Slope	0 deg
Axis Heading	0 deg		

Middle Level Clouds

Start Time	123.00 s	Type	Stratocumulus
Coverage	4/8	Base	1000 ft
Height	5000 ft	Slope	0 deg
Axis Heading	0 deg		

Middle Level Clouds

Start Time	126.00 s	Type	Stratocumulus
Coverage	3/8	Base	1000 ft
Height	5000 ft	Slope	0 deg
Axis Heading	0 deg		

Voice Message

Start Time	146.00 s	Message Name	DF_2_1_5.wav
Duration	4.31 s	Volume	50
Message: "Oscar Alpha Lima continue direct Hotel November Lima V O R"			

Condition

Start Time	151.00 s	Condition	Distance < 2.00 mile(s) from Lat : 21° 18' 29.91"
------------	----------	-----------	--

Voice Message

Start Time	152.00 s	Message Name	DF_2_1_6.wav
Duration	5.59 s	Volume	50
Message: "Oscar Alpha Lima after passing Hotel November Lima V O R make base turn as published"			

Condition

Start Time	151.00 s	Condition	Distance > 3.00 mile(s) from Lat : 21° 18' 29.91"
------------	----------	-----------	--

Voice Message

Start Time	159.00 s	Message Name	DF_2_1_7.wav
Duration	3.54 s	Volume	50
Message: "Oscar Alpha Lima climb altitude 4 thousand feet"			

Middle Level Clouds

Start Time	160.00 s	Type	Stratocumulus
Coverage	4/8	Base	1000 ft
Height	5000 ft	Slope	0 deg
Axis Heading	0 deg		

Middle Level Clouds

Start Time	160.50 s	Type	Stratocumulus
Coverage	5/8	Base	1000 ft
Height	5000 ft	Slope	0 deg
Axis Heading	0 deg		

Middle Level Clouds

Start Time	161.50 s	Type	Stratocumulus
Coverage	8/8	Base	1000 ft
Height	5000 ft	Slope	0 deg
Axis Heading	0 deg		

Condition

Start Time	163.00 s	Condition	Distance > 4.00 mile(s) from Lat : 21° 18' 29.91
------------	----------	-----------	---

Condition

Start Time	164.00 s	Condition	Roll Angle < -5.00 deg
------------	----------	-----------	------------------------

Pitch

Start Time	165.00 s	Command Type	Position
Position	5.00 deg	Velocity	1.00 deg/s
Acceleration	0.30 deg/s ²	Duration	8.33 s

Roll

Start Time	165.00 s	Command Type	Position
Position	-3.00 deg	Velocity	0.30 deg/s
Acceleration	0.30 deg/s ²	Duration	11.00 s

Yaw

Start Time	165.00 s	Command Type	Velocity
Position	-16.00 deg/s	Velocity	0.50 deg/s ²
Acceleration	32.00 s		

Condition

Start Time	198.00 s	Condition	Heading < 275.00 deg
------------	----------	-----------	----------------------

Condition

Start Time	199.00 s	Condition	Roll Angle > -10.00 deg
------------	----------	-----------	-------------------------

Pitch

Start Time	200.00 s	Command Type	Position
Position	0.00 deg	Velocity	1.00 deg/s
Acceleration	0.30 deg/s ²	Duration	8.33 s

Roll

Start Time	200.00 s	Command Type	Position
Position	3.00 deg	Velocity	4.00 deg/s
Acceleration	10.00 deg/s ²	Duration	1.90 s

Yaw

Start Time	200.00 s	Command Type	Velocity
Position	0.00 deg/s	Velocity	2.00 deg/s ²
Acceleration	8.00 s		

Roll

Start Time	201.90 s	Command Type	Position
Position	0.00 deg	Velocity	0.20 deg/s
Acceleration	0.10 deg/s ²	Duration	17.00 s

Condition

Start Time	220.00 s	Condition	Distance < 3.00 mile(s) from Lat : 21° 18' 29.91"
------------	----------	-----------	--

Voice Message

Start Time	221.00 s	Message Name	DF_2_1_8.wav
Duration	4.06 s	Volume	50
Message: "Oscar Alpha Lima hold over Hotel November Lima as publised"			

Condition

Start Time	225.00 s	Condition	Longitude < -157° 57' 31.38"
------------	----------	-----------	------------------------------

Middle Level Clouds

Start Time	225.20 s	Type	Stratocumulus
Coverage	5/8	Base	1000 ft
Height	5000 ft	Slope	0 deg
Axis Heading	0 deg		

Middle Level Clouds

Start Time	225.80 s	Type	Stratocumulus
Coverage	4/8	Base	1000 ft
Height	5000 ft	Slope	0 deg
Axis Heading	0 deg		

Middle Level Clouds

Start Time	225.90 s	Type	Stratocumulus
Coverage	2/8	Base	1000 ft
Height	5000 ft	Slope	0 deg
Axis Heading	0 deg		

Condition

Start Time	226.00 s	Condition	Longitude > -157° 56' 0.29"
------------	----------	-----------	-----------------------------

Condition

Start Time	227.00 s	Condition	Roll Angle < -5.00 deg
------------	----------	-----------	------------------------

Yaw

Start Time	228.00 s	Command Type	Velocity
Position	-60.00 deg/s	Velocity	2.00 deg/s ²
Acceleration	30.00 s		

Condition

Start Time	259.00 s	Condition	Heading not between 10.00 and 190.00 deg
------------	----------	-----------	--

Voice Message

Start Time	260.00 s	Message Name	DF_2_1_9.wav
Duration	3.73 s	Volume	50
Message: "Oscar Alpha Lima can you check that the com speaker is off?"			

Condition

Start Time	264.00 s	Condition	Heading < 290.00 deg
------------	----------	-----------	----------------------

Condition

Start Time	265.00 s	Condition	Roll Angle > -8.00 deg
------------	----------	-----------	------------------------

Yaw

Start Time	266.00 s	Command Type	Velocity
Position	0.00 deg/s	Velocity	1.00 deg/s ²
Acceleration	60.00 s		

Condition

Start Time	327.00 s	Condition	Longitude < -157° 57' 31.38"
------------	----------	-----------	------------------------------

Condition

Start Time	328.00 s	Condition	Longitude > -157° 57' 31.38"
------------	----------	-----------	------------------------------

Condition

Start Time	329.00 s	Condition	Longitude > -157° 56' 0.29"
------------	----------	-----------	-----------------------------

Condition

Start Time	330.00 s	Condition	Longitude < -157° 57' 31.38"
------------	----------	-----------	------------------------------

Condition

Start Time	331.00 s	Condition	Heading < 150.00 deg
------------	----------	-----------	----------------------

Voice Message

Start Time	332.00 s	Message Name	DF_2_1_11.wav
Duration	5.80 s	Volume	50
Message: "Oscar Alpha Lima after passing Hotel November Lima V O R intercept radial 1 3 8"			

Middle Level Clouds

Start Time	400.00 s	Type	Stratocumulus
Coverage	3/8	Base	1000 ft
Height	5000 ft	Slope	0 deg
Axis Heading	0 deg		

Middle Level Clouds

Start Time	402.00 s	Type	Stratocumulus
Coverage	4/8	Base	1000 ft
Height	5000 ft	Slope	0 deg
Axis Heading	0 deg		

Middle Level Clouds

Start Time	403.00 s	Type	Stratocumulus
Coverage	4/8	Base	1000 ft
Height	5000 ft	Slope	0 deg
Axis Heading	0 deg		

Condition

Start Time	404.00 s	Condition	Distance > 3.00 mile(s) from Lat : 21° 18' 29.91"
------------	----------	-----------	--

Middle Level Clouds

Start Time	404.50 s	Type	Stratocumulus
Coverage	8/8	Base	1000 ft
Height	5000 ft	Slope	0 deg
Axis Heading	0 deg		

Voice Message

Start Time	405.00 s	Message Name	DF_2_1_12.wav
Duration	7.16 s	Volume	50
Message: "Oscar Alpha Lima descend altitude 3 thousand feet and continue continue 5 miles D M E from Hotel November Lima V O R and make a right procedure"			

Condition

Start Time	412.00 s	Condition	Heading > 170.00 deg
------------	----------	-----------	----------------------

Condition

Start Time	463.00 s	Condition	Roll Angle < -5.00 deg
------------	----------	-----------	------------------------

Yaw

Start Time	464.00 s	Command Type	Velocity
Position	-60.00 deg/s	Velocity	1.50 deg/s ²
Acceleration	40.00 s		

Condition

Start Time	505.00 s	Condition	Heading > 330.00 deg
------------	----------	-----------	----------------------

Condition

Start Time	506.00 s	Condition	Roll Angle > -15.00 deg
------------	----------	-----------	-------------------------

Yaw

Start Time	507.00 s	Command Type	Velocity
Position	0.00 deg/s	Velocity	12.00 deg/s ²
Acceleration	5.01 s		

Profile End

Profile End Time	800.00 s
------------------	----------

Appendix 3
Flight profile 3 for Stage 1

PROFILE 3 for Stage 1

Voice Message

Start Time	27.00 s	Message Name	DF_3_1_1.wav
Duration	6.94 s	Volume	50
Message: "Oscar Kilo Romeo Alpha Lima runway 0 4 cleared for take off, climb altitude 3 thousand feet"			

Condition

Start Time	34.00 s	Condition	Heading > 160.00 deg
------------	---------	-----------	----------------------

Voice Message

Start Time	35.00 s	Message Name	DF_3_1_2.wav
Duration	4.95 s	Volume	50
Message: "Oscar Alpha Lima contact Honolulu Approach 1 2 4 decimal 7"			

Voice Message

Start Time	55.00 s	Message Name	DF_3_1_3.wav
Duration	4.24 s	Volume	50
Message: "Oscar Kilo Romeo Alpha Lima, good day, radar contact"			

Condition

Start Time	59.00 s	Condition	Heading > 140.00 deg
------------	---------	-----------	----------------------

Visibility

Start Time	59.01 s	Condition	Haze
Visibility Distance	30 mi	Top	200 ft
BrownOut	Disabled	WhiteOut	Disabled

Visibility

Start Time	59.50 s	Condition	Haze
Visibility Distance	20 mi	Top	200 ft
BrownOut	Disabled	WhiteOut	Disabled

Visibility

Start Time	60.00 s	Condition	Haze
Visibility Distance	10 mi	Top	200 ft
BrownOut	Disabled	WhiteOut	Disabled

Condition

Start Time	60.00 s	Condition	Altitude (MSL) > 2800.00 ft
------------	---------	-----------	-----------------------------

Low Level Clouds

Start Time	60.50 s	Type	AltoCumulus
Coverage	2/8	Base	500 ft
Height	4000 ft	Slope	0 deg
Axis Heading	0 deg		

Low Level Clouds

Start Time	63.00 s	Type	AltoCumulus
Coverage	3/8	Base	500 ft
Height	4000 ft	Slope	0 deg
Axis Heading	0 deg		

Low Level Clouds

Start Time	69.00 s	Type	AltoCumulus
Coverage	5/8	Base	500 ft
Height	4000 ft	Slope	0 deg
Axis Heading	0 deg		

Low Level Clouds

Start Time	72.00 s	Type	AltoCumulus
Coverage	8/8	Base	500 ft
Height	4000 ft	Slope	0 deg
Axis Heading	0 deg		

Voice Message

Start Time	75.00 s	Message Name	DF_3_1_4.wav
Duration	4.44 s	Volume	50
Message: "Oscar Alpha Lima turn Right inbound Hotel November Lima V O R"			

Condition

Start Time	80.00 s	Condition	Roll Angle > 5.00 deg
------------	---------	-----------	-----------------------

Yaw

Start Time	81.00 s	Command Type	Velocity
Position	60.00 deg/s	Velocity	1.50 deg/s ²
Acceleration	40.00 s		

Condition

Start Time	122.00 s	Condition	Roll Angle < 8.00 deg
------------	----------	-----------	-----------------------

Yaw

Start Time	123.00 s	Command Type	Velocity
Position	0.00 deg/s	Velocity	12.00 deg/s ²
Acceleration	5.01 s		

Visibility

Start Time	125.00 s	Condition	Haze
Visibility Distance	30 mi	Top	200 ft
BrownOut	Disabled	WhiteOut	Disabled

Low Level Clouds

Start Time	126.00 s	Type	AltoCumulus
Coverage	5/8	Base	500 ft
Height	4000 ft	Slope	0 deg
Axis Heading	0 deg		

Low Level Clouds

Start Time	129.00 s	Type	AltoCumulus
Coverage	4/8	Base	500 ft
Height	4000 ft	Slope	0 deg
Axis Heading	0 deg		

Low Level Clouds

Start Time	132.00 s	Type	AltoCumulus
Coverage	3/8	Base	500 ft
Height	4000 ft	Slope	0 deg
Axis Heading	0 deg		

Low Level Clouds

Start Time	135.00 s	Type	AltoCumulus
Coverage	2/8	Base	500 ft
Height	4000 ft	Slope	0 deg
Axis Heading	0 deg		

Voice Message

Start Time	173.00 s	Message Name	DF_3_1_5.wav
Duration	9.42 s	Volume	50
Message: "Oscar Alpha Lima after passing Hotel November Lima V O R, cleared for localizer approach runway 0 4 right, report established"			

Condition

Start Time	182.00 s	Condition	Heading between 227.00 and 237.00 deg
------------	----------	-----------	---------------------------------------

Condition

Start Time	184.00 s	Condition	Distance > 6.00 mile(s) from Lat : 21° 18' 29.91
------------	----------	-----------	--

Condition

Start Time	185.00 s	Condition	Heading between 182.00 and 192.00 deg
------------	----------	-----------	---------------------------------------

Low Level Clouds

Start Time	186.00 s	Type	AltoCumulus
Coverage	3/8	Base	500 ft
Height	4000 ft	Slope	0 deg
Axis Heading	0 deg		

Low Level Clouds

Start Time	189.00 s	Type	AltoCumulus
Coverage	4/8	Base	500 ft
Height	4000 ft	Slope	0 deg
Axis Heading	0 deg		

Low Level Clouds

Start Time	192.00 s	Type	AltoCumulus
Coverage	5/8	Base	500 ft
Height	4000 ft	Slope	0 deg
Axis Heading	0 deg		

Low Level Clouds

Start Time	195.00 s	Type	AltoCumulus
Coverage	8/8	Base	500 ft
Height	4000 ft	Slope	0 deg
Axis Heading	0 deg		

Visibility

Start Time	197.00 s	Condition	Haze
Visibility Distance	20 mi	Top	200 ft
BrownOut	Disabled	WhiteOut	Disabled

Condition

Start Time	226.00 s	Condition	Roll Angle > 5.00 deg
------------	----------	-----------	-----------------------

Roll

Start Time	227.00 s	Command Type	Position
Position	3.00 deg	Velocity	0.30 deg/s
Acceleration	0.30 deg/s ²	Duration	11.00 s

Yaw

Start Time	227.00 s	Command Type	Velocity
Position	16.00 deg/s	Velocity	0.50 deg/s ²
Acceleration	32.00 s		

Condition

Start Time	260.00 s	Condition	Roll Angle < 8.00 deg
------------	----------	-----------	-----------------------

Roll

Start Time	261.00 s	Command Type	Position
Position	-3.00 deg	Velocity	4.00 deg/s
Acceleration	10.00 deg/s ²	Duration	1.90 s

Yaw

Start Time	261.00 s	Command Type	Velocity
Position	0.00 deg/s	Velocity	2.00 deg/s ²
Acceleration	8.00 s		

Roll

Start Time	262.90 s	Command Type	Position
Position	0.00 deg	Velocity	0.20 deg/s
Acceleration	0.10 deg/s ²	Duration	17.00 s

Low Level Clouds

Start Time	263.00 s	Type	AltoCumulus
Coverage	5/8	Base	500 ft
Height	4000 ft	Slope	0 deg
Axis Heading	0 deg		

Visibility

Start Time	265.00 s	Condition	Haze
Visibility Distance	7 mi	Top	200 ft
BrownOut	Disabled	WhiteOut	Disabled

Low Level Clouds

Start Time	266.00 s	Type	AltoCumulus
Coverage	4/8	Base	500 ft
Height	4000 ft	Slope	0 deg
Axis Heading	0 deg		

Visibility

Start Time	268.00 s	Condition	Haze
Visibility Distance	3.5 mi	Top	200 ft
BrownOut	Disabled	WhiteOut	Disabled

Visibility

Start Time	270.00 s	Condition	Haze
Visibility Distance	1 mi	Top	200 ft
BrownOut	Disabled	WhiteOut	Disabled

Visibility

Start Time	273.00 s	Condition	Haze
Visibility Distance	0.2 mi	Top	200 ft
BrownOut	Disabled	WhiteOut	Disabled

Condition

Start Time	281.00 s	Condition	Altitude (MSL) < 550.00 ft
------------	----------	-----------	----------------------------

Condition

Start Time	282.00 s	Condition	Pitch Angle > 5.00 deg
------------	----------	-----------	------------------------

Pitch

Start Time	283.00 s	Command Type	Position
Position	12.00 deg	Velocity	4.00 deg/s
Acceleration	1.30 deg/s ²	Duration	6.08 s

Pitch

Start Time	289.10 s	Command Type	Position
Position	0.00 deg	Velocity	1.00 deg/s
Acceleration	0.30 deg/s ²	Duration	15.33 s

Visibility

Start Time	298.00 s	Condition	Haze
Visibility Distance	3 mi	Top	200 ft
BrownOut	Disabled	WhiteOut	Disabled

Visibility

Start Time	300.00 s	Condition	Haze
Visibility Distance	15 mi	Top	200 ft
BrownOut	Disabled	WhiteOut	Disabled

Visibility

Start Time	303.50 s	Condition	Haze
Visibility Distance	20 mi	Top	200 ft
BrownOut	Disabled	WhiteOut	Disabled

Visibility

Start Time	305.00 s	Condition	Haze
Visibility Distance	25 mi	Top	200 ft
BrownOut	Disabled	WhiteOut	Disabled

Condition

Start Time	306.00 s	Condition	Distance > 8.00 mile(s) from Lat : 21° 18' 29.91
------------	----------	-----------	---

Condition

Start Time	307.00 s	Condition	Distance < 7.00 mile(s) from Lat : 21° 18' 29.91
------------	----------	-----------	---

Condition

Start Time	308.00 s	Condition	Roll Angle > 5.00 deg
------------	----------	-----------	-----------------------

Yaw

Start Time	309.00 s	Command Type	Velocity
Position	60.00 deg/s	Velocity	2.00 deg/s ²
Acceleration	30.00 s		

Condition

Start Time	340.00 s	Condition	Heading > 91.00 deg
------------	----------	-----------	---------------------

Voice Message

Start Time	341.00 s	Message Name	DF_3_1_6.wav
Duration	8.52 s	Volume	50
Message: "OSKAR ALPHA Lima, this is Joe, could you please check you have the speaker off? The button is located on the left panel slightly behind you"			

Condition

Start Time	350.00 s	Condition	Roll Angle < 8.00 deg
------------	----------	-----------	-----------------------

Yaw

Start Time	351.00 s	Command Type	Velocity
Position	0.00 deg/s	Velocity	1.00 deg/s ²
Acceleration	60.00 s		

Voice Message

Start Time	416.00 s	Message Name	DF_3_1_7.wav
Duration	3.59 s	Volume	50
Message: "Oscar Alpha Lima climb altitude 4 thousand feet"			

Condition

Start Time	420.00 s	Condition	Distance > 8.00 mile(s) from Lat : 21° 18' 29.91
------------	----------	-----------	---

Voice Message

Start Time	476.00 s	Message Name	DF_3_1_8.wav
Duration	5.81 s	Volume	50
Message: "Oscar Alpha Lima, after passing ALANA, continue direct Hotel November N D B"			

Profile End

Profile End Time	800.00 s
------------------	----------

Appendix 4

Flight profile 1 for Stage 2

PROFILE 1 for Stage 2, without illusions

Voice Message

Start Time	30.00 s	Message Name	DF_2CAST_1_01.wav
Duration	10.13 s	Volume	50
Message: "Oscar Kilo Romeo Alpha Lima runway 0 8 right cleared for take off, when airborne maintain runway heading and climb altitude 1 thousand 5 hundred feet "			

Condition

Start Time	54.00 s	Condition	Altitude (MSL) > 1450.00 ft
------------	---------	-----------	-----------------------------

Voice Message

Start Time	69.00 s	Message Name	DF_2CAST_1_02.wav
Duration	3.13 s	Volume	50
Message: "Oscar Alpha Lima, turn right heading 1 6 0 "			

Condition

Start Time	70.00 s	Condition	Heading > 167.00 deg
------------	---------	-----------	----------------------

Voice Message

Start Time	90.00 s	Message Name	DF_2CAST_1_03.wav
Duration	3.42 s	Volume	50
Message: "Oscar Alpha Lima, climb altitude 2 thousand feet "			

Condition

Start Time	91.00 s	Condition	Altitude (MSL) > 1950.00 ft
------------	---------	-----------	-----------------------------

Low Level Clouds

Start Time	92.00 s	Type	AltoCumulus
Coverage	8/8	Base	1000 ft
Height	4000 ft	Slope	0 deg
Axis Heading	0 deg		

Visibility

Start Time	92.00 s	Condition	Clear
Visibility Distance	5 mi	Top	200 ft
BrownOut	Disabled	WhiteOut	Disabled

Voice Message

Start Time	114.00 s	Message Name	DF_2CAST_1_04.wav
Duration	3.37 s	Volume	50
Message: "Oscar Alpha Lima, turn left heading 2 7 0 "			

Condition

Start Time	115.00 s	Condition	Heading between 275.00 and 285.00 deg
------------	----------	-----------	---------------------------------------

Condition

Start Time	116.00 s	Condition	Roll Angle > -8.00 deg
------------	----------	-----------	------------------------

Voice Message

Start Time	175.00 s	Message Name	DF_2CAST_1_06.wav
Duration	4.33 s	Volume	50
Message: "Oscar Alpha Lima, turn right direct Hotel November Lima V O R "			

Condition

Start Time	176.00 s	Condition	Roll Angle < 5.00 deg
------------	----------	-----------	-----------------------

Condition

Start Time	177.00 s	Condition	Distance < 2.00 mile(s) from Lat : 21° 18' 29.91
------------	----------	-----------	---

Voice Message

Start Time	178.00 s	Message Name	DF_2CAST_1_08.wav
Duration	5.83 s	Volume	50
Message: "Oscar Alpha Lima, after passing Hotel November Lima V O R turn left heading 2 5 0 "			

Condition

Start Time	179.00 s	Condition	Heading < 262.00 deg
------------	----------	-----------	----------------------

Voice Message

Start Time	199.00 s	Message Name	DF_2CAST_1_07.wav
Duration	4.03 s	Volume	50
Message: "Oscar Alpha Lima, descend altitude 1 thousand 5 hundred feet "			

Condition

Start Time	200.00 s	Condition	Longitude < -158° 1' 48.00"
------------	----------	-----------	-----------------------------

Voice Message

Start Time	201.00 s	Message Name	DF_2CAST_1_10.wav
Duration	3.47 s	Volume	50
Message: "Oscar Alpha Lima, turn left heading 0 4 5 "			

Condition

Start Time	253.00 s	Condition	Heading < 60.00 deg
------------	----------	-----------	---------------------

Voice Message

Start Time	273.00 s	Message Name	DF_2CAST_1_11.wav
Duration	3.58 s	Volume	50
Message: "Oscar Alpha Lima, descend altitude 8 hundred feet "			

Condition

Start Time	274.00 s	Condition	Latitude > 21° 17' 57.00"
------------	----------	-----------	---------------------------

Voice Message

Start Time	275.00 s	Message Name	DF_2CAST_1_12.wav
Duration	6.28 s	Volume	50
Message: "Oscar Alpha Lima, turn right heading 0 8 0 and runway 0 8 right cleared to land "			

Profile End

Profile End Time	1000.00 s
------------------	-----------

PROFILE 1 for Stage 2, with illusions

Voice Message

Start Time	30.00 s	Message Name	DF_2CAST_1_01.wav
Duration	10.13 s	Volume	50
Message: "Oscar Kilo Romeo Alpha Lima runway 0 8 right cleared for take off, when airborne maintain runway heading and climb altitude 1 thousand 5 hundred feet "			

Condition

Start Time	31.00 s	Condition	Pitch Angle > 5.00 deg
------------	---------	-----------	------------------------

Pitch

Start Time	32.00 s	Command Type	Position
Position	12.00 deg	Velocity	4.00 deg/s
Acceleration	1.30 deg/s ²	Duration	6.08 s

Pitch

Start Time	38.00 s	Command Type	Position
Position	0.00 deg	Velocity	1.00 deg/s
Acceleration	0.30 deg/s ²	Duration	15.68 s

Condition

Start Time	54.00 s	Condition	Altitude (MSL) > 1450.00 ft
------------	---------	-----------	-----------------------------

Voice Message

Start Time	69.00 s	Message Name	DF_2CAST_1_02.wav
Duration	3.13 s	Volume	50
Message: "Oscar Alpha Lima, turn right heading 1 6 0 "			

Condition

Start Time	70.00 s	Condition	Heading > 167.00 deg
------------	---------	-----------	----------------------

Voice Message

Start Time	90.00 s	Message Name	DF_2CAST_1_03.wav
Duration	3.42 s	Volume	50
Message: "Oscar Alpha Lima, climb altitude 2 thousand feet "			

Condition

Start Time	91.00 s	Condition	Altitude (MSL) > 1950.00 ft
------------	---------	-----------	-----------------------------

Low Level Clouds

Start Time	92.00 s	Type	AltoCumulus
Coverage	8/8	Base	1000 ft
Height	4000 ft	Slope	0 deg
Axis Heading	0 deg		

Visibility

Start Time	92.00 s	Condition	Clear
Visibility Distance	5 mi	Top	200 ft
BrownOut	Disabled	WhiteOut	Disabled

Voice Message

Start Time	114.00 s	Message Name	DF_2CAST_1_04.wav
Duration	3.37 s	Volume	50
Message: "Oscar Alpha Lima, turn left heading 2 7 0 "			

Condition

Start Time	115.00 s	Condition	Heading < 170.00 deg
------------	----------	-----------	----------------------

Condition

Start Time	116.00 s	Condition	Roll Angle < -5.00 deg
------------	----------	-----------	------------------------

Yaw

Start Time	117.00 s	Command Type	Velocity
Position	-60.00 deg/s	Velocity	2.00 deg/s ²
Acceleration	30.00 s		

Condition

Start Time	148.00 s	Condition	Heading < 45.00 deg
------------	----------	-----------	---------------------

Voice Message

Start Time	149.00 s	Message Name	DF_2CAST_1_05.wav
Duration	7.30 s	Volume	50
Message: "Oscar Alpha Lima, can you read the number on the plate? The plate is located on the left panel slightly behind you "			

Condition

Start Time	150.00 s	Condition	Heading < 275.00 deg
------------	----------	-----------	----------------------

Condition

Start Time	151.00 s	Condition	Roll Angle > -8.00 deg
------------	----------	-----------	------------------------

Yaw

Start Time	152.00 s	Command Type	Velocity
Position	0.00 deg/s	Velocity	1.00 deg/s ²
Acceleration	60.00 s		

Voice Message

Start Time	214.00 s	Message Name	DF_2CAST_1_06.wav
Duration	4.33 s	Volume	50
Message: "Oscar Alpha Lima, turn right direct Hotel November Lima V O R "			

Condition

Start Time	215.00 s	Condition	Roll Angle < 5.00 deg
------------	----------	-----------	-----------------------

Condition

Start Time	216.00 s	Condition	Distance < 2.00 mile(s) from Lat : 21° 18' 29.91
------------	----------	-----------	---

Voice Message

Start Time	217.00 s	Message Name	DF_2CAST_1_08.wav
Duration	5.83 s	Volume	50
Message: "Oscar Alpha Lima, after passing Hotel November Lima V O R turn left heading 2 5 0 "			

Condition

Start Time	218.00 s	Condition	Heading < 262.00 deg
------------	----------	-----------	----------------------

Voice Message

Start Time	238.00 s	Message Name	DF_2CAST_1_07.wav
Duration	4.03 s	Volume	50
Message: "Oscar Alpha Lima, descend altitude 1 thousand 5 hundred feet "			

Condition

Start Time	239.00 s	Condition	Longitude < -158° 1' 48.00"
------------	----------	-----------	-----------------------------

Voice Message

Start Time	240.00 s	Message Name	DF_2CAST_1_10.wav
Duration	3.47 s	Volume	50
Message: "Oscar Alpha Lima, turn left heading 0 4 5 "			

Condition

Start Time	241.00 s	Condition	Heading < 260.00 deg
------------	----------	-----------	----------------------

Condition

Start Time	242.00 s	Condition	Roll Angle < -5.00 deg
------------	----------	-----------	------------------------

Yaw

Start Time	243.00 s	Command Type	Velocity
Position	-60.00 deg/s	Velocity	1.50 deg/s ²
Acceleration	40.00 s		

Condition

Start Time	284.00 s	Condition	Heading < 65.00 deg
------------	----------	-----------	---------------------

Condition

Start Time	285.00 s	Condition	Roll Angle > -15.00 deg
------------	----------	-----------	-------------------------

Yaw

Start Time	286.00 s	Command Type	Velocity
Position	0.00 deg/s	Velocity	12.00 deg/s ²
Acceleration	5.01 s		

Condition

Start Time	292.00 s	Condition	Heading < 60.00 deg
------------	----------	-----------	---------------------

Voice Message

Start Time	312.00 s	Message Name	DF_2CAST_1_11.wav
Duration	3.58 s	Volume	50
Message: "Oscar Alpha Lima, descend altitude 8 hundred feet "			

Condition

Start Time	313.00 s	Condition	Latitude > 21° 17' 57.00"
------------	----------	-----------	---------------------------

Voice Message

Start Time	314.00 s	Message Name	DF_2CAST_1_12.wav
Duration	6.28 s	Volume	50
Message: "Oscar Alpha Lima, turn right heading 0 8 0 and runway 0 8 right cleared to land "			

Profile End

Profile End Time	1000.00 s
------------------	-----------

Appendix 5

Flight profile 2 for Stage 2

PROFILE 2 for Stage 2, without illusions

Voice Message

Start Time	30.00 s	Message Name	DF_2CAST_2_01.wav
Duration	10.19 s	Volume	50
Message: "Oscar Kilo Romeo Alpha Lima runway 0 4 right cleared for take off, when airborne maintain runway heading and climb altitude 1 thousand 5 hundred feet "			

Condition

Start Time	55.00 s	Condition	Latitude > 21° 19' 50.00"
------------	---------	-----------	---------------------------

Voice Message

Start Time	56.00 s	Message Name	DF_2CAST_2_02.wav
Duration	5.81 s	Volume	50
Message: "Oscar Alpha Lima, turn left heading 3 0 0 and climb altitude 2000 ft "			

Condition

Start Time	58.00 s	Condition	Altitude (MSL) > 1950.00 ft
------------	---------	-----------	-----------------------------

Condition

Start Time	59.00 s	Condition	Longitude < -157° 56' 60.00"
------------	---------	-----------	------------------------------

Low Level Clouds

Start Time	60.00 s	Type	AltoCumulus
Coverage	8/8	Base	1000 ft
Height	4000 ft	Slope	0 deg
Axis Heading	0 deg		

Visibility

Start Time	60.00 s	Condition	Clear
Visibility Distance	5 mi	Top	200 ft
BrownOut	Disabled	WhiteOut	Disabled

Voice Message

Start Time	61.00 s	Message Name	DF_2CAST_2_03.wav
Duration	3.09 s	Volume	50
Message: "Oscar Alpha Lima, turn rght heading 190 "			

Voice Message

Start Time	161.00 s	Message Name	DF_2CAST_2_05.wav
Duration	4.15 s	Volume	50
Message: "Oscar Alpha Lima, continue direct Hotel November Lima V O R "			

Condition

Start Time	163.00 s	Condition	Distance < 2.00 mile(s) from Lat : 21° 18' 29.91
------------	----------	-----------	---

Voice Message

Start Time	164.00 s	Message Name	DF_2CAST_2_06.wav
Duration	5.62 s	Volume	50
Message: "Oscar Alpha Lima, after passing Hotel November Lima V O R turn left heading 110 "			

Condition

Start Time	165.00 s	Condition	Heading < 122.00 deg
------------	----------	-----------	----------------------

Voice Message

Start Time	185.00 s	Message Name	DF_2CAST_2_06_5.wav
Duration	4.03 s	Volume	50
Message: "Oscar Alpha Lima, descend altitude 1 thousand 5 hundred feet "			

Condition

Start Time	186.00 s	Condition	Longitude > -157° 49' 48.00"
------------	----------	-----------	------------------------------

Voice Message

Start Time	189.00 s	Message Name	DF_2CAST_2_07.wav
Duration	3.43 s	Volume	50
Message: "Oscar Alpha Lima, turn right heading 3 1 5 "			

Condition

Start Time	241.00 s	Condition	Heading > 320.00 deg
------------	----------	-----------	----------------------

Voice Message

Start Time	261.00 s	Message Name	DF_2CAST_2_08.wav
Duration	3.58 s	Volume	50
Message: "Oscar Alpha Lima, descend altitude 8 hundred feet "			

Condition

Start Time	262.00 s	Condition	Latitude > 21° 17' 57.00"
------------	----------	-----------	---------------------------

Voice Message

Start Time	263.00 s	Message Name	DF_2CAST_2_09.wav
Duration	6.25 s	Volume	50
Message: "Oscar Alpha Lima, turn left heading 2 6 0 and runway 2 6 right cleared to land "			

Profile End

Profile End Time	1000.00 s
------------------	-----------

PROFILE 2 for Stage 2, with illusions

Voice Message

Start Time	30.00 s	Message Name	DF_2CAST_2_01.wav
Duration	10.19 s	Volume	50
Message: "Oscar Kilo Romeo Alpha Lima runway 0 4 right cleared for take off, when airborne maintain runway heading and climb altitude 1 thousand 5 hundred feet "			

Condition

Start Time	31.00 s	Condition	Pitch Angle > 5.00 deg
------------	---------	-----------	------------------------

Pitch

Start Time	32.00 s	Command Type	Position
Position	12.00 deg	Velocity	4.00 deg/s
Acceleration	1.30 deg/s ²	Duration	6.08 s

Pitch

Start Time	38.00 s	Command Type	Position
Position	0.00 deg	Velocity	1.00 deg/s
Acceleration	0.30 deg/s ²	Duration	15.68 s

Condition

Start Time	55.00 s	Condition	Latitude > 21° 19' 50.00"
------------	---------	-----------	---------------------------

Voice Message

Start Time	56.00 s	Message Name	DF_2CAST_2_02.wav
Duration	5.81 s	Volume	50
Message: "Oscar Alpha Lima, turn left heading 3 0 0 and climb altitude 2000 ft "			

Condition

Start Time	58.00 s	Condition	Altitude (MSL) > 1950.00 ft
------------	---------	-----------	-----------------------------

Condition

Start Time	59.00 s	Condition	Longitude < -157° 56' 60.00"
------------	---------	-----------	------------------------------

Low Level Clouds

Start Time	60.00 s	Type	AltoCumulus
Coverage	8/8	Base	1000 ft
Height	4000 ft	Slope	0 deg
Axis Heading	0 deg		

Visibility

Start Time	60.00 s	Condition	Clear
Visibility Distance	5 mi	Top	200 ft
BrownOut	Disabled	WhiteOut	Disabled

Voice Message

Start Time	61.00 s	Message Name	DF_2CAST_2_03.wav
Duration	3.09 s	Volume	50
Message: "Oscar Alpha Lima, turn right heading 190 "			

Condition

Start Time	62.00 s	Condition	Heading > 310.00 deg
------------	---------	-----------	----------------------

Condition

Start Time	63.00 s	Condition	Roll Angle > 5.00 deg
------------	---------	-----------	-----------------------

Yaw

Start Time	64.00 s	Command Type	Velocity
Position	-60.00 deg/s	Velocity	2.00 deg/s ²
Acceleration	30.00 s		

Condition

Start Time	95.00 s	Condition	Heading > 75.00 deg
------------	---------	-----------	---------------------

Voice Message

Start Time	96.00 s	Message Name	DF_2CAST_2_04.wav
Duration	7.30 s	Volume	50
Message: "Oscar Alpha Lima, can you read the number on the plate? The plate is located on the left panel slightly behind you "			

Condition

Start Time	97.00 s	Condition	Heading > 195.00 deg
------------	---------	-----------	----------------------

Condition

Start Time	98.00 s	Condition	Roll Angle < 8.00 deg
------------	---------	-----------	-----------------------

Yaw

Start Time	99.00 s	Command Type	Velocity
Position	0.00 deg/s	Velocity	1.00 deg/s ²
Acceleration	60.00 s		

Voice Message

Start Time	161.00 s	Message Name	DF_2CAST_2_05.wav
Duration	4.15 s	Volume	50
Message: "Oscar Alpha Lima, continue direct Hotel November Lima V O R "			

Condition

Start Time	163.00 s	Condition	Distance < 2.00 mile(s) from Lat : 21° 18' 29.91
------------	----------	-----------	---

Voice Message

Start Time	164.00 s	Message Name	DF_2CAST_2_06.wav
Duration	5.62 s	Volume	50
Message: "Oscar Alpha Lima, after passing Hotel November Lima V O R turn left heading 110 "			

Condition

Start Time	165.00 s	Condition	Heading < 122.00 deg
------------	----------	-----------	----------------------

Voice Message

Start Time	185.00 s	Message Name	DF_2CAST_2_06_5.wav
Duration	4.03 s	Volume	50
Message: "Oscar Alpha Lima, descend altitude 1 thousand 5 hundred feet "			

Condition

Start Time	186.00 s	Condition	Longitude > -157° 49' 48.00"
------------	----------	-----------	------------------------------

Voice Message

Start Time	189.00 s	Message Name	DF_2CAST_2_07.wav
Duration	3.43 s	Volume	50
Message: "Oscar Alpha Lima, turn right heading 3 1 5 "			

Condition

Start Time	190.00 s	Condition	Heading > 120.00 deg
------------	----------	-----------	----------------------

Condition

Start Time	191.00 s	Condition	Roll Angle > 5.00 deg
------------	----------	-----------	-----------------------

Yaw

Start Time	192.00 s	Command Type	Velocity
Position	-60.00 deg/s	Velocity	1.50 deg/s ²
Acceleration	40.00 s		

Condition

Start Time	233.00 s	Condition	Heading > 315.00 deg
------------	----------	-----------	----------------------

Condition

Start Time	234.00 s	Condition	Roll Angle < 15.00 deg
------------	----------	-----------	------------------------

Yaw

Start Time	235.00 s	Command Type	Velocity
Position	0.00 deg/s	Velocity	12.00 deg/s ²
Acceleration	5.01 s		

Condition

Start Time	241.00 s	Condition	Heading > 320.00 deg
------------	----------	-----------	----------------------

Voice Message

Start Time	261.00 s	Message Name	DF_2CAST_2_08.wav
Duration	3.58 s	Volume	50
Message: "Oscar Alpha Lima, descend altitude 8 hundred feet "			

Condition

Start Time	262.00 s	Condition	Latitude > 21° 17' 57.00"
------------	----------	-----------	---------------------------

Voice Message

Start Time	263.00 s	Message Name	DF_2CAST_2_09.wav
Duration	6.25 s	Volume	50
Message: "Oscar Alpha Lima, turn left heading 2 6 0 and runway 2 6 right cleared to land "			

Profile End

Profile End Time	1000.00 s
------------------	-----------